The Dissertation Committee for Ashkan Khakparvar Yazdi
certifies that this is the approved version of the following dissertation:

Carrier-Free High-Dose Dry-Powder Inhaler Formulation of

Non-Steroidal Anti-Inflammatory Drugs

_____
Hugh D.C. Smyth, Supervisor

_____
Robert O. Williams III

_____
Christopher R. Frei

_____
Alan B. Watts

_____
Bennie C. McWilliams

Carrier-Free High-Dose Dry-Powder Inhaler Formulation of Non-Steroidal Anti-Inflammatory Drugs

by

Ashkan Khakparvar Yazdi, Pharm.D.

Dissertation

Presented to the Faculty of the Graduate School of

the University of Texas at Austin

in Partial Fulfillment

of the Requirements

for the Degree of

Doctor of Philosophy

The University of Texas at Austin

August 2016

Dedications

To Meredith, my wife

To my beloved parents

Acknowledgements

I would like to thank my supervisor, Dr. Hugh D.C. Smyth, for giving me the opportunity to work in his lab and for providing the guidance and support throughout my Ph.D. tenure. I would like to thank my committee members Dr. Robert O. Williams III, Dr. Cristopher R. Frei, Dr. Alan B. Watts, and Dr. Bennie C. McWilliams for their time and advice throughout my research project. Furthermore, I would like to thank Dr. James W. McGinity for his teaching and advice throughout the course of my tenure.

I would like to specially thank Dr. Kristin R. Fathe, our immediate-past lab manager, for her editorial help. I would also like to thank Dr. Zachary Warnken for his help with the initial preliminary studies. I would also like to thank the Division of Pharmaceutics faculty and staff specially Yolanda Camacho, Pharmaceutics Program and Division Coordinator for their support. I would also like to thank the Learning Resource Center staff for their technological support: Belinda Lehmkuhle, Jay Hamman, John Reineke. I would also like to thank Herman Schwarzer and Joe D. Adcock in Business office and Sharla Brewer, the Building Manager.

I would like to also thank previous and current post doctoral fellows: Dr. Andy Maloney, Dr. Nihal Bandara, and Dr. Silvia Ferrati. Moreover, I would like to thank previous and current fellow graduate students in the lab: Dr. Martin Donovan, Dr. Srimahitha Kaliki, Dr. Ping Du, Dr. Ju Du, Dr. Matthew Herpin, Daniel Moraga-Espinoza, Tania Bahamondez, Dr. Zacharey Warnken, Jasmim Leal, and Patricia Martins for their support and camaraderie. Finally, I would like to thank the former and current

fellow graduate students in the division of Pharmaceutics for their scientific discussions: Dr. Javier Morales, Dr. Yoen-Ju Son, Dr. Sumalee Thitinan, Dr. Shi-Fan Jang, Dr. Thiago Carvalho, Dr. Simone Carvalho, Dr. Ryan Bennett, Dr. Stephanie Bosselmann, Dr. Chris Brough, Dr. Jin Huk Coi, Dr. Justin Hughey, Dr. Justin Keen, Dr. Amit Kumar, Dr. Bo Lang, Dr. Xinran Li, Dr. Kevin O'Donnell, Dr. Letty Rodriguez, Dr. Yibo Wang, Dr. Youssef Naguib, Dr. Hannah OMary, Michael Sandoval, Dayel, Solange, Soraya Hengsawas, Siyuan Huang, Justin LaFountaine, Xu Liu, Julien Maincent, Abbe Miller, Leena Prasad, and Sachin Thakkar.

I would like to acknowledge Meredith Gutierrez, my college sweetheart, and my wife for her kindness, support, and encouragement during the past five years. I would also like to thank Dr. Iman Yazdi, my brother, my friend, and my role model. Finally, I am grateful for having supportive parents who immigrated to the United States and provided endless opportunities for my brother and me.

Carrier-Free High-Dose Dry-Powder Inhaler Formulation of

Non-Steroidal Anti-Inflammatory Drugs

Ashkan Khakparvar Yazdi, Ph.D.

The University of Texas at Austin, 2016

SUPERVISOR: Hugh D.C. Smyth

Ibuprofen (IBU) is a non-steroidal anti-inflammatory agent (NSAID) is administered orally as tablets and suspensions. It is indicated for pain, fever, and other inflammatory conditions. More recently, a slower rate of respiratory decline is shown in cystic fibrosis (CF) patients on high, oral doses of IBU in comparison to placebo. The use of this treatment modality has not been well adopted or widespread due to high doses, side effects, contraindications, and black box warnings regarding the use of IBU.

Pulmonary delivery may be an attractive alternative to high-dose oral administration in CF since lungs are the desired targets for the anti-inflammatory and antibiotic activities of IBU. Typically with inhaled powders, a binary formulation of a drug with a carrier, such as lactose, significantly improves their performance; however, this strategy is not practical for the delivery of a large drug dose via a dry powder inhaler (DPI). Other inhalation devices such as nebulizers require significantly more time for drug delivery and metered dose inhalers may be incapable of metering sufficiently large drug doses. Therefore, carrier-free DPIs have been explored for large drug dose delivery.

IBU exists as the stable polymorph I (in its acicular crystal habit), or as the less stable polymorph II. Low melting point (75.85°C), water solubility, and crystal habit of ibuprofen make its processing challenging. A novel air-jet milled carrier-free formulation of IBU was developed using the design of experiment approach, which possessed superior flowability, *in-vitro* aerodynamic performance determined by Next Generation Impactor. Furthermore, the developed formulation possessed at least one-year stability at room temperature in the desiccator under vacuum.

TABLE OF CONTENTS

LIST OF TABLES

CHAPTER I

CHAPTER III

CHAPTER IV

LIST OF FIGURES

CHAPTER I

CHAPTER III

CHAPTER IV

CHAPTER I

Material and Process Considerations in Particle Engineering Technologies

Authors:

Ashkan K. Yazdi[1], Hugh D.C. Smyth[1]

[1]PHR 4.214, Division of Pharmaceutics, College of Pharmacy, The University of Texas at Austin, 2409 University Ave Stop A1920, Austin TX 78712-1119

Corresponding Author:

Hugh D. C. Smyth

Office: 512 471 3383

Fax: 512 471 7474

Email: hugh.smyth@austin.utexas.edu

Keywords:

Bottom-up, Top-down, Micronization, Homogenization, Spray-drying, Crystallization, Supercritical fluid, Polymorphism, Surface energy, Mechanochemical transformation

Abstract:

Objective: To provide a survey of common particle engineering technologies used for the preparation of nanoparticles and microparticles, to evaluate the effect of these technologies on the properties of end-product, and to discuss the critical properties of compounds, which dictates the type technologies to be utilized to process a specific compound.

Background: Microparticles and nanoparticles are intended to increase the bioavailability of compounds with low water solubility. Furthermore, microparticles are utilized to deliver to a specific cite such as lungs. Finally, microparticles and nanoparticles are of great importance in preparation of stable suspensions.

Results: From the top-down and bottom-up particle engineering techniques, the top-down particle engineering techniques, namely different milling techniques, have been utilized the most to produce nanoparticles and microparticles. The most common bottom-up process in particle engineering is spray drying, which allows for the production amorphous and crystalline particles with different morphologies. The popularities of these techniques lie in the ability to scale-up from laboratory to commercial. Particle engineering technologies may influence the phase of final product through mechanochemical transformation and induce the transition of a crystalline to an amorphous phase or vice-versa. Finally, physicochemical properties of drugs such melting point and crystal lattice strength dictate the particle engineering technologies, which can be utilized to produce nanoparticles and microparticles.

Conclusion: There have been tremendous advances in the development of particle engineering technologies. Mechanochemical transformation constitutes the primary influence of these technologies on the properties of the final product. Physicochemical properties of starting material should dictate the type of processing methods in nanoparticle and microparticle engineering.

1. Introduction

The primary purpose of the transformation of active pharmaceutical ingredients (APIs) into a fine powder is to enhance their bioavailability through an increase in the dissolution rate. Other purposes for this transformation are to target the formulation to respiratory route and to formulate stable suspensions. One, or more particle engineering steps are usually required during formulation development since almost all formulations start from a solid active pharmaceutical ingredient (API) directly from a manufacturer as a bulk material, or there is a distinct downstream particle-engineering step.

Particle engineering methods utilized for the production of fine powders include bottom-up and top-down processes. Bottom-up processes include controlled crystallization, spray chilling, melt-emulsification, spray drying, and the rapid expansion of supercritical solutions. Top-down processes, also known as comminution methods include dry-milling, wet-milling, and high-pressure homogenization. The processing method selection criteria include the desired particle size range, as well as physicochemical properties of the material including polymorphism, solubility, and stability.

In this review, an overview of different particle engineering techniques will be provided. Furthermore, strengths and limitations of each method will be discussed. Finally, API properties affecting decision making for the use of one method over another method will be discussed.

1.1. Dissolution rate

As of 2006, about 40% of top 200 drugs sold in the United States were considered to be practically insoluble in water (Takagi et al., 2006) and significantly higher percentage of drug candidates in development belong to this category and present significant challenges for drug development. Specifically, drug candidates, belonging to the biopharmaceutic classification system (BCS) class II, possess high membrane permeability and low aqueous solubility. Therefore, their bioavailability will suffer from erratic or incomplete absorption due to poor aqueous solubility (Amidon et al., 1995). One approach for increasing the bioavailability these drug candidates is to increase their dissolution rate.

According to Nernst-Brunner equation (Equation 1), drug dissolution rate (dC/dt) increases with an increase in drug surface area (S), which can be achieved through particle size reduction (Dokoumetzidis and Macheras, 2006). Other variables in this equation are drug diffusion coefficient (D), drug concentration surrounding the drug particles in the diffusion layer (C_s), drug concentration in bulk dissolution media (C), the volume of the dissolution medium (V), and diffusion layer thickness (h).

$$\frac{dC}{dt} = \frac{D\,S}{V\,h}(C_s - C) \qquad \text{Equation 1}$$

Furthermore, saturation solubility is a function of particle size, and their relationship is explained by the Ostwald-Freundlich equation (Equation 2), where smaller particle sizes are associated with an increase in the saturation solubility (Simonell.ap et al., 1970). In this equation, $C_{s,r}$ and $C_{s,\infty}$ are the solubilities for a particle with a radius of r

and a very large particle; γ is the interfacial tension; V_m is the molar volume; R is the gas constant; and T is the absolute temperature.

$$ln\frac{C_{s,r}}{C_{s,\infty}} = \frac{2\,\gamma\,V_m}{rRT} \qquad \text{Equation 2}$$

1.2. Suspensions

Particle size significantly affects the physical stability of a suspension. Specifically, sedimentation velocity for spherical particles in a suspension is governed by the Stokes' law (Equation 3).

$$v = \frac{2r^2(\rho_1-\rho_2)g}{9\eta} \qquad \text{Equation 3}$$

In this equation, r is the radius of particles, ρ_1 and ρ_2 are densities of the dispersed phase and dispersion medium, g is the gravitational acceleration and η is the Newtonian viscosity of the dispersion medium. According to the Stokes' law, suspensions with smaller particle size are expected to have a slower sedimentation velocity. Furthermore, higher interparticulate interactions in these suspensions due to the increased surface area may lead to a favorable increase in the viscosity and the stability of the suspension. Conversely, suspensions with smaller particles may be prone to caking if they are not flocculated (Kulshreshtha et al., 2009).

A mono-dispersed particle size distributions are preferred over poly-dispersed particle size distribution for the development of stable suspension systems as they will be associated with a more uniform sedimentation velocity. Additionally, flocculated suspensions from mono-dispersed distributions will be less dense than ones from poly-

dispersed distributions where small particles fill voids between larger particles. Finally, poly-dispersed distributions suffer to a greater extent from Oswald ripening where temperature fluctuations lead to the dissolution of smaller particles and crystal growth on larger particles.

1.3. Pulmonary drug delivery

The pulmonary route represents an alternative to the oral and the parenteral route of delivery for local and systemic delivery small molecules but more specifically protein and peptide drugs (Patton and Platz, 1992). Drug physicochemical properties administered via inhalation vary significantly: logP [–2 (albuterol sulfate) to 5 (fluticasone propionate)], solubility [0.1 μg/mL (fluticasone propionate) to 250 mg/mL (albuterol sulfate)]. Lung fluid is composed of water mainly (96%), salts, phospholipids, proteins, and mucin with pH of about 6.6 in healthy individuals (Olsson et al., 2011). Moreover, the total liquid volume available for dissolution is approximately 10 – 30 mL with 5 – 10 μm thickness in conducting airways and much lower thickness of 0.01 – 0.08 μm with the maximum of several microns thick in some regions in the alveoli (John S., 1996). The large absorptive surface area of approximately 100 m^2 and superior blood perfusion enable the rapid absorption and onset of action of drugs (Labiris and Dolovich, 2003). Furthermore, systemic absorption from lungs is associated with minimal hepatic first-pass metabolism (Patton et al., 2004). Alternatively, local lung delivery with minimal systemic absorption is associated with therapeutic local concentration and

minimal drug distributions in other tissues. Tissue-selective distribution limits side effects and increases therapeutic indices.

Respiratory system structural design, its primary protective mechanism, prevents alveoli deposition of all particles except particles with a narrow aerodynamic diameter size range between 0.5 to 5 μm. Successful deep lung deposition for dry powder inhaler (DPI) formulations, is strongly correlated to the percentage of particles with an aerodynamic diameter less than 3 μm and particles and particles larger than this size are deposited in the upper airways (Newman and Chan, 2008). As depicted in Equation 1, for spherical, solid particles, the aerodynamic diameter is equal to the geometric diameter (D_{eq}) where particle density (ρ_p) is equal to unit density (ρ_o) and the dynamic shape factor (χ) is equal to one (Telko and Hickey, 2005).

$$D_{ae} = D_{eq}\sqrt{\frac{\rho_p}{\rho_o \chi}} \qquad \textit{(Equation 4)}$$

Pulmonary formulations are delivered to the lungs via three distinct classes of devices including dry powder inhalers (DPIs), pressurized meter dose inhalers (pMDIs), and nebulizers (Frijlink and de Boer, 2005). Aerosol deposition in the airways is a function of the physical structures of the airways, the physics of particle motion, and airflow dynamics. If inhaled particles are not exhaled due to the particle size less than 0.5 μm, they may deposit in the various regions of the respiratory system by the action of five different deposition mechanisms: interception, inertial impaction, diffusion, gravitational settling, and electrostatic attraction (Hinds, 2012).

2. Particle engineering technologies

As it was previously discussed, particle-engineering technologies are utilized to produce microparticles and nanoparticles to enable route specific delivery and to improve saturation solubility, dissolution rate, and formulation stability.

2.1. Top-down approaches

Top-down approaches also known as destructive approaches are the most widely used technologies to produce microparticles and nanoparticles. Milling methods can be classified as shear milling, compression milling, and impaction milling where relatively larger particles are produced by shear milling and the smallest particles are produced by impact milling.

2.1.1. Milling

Various milling techniques are capable of producing particles with different particle sizes ranging from very fine to colloidal particles (Zheng, 2009). Table 1.1 depicts the various dry and wet milling techniques and size ranges associated with them. Milling methods can be divided into dry-milling where the milling media is gas, or wet-milling where the milling media is liquid methods. Particle-size reduction occurs by compression, impaction, and attrition through collision of particles with the surfaces of the equipment as well as with each other (Clement and Purutyan, 2002; Friedrich, 2001). Furthermore, during the wet-milling process, the liquid milling media exhibits shearing and cavitational forces contributing to the particle-size reduction (Sharma et al., 2009).

Regardless of milling technique, particle density and residence time of particles can affect both the milling rate and its efficiency.

2.1.1.1. Ball milling

Ball mill is composed of a rotating vessel filled partially with balls where comminution is caused by attrition and impaction. In a wet ball mall, the vessel is filled three-quarters way with pearl balls along with a suspension of the drug with stabilizers and in contrast to the high-pressure homogenization, micronized drug are obtained using a lower energy input. Most notably, a wet ball mill is branded as NanoCrystal® technology, and the API for processing is suspended in the dispersion medium. Suspensions for oral and parenteral use are stabilized using surfactants and there no requirement for subsequent drying due to stability concerns.

2.1.1.2. Fluid energy milling

Fluid energy mills can be classified into two general categories of loop/spiral mills also known as air-jet mills and attrition mills also known as fluidized bed jet mill. This classification is based on whether the jets of grinding gas are introduced tangentially in the direction of airflow, or are impinging at a central point where maximal particle-particle collisions are expected to result in breakage. Milling pressure is between 3 and 10 bar corresponding to 43.5 and 145 psi (Rasenack and Müller, 2004). Fluidized bed jet mills can mill harder materials in comparison with spiral jet mills. Furthermore, a classifier prevents the premature departure of unmilled solid from the milling chamber in the fluidized bed jet-mills as opposed to spiral jet mills. For fluidized bed jet mills with a

rotatory classifier, specific surface area is a function of grinding pressure and the speed of rotation for the classifier (Nakach et al., 2004). Spiral jet mills benefit from an internal classifier where larger particles stay on the periphery of the grinding chamber and finer particles, entrained in the air current, exit the grinding chamber. Fine particles may be fractionated further using a cyclone separator at a specific particle cutoff size.

2.1.1.3. Cryogenic milling

Two different processes involving cryogenic conditions constitute cryogenic milling or cryomilling. The first process is a ball milling, where the cryogenic liquid is added to the grinding chamber and material is in direct contact with the cryogenic liquid. The second process involves cooling down the grinding chamber where material is not in direct contact with the cryogenic liquid. In cryomilling, particle size reduction occurs at controlled low temperatures where material brittleness favors particle fracture upon compression, impaction, and attrition (Witkin and Lavernia, 2006). One significant advantage of this method is to process heat-sensitive materials; however, particle aggregation induced by moisture condensation during sample recovery and cryogenic liquid removal is a major drawback (Fisher, 2013). Other drawbacks includes amorphization with prolonged duration of milling (Macfhionnghaile et al., 2014).

2.1.1.4. Sonofragmentation

Sonofragmentation is the process during which ultrasound is used to decrease particle size. Ultrasound waves possess alternating periods of compression and expansion while propagating through a liquid. Its chemical and physical effects on materials arise

from acoustic cavitation, the formation, growth, and implosive collapse of bubbles in the liquid during ultrasound expansion periods. The implosive collapse of bubbles creates shockwaves with velocities of ~4000 m/s and amplitudes of 10^6 KPa (Suslick, 1989). Isolated sub-micron reactors are predicted to have local temperatures of ~5000 K, pressures of ~ 10^5 KPa, and heating and cooling rates above 10^9 K/s and are responsible for sonochemistry (Suslick, 1990). Zeiger and Suslick ruled out interparticle, particle-horn, and particle-wall collisions as potential mechanisms for sonofragmentation and proposed particle-shockwave interactions as the mechanism for this process (Zeiger and Suslick, 2011). Pérez-Maqueda et al. processed down talc to submicron particles using sonofragmentation and observed delamination and lateral particle size reduction followed by agglomeration with further particle size reduction when ultrasound was applied for longer than 40 h (Pérez-Maqueda et al., 2005).

2.1.2. High-pressure homogenization

Homogenization is a particle-size reduction process for the preparation of emulsions; however, it has been utilized to reduce the particle size of suspensions. Through this process, the polydispersity of sample particle size distribution is decreased. The sample is "homogenized" due to fluidic turbulence, cavitation, and shear. The type of homogenizer (i.e. piston-gap vs. jet-stream) along with the physical properties of the bulk powder determines which of these mechanisms will be more dominant in particle-size reduction.

2.1.2.1. Piston-gap homogenization

A piston-gap homogenizer forces a macrosuspension consisting of a drug dispersed in an aqueous surfactant solution through a 5 to 20 μm gap using a piston under pressures up to 4000 bars and is also known as DissoCubes™ technology (Muller et al., 1999). An increase in the dynamic pressure caused by a high streaming velocity in the gap is compensated by a decrease in the static pressure below the vapor pressure of water, which causes it to boil and to form gas bubbles. Cavitation occurs with the collapse of gas bubbles immediately after the gap, creates high power shockwaves, and results in particle size reduction (Shegokar and Mueller, 2010).

Nanopure® technology is a piston-gap homogenizer variant where non-aqueous liquids with low vapor pressure (i.e. oils, polyethylene glycol) are used instead of water. Due to the absence of cavitation with low vapor pressure, hydrodynamic shear forces and drug particle collisions are responsible for particle size reduction.

2.1.2.2. Jet-stream homogenization

Also known as a microfluidizer, a jet-stream homogenizer operates based on the jet stream principle where two fluid streams collide under pressures up to 1700 bars in a Y-type or Z-type chamber. Forces of shear, impaction, and cavitation in the collision chamber are responsible for particle size reduction and surfactants are added to stabilize these particles. Strydom et al. prepared nanoparticle complexes of sulfadiazine, silver, and poly(amidoamine) dendrimers using jet-stream homogenization technique to create a

uniform distribution of these nanoparticles with increasing the number of process cycles (Strydom et al., 2013).

2.2. Bottom-up approaches

2.2.1. Spray-drying

Spray-drying is a one-step, scalable, constructive particle engineering process as opposed to milling, a destructive particle engineering process, for the production of drug aerosol particles (Xu and Hickey, 2011). The first patent on spray-drying was filed in 1872 by Peroy, SR (Drying, 1872). In the spray-drying method, a solution, a coarse suspension, fine suspension, a colloidal dispersion (e.g. emulsion, liposomes, etc.), or paste of an active pharmaceutical ingredients (API) alone, or with other excipients are atomized and are dried by contact with hot air (Mujumdar, 2006). Atomization methods used include centrifugal (e.g. spinning disk), kinetic (e.g. pneumatic), high pressure, ultrasonic, electrostatic, and effervescent. Separation occurs via the use of a cyclone, electrostatic precipitator, or a bag filter (Van Oort and Sacchetti, 2007).

Advantages of spray drying for particle engineering include processing of materials, which are heat labile and have low aqueous solubility. Furthermore, it is a scalable continuous processing method, which allows for a high degree of tunability for product properties (e.g. particle size, size distribution, particle shape, density, and macroscopic powder properties such as bulk density, flowability, and dispersibility). Finally, process optimizations allow for the production of aerosolizable powder would not require post-processing modification such as lyophilization (Van Oort and Sacchetti,

2007). Disadvantages of spray drying include low material bulk desnsities, liquid vehicle dependent operation, and the requirement for pumpable feed material (Mujumdar, 2006).

2.2.2. Cryogenic technologies

In these methods, cryogenic liquid most commonly liquid nitrogen is utilized to improve the solubility and dissolution of poorly water-soluble drugs by freezing a feed formulation with subsequent solvent removal (Yang et al., 2012).

2.2.2.1. Spray-freeze drying

As oppose to spray drying with atomization and drying steps, spray-freeze drying (SFD) consists of three steps: atomization, freezing, and sublimation. The atomization step is conducted on a feed solution, emulsion, or suspension of a drug alone or in combination with other excipients. The freezing step involves the freezing of the atomized droplets using the cryogenic liquid. The final step of sublimation involves the solvent removal from the frozen particle. The final product usually yields an amorphous powder. This method was first used to process proteins and peptides, because unlike spray drying techniques, no heat is required, which prevents proteins and peptides denaturation (Benson and Ellis, 1948). It is only in the early 1990s that SFD started to be used by pharmaceutical industries to prepare amorphous forms of poorly water-soluble drugs (Mumenthaler and Leuenberger, 1991; Zijlstra et al., 2007).

2.2.2.2. Spray freezing into liquid

Developed and patented by Williams, et al. (Williams et al., 2005) and commercialized by Dow Chemical Company, and Enavail LLC, spray freezing into

liquid (SFL) involves steps akin to spray-freeze drying; however, the atomization process occurs in the cryogenic liquid were the atomized droplets are frozen upon contact with the cryogenic liquid resulting in better stability profile (Yu et al., 2006). The powders processed with the SFL technology are micron size nanostructures with an amorphous morphology, high porosity, hence, they possess high surface area (Hu et al., 2004a), which improve the wettability and enhance dissolution properties of the poorly water-soluble drugs processed by SFL (Hu et al., 2004b).

2.2.2.3. Thin film freezing

Similarly to the SFL and the SFD technologies, the thin film freezing (TFF) process starts with a feed solution containing the drug alone, or in combination with other pharmaceutical excipients. The feed solution is frozen dropwise on a pre-cooled (below the lowest freezing temperature of the solvent used to dissolve the drug and the excipients) rotating cryogenic substrate. Similar to the SFD and SFL technologies, the solvents are removed by freeze-drying to obtain dry powders (Beinborn et al., 2012). This process is utilized to created micro-aggregates containing primary nanoparticle structures of amorphous or crystalline materials and to improve the dissolution of poorly water-soluble drugs by increasing the specific surface area of the particles and modifying their crystal structure (Overhoff et al., 2007). The cooling rate of the TFF process (~102 K/s) produces rapid nucleation and significantly prevents particle growth, as the particles are immobilized in the frozen state. The size of the primary structures is controlled by the process parameters and the formulation composition: the solvent composition, the

percentage of dissolved solids in the feed solution and the temperature of the cryogenic surface (Beinborn et al., 2012; Engstrom et al., 2008).

2.2.3. Controlled precipitation technologies

Controlled crystallization or precipitation processes allow for the particle size control of APIs and production of narrowly distributed particle sizes (Am Ende and Brenek, 2004). Crystallization driving force is supersaturation, which is achieved with thermal swing and antisolvent addition and is followed by nucleation and crystal growth (Mullin, 2001). Alternatively, if the amorphous phase growth rate is greater than the crystalline phase growth rate, the resulting phase will be amorphous. A critical step to control the crystal particle size distribution is to stabilize the particles using surface-active agents.

2.2.3.1. Solvent antisolvent precipitation

During this bottom-up particle engineering method, nanoparticles and microparticles are formed with the addition of an antisolvent to a drug solution where the solvent and the antisolvent are miscible. The addition of the miscible antisolvent decreases the saturation solubility of the drug in solution and results in supersaturation, which is followed by nucleation and precipitation. Generated particles are crystalline; however, there have been reports for the generation of amorphous particles using solvent-antisolvent precipitation technique. Viçosa et al. generated amorphous rifampicin nanoparticles from a room temperature ionic liquid (RTIL) with a phosphate buffer as antisolvent (Viçosa et al., 2012). RTIL are organic salts, which are liquid at room

temperature. Particle size control is the primary challenge regarding this method as a high concentration of surfactants is required to control it.

2.2.3.2. Evaporative precipitation into aqueous solution (EPAS)

EPAS process allows for the formation of submicron particles coated with hydrophilic stabilizer. During this process, the drug is dissolved in an organic solvent and is atomized into an aqueous solution of hydrophilic stabilizer (Chen et al., 2002). During the atomization step, the organic solvent evaporates, supersaturation is reached, and particle formation ensues. Generated particles using EPAS method have been reported to be amorphous since amorphous phase growth rate exceeds the crystalline phase growth rate, and the hydrophilic stabilizer is thought to prevent crystallization (De Yoreo and Vekilov, 2003).

2.2.3.3. Emulsion templates

Emulsion templates are a group of particle engineering techniques including the emulsion solvent evaporation method, which involves the formation of stable emulsions followed by solvent evaporation. Emulsions may consist of oil-in-water, water-in-oil-in-water, or water-in-oil. The utilized solvent evaporation techniques include: vacuum drying, lyophilization, spray drying, one of the cryogenic technologies and followed by sublimation. The formation of stable emulsions is the key step in particle engineering using this technology. Emulsions are thermodynamically unstable system since they possess a positive free energy of emulsion formation (ΔG) due their large interfacial

energy ($\lambda\Delta A$) in comparison with the entropy of droplet formation (ΔS_i) as it is depicted in Equation 5.

$$\Delta G = \lambda \Delta A - T \Delta S \qquad \text{Equation 5}$$

2.2.3.4. Sonocrystallization

As opposed to passive crystallization technologies, which were previously discussed, sonocrystallization utilizes ultrasound during the crystallization process. Independent of supersaturation level during the crystallization process, ultrasound induces nucleation and decreases induction time, the time elapsed from supersaturation to the formation and detection of crystals (Sander et al., 2014). Ultrasonic shockwaves increase the nucleation rate, and cavitation bubbles increase the number of nucleation sites thereby sonocrystallization yield particles with narrow size distribution in comparison with passive crystallization techniques (Nalajala and Moholkar, 2011).

2.2.4. Supercritical fluid technologies

Supercritical fluid (SCF) is a fluid that was compressed beyond its critical pressure (P_c) or was heated above its critical temperature (T_c). Small changes in pressure lead to significant changes in SCF densities leading to significant variations in diffusivity, viscosity, as well as the solubility of other solvents and small solutes. Furthermore, SCFs' diffusivities are ~100 times greater, and their viscosities are ~100 times lower than that for liquids, and they lead to rapid supersaturation and nucleation and favor the production of small particles. With a relatively low T_c and an average P_c supercritical carbon dioxide (CO_2) is the most prevalent SCF since it is inexpensive,

nonflammable, and nontoxic. Depending on the solubility of API in SCF, different methods have been developed for particle engineering.

2.2.4.1. Gas antisolvent precipitation (GAS)

Gas antisolvent precipitation method is based on a low solubility of API in the SCF, and the miscibility of SCF and the API solvent. Particles are produced through the addition of SCF to a solution of API in the solvent, where the solubility strength of solvent for the API is decreased, and the supersaturation is followed by the nucleation and precipitation (Martin and Cocero, 2008). Formulations of API and excipients are prepared when initially the API and excipients are dissolved in the solvent and SCF is the antisolvent for all components. Key process parameters include pressure and temperature of precipitation chamber, solvent selection, and SCF addition rate (Muhrer et al., 2003). Both crystalline and amorphous particles have been produced utilizing the GAS method (Muller et al., 2000). Particle size distributions with average particle sizes between 200 nm and 10 μm can be fine tuned through adjusting the addition rate of the SCF (Muhrer et al., 2003). There also has been the report of cases where average particle size was independent of SCF addition rate (Fusaro et al., 2004). Muhrer's model shows that where primary nucleation is dominant over secondary nucleation, the SCF addition rate will affect the average particle size. On the other hand, if secondary nucleation is dominant over primary nucleation, average particle size is independent of the SCF addition rate (Muhrer et al., 2002).

2.2.4.2. Precipitation with a compressed antisolvent (PCA)

PCA processes can further be broken down to aerosol solvent extraction system (ASES), solution-enhanced dispersion by supercritical fluids (SEDS), and supercritical antisolvent (SAS). During a PCA process, a solution of formulation in an organic solvent is sprayed in the SCF where the organic solvent is miscible with the SCF and SCF is an antisolvent for the formulation. In comparison with GAS, smaller particles are produced during a PCA process with an increased surface area due to the atomization of the organic solution.

2.2.4.3. Rapid expansion of supercritical solutions (RESS)

In this technology, the SCF serves as the solvent, where the drug and additional stabilizers are dissolved in. The preheated mixture is passed through the saturator and is atomized with a heated nozzle into a collection chamber. The rapid depressurization to the atmospheric pressure induces the vaporization of the SCF causing homogenous supersaturation, nucleation, and precipitation of mono-dispersed drug particulates. The rapid depressurization generates an intense turbulence, which instantaneously creates evenly distributed supersaturation regions. The intense degree of nucleation produced leads to the production of small monodispersed particles (Rowe and Johnston, 2012). The temperatures and pressure of the extraction unit are critical and affect the final particles characteristics.

3. Process considerations and their effects on final product

In this section, a closer look is given to milling and spray-drying and how they may affect the properties of the final product.

3.1. Milling

During milling, the opportunities to control important product characteristics such as size, shape, morphology, surface properties and electrostatic charge are limited. However, milling processes not only reduce the particle size but also affect other properties of the milled material.

3.1.1. Polymorphism

Mechanochemical transformation is one of the concerns during milling where the material can undergoes polymorphic transformation or amorphization (Boldyrev, 2004). Another form of mechanochemical transformation, which does not directly involve amorphization, has been observed for talc during sonofragmentation where milled material release more water at low temperature and the dehydroxylation temperature dropped with further micronization (Pérez-Maqueda et al., 2005). Mechanochemical transformation occurs due to compression or impaction forces and due to elevated temperatures. The key determinants of this process are the milling temperature and glass transition temperature (T_g). The amorphization tendency of the milled material is increased when the milling temperature is below T_g. However, the polymorphic transformation from one polymorph to another is favored when the milling temperature is above T_g for compounds with polymorphs. Both amorphization and polymorphic

transformation can occur when the milling temperature is in the T_g range depending on the milling intensity (Descamps et al., 2007).

This transformation may occur completely as described before, or it may occur to a limited degree. Even though the amorphous content is significantly small, a significant percentage of amorphous content is localized on the surface of the milled material. This transformation can significantly impact particle-particle interactions (Newell et al., 2001; Steckel et al., 2003; Ticehurst et al., 2000), alter flow properties (Feeley et al., 1998; Mackin et al., 2002), and wettability (Rasenack and Müller, 2004). Thus, it can improve the aqueous solubility and dissolution rate as well as compressibility (Yu, 2001).

However, mechanochemical transformation can cause stability concerns during storage through the alteration of particle size distribution and specific surface area (Guinot and Leveiller, 1999). During post-milling storage, the particle size distribution of milled material may shift to the right with "surface re-crystallization" or to the left "stress relaxation" accordingly. The two phenomena may occur at the same time in a competitive manner. Milled particles form agglomerates and surface re-crystallization of amorphous domains on adjacent particles in these agglomerates increase their effective particle size with the formation of interparticulate bridges (Brodka-Pfeiffer et al., 2003). Conversely, stress relaxation in a single crystalline particle can be followed with the introduction of new fractures with the reorientation of molecules in the crystalline structure (Joshi et al., 2002). Conditioning through modulation of storage humidity and temperature can allow

for controlled recrystallization of the amorphous domains on the particle surfaces following powder micronization (Brodka-Pfeiffer et al., 2003).

Thermodynamic modeling has allowed the prediction of mechanochemical transformation for a crystalline compound where key physical properties are known (Wildfong et al., 2006). Moreover, this phenomenon has been reported for many compounds such as piroxicam (Shakhtshneider, 1997), budesonide (Dudognon et al., 2006), naproxen (Kayaert and Van den Mooter, 2012), and indomethacin (Planinšek et al., 2010). More recently, there has been a report of amorphization as well as milling-induced polymorphic transformation during milling process following ball milling and cryomilling. The polymorphic transformation can be direct, or possess a transient amorphization or crystalline intermediate phase. MacFhionnghaile et al. studied the effects of ball-milling and cryomilling on polymorphs of sulfamerazine (SMZ). Cryomilling of SMZ resulted in a complete amorphization; however, balling milling resulted in a mixture of amorphous and crystalline SMZ. Milling time also affects the polymorphism in SMZ in addition to milling temperature. Furthermore, authors reported the spontaneous formation of sulfamerazine/oxalic acid cocrystals upon storage following co-milling and amorphization (Macfhionnghaile et al., 2014).

Co-milling a physical mixture of solids usually yields a solid physical mixture with a smaller PSD; however, this process could yield co-crystals or solid solutions. One of the proposed mechanisms for the formation of co-crystal from two solid phases involves the creation of a high interfacial area between the two, which allows for the

formation of a liquid phase and eventual co-crystal formation from the liquid phase. Further milling allows for the formation of an additional interfacial area to allow for this process to repeat until complete transformation into co-crystals is achieved (Chadwick et al., 2007). Alternatively, if each crystalline phase is expected to undergo amorphization, the co-milled sample will form a solid solution. As it was discussed previously, it is necessary for the milling temperature to be lower than the T_g for the solid solution (Descamps et al., 2007).

3.1.2. Morphology

Milling alters the shape and surface roughness of engineered particles and yields particle, which are rarely isometric or spherical in shape. The significances of these changes become apparent in the development of inhalable dry powder formulations. Effects of morphological changes in drug dissolution, solubility and bioavailability are less known; however, there is evidence that particle shape factors closely correspond with dissolution rates and profiles (Dali and Carstensen, 1996; Fini et al., 1995).

3.1.3. Surface energy

Different processing techniques (e.g. ball milling, air-jet milling, etc.) can induce the formation of amorphous pockets on the surface of API/excipient crystal and can have significant implications on the surface energy of particles (Newell et al., 2001)**.** Surface energy is composed of dispersive and polar components and milling can affect each component to a different degree. Puri et al. showed that the dispersive components of surface energy for crystalline and amorphous celecoxib were approximately equal;

however, amorphous celecoxib had a higher polar component of surface energy in comparison to the crystalline form, which showed no measurable interaction. Furthermore, amorphous CLB absorbed a small amount of water, which is evidence for higher polar surface energy (Puri et al., 2010).

3.2. Spray-drying

3.2.1. Morphology

Morphology of spray-dried particles is heavily dependent on drying conditions and material properties. Maas, et al. investigated the influence of different outlet temperature on the surface roughness of spray-dried mannitol particles and used confocal laser-scanning microscopy to quantify the surface roughness of mannitol particles. Different particle surface roughness was attributed to different crystallization mechanisms (Maas et al., 2011). The dispersion of powder is influenced by the adhesion, cohesion, and gas fluidization properties of the powder and it is related particle geometry which plays a key role in the adhesion force (Mullins et al., 1992). In comparison with air-jet-milled particles, spray-dried particles possess a greater extent of dispersibility due to a smaller contact surface between neighboring particles and a smaller radius of curvature (Weiler et al., 2010). Weiler et al. investigated the effect of particle morphology and corrugation on cohesion forces and aerosol performance of spray-dried powders for inhalation and showed that increasing corrugation improved dispersibility of the spray-dried particles with up to 90% decrease in cohesion for corrugated particles compared with spherical particles (Weiler et al., 2010).

3.2.2. Mechanical strength

Littringer, et al. showed that spray-dried particles of mannitol showed higher breaking strength at higher inlet temperature and lower breaking strength at higher feed rates and attributed it to possible changing of the mechanism of the particle formation thus affecting the internal structure of particles. The prepared spray-dried particles were either the stable polymorph I of mannitol (96.9 %) or a mixture of polymorphs I and II (Littringer et al., 2012).

3.2.3. Polymorphism

Amorphous particles are recovered following spray drying since drying time is about one second or less (Van Oort and Sacchetti, 2007); however, there has been a report of crystalline particles following spray drying. Furthermore, altering processing condition such as inlet temperature (T_{in}) can result in the production of alternative polymorphs. Amorphous versus crystalline character of the powder is dependent on the rate of drying. Fast rate of drying results in the amorphous state of the powder or aggregates of small crystals and slow rate of drying results in particles composed of single crystal (Masuda and Ebooks Corporation, 2006). Matsuda, et al. spray-dried phenylbutazone from solution and obtained three different polymorphs (i.e. α, β, ε) by altering the T_{in} (Matsuda et al., 1984). Alternatively, in the case of griseofulvin, solvate pseudopolymorph of the compound was isolated from the drying chamber (Corrigan, 1995). Alhalaweh, et al. developed pharmaceutical co-crystals of different APIs with glutaric acid, nicotinamide, succinic acid, and oxalic acid via spray drying. Simple spray

drying technique proved to be a viable method for the production of cocrystal and its scale up (Alhalaweh and Velaga, 2010).

4. Material Properties and process selection

As particle-engineering technologies affect the properties of the final product, material's intrinsic characteristics may dictate how a material behaves while undergoing particle engineering. Milling and Spray-drying will be looked at to illustrate this point.

4.1. Milling

A mechanistic model of impact attrition of solids with a semi-brittle failure mode relates the attrition propensity (η), a dimensionless parameter, to material properties and impact conditions (Equation 6) including: the particle density (ρ), the impact velocity (v), the particle size (l), the hardness (H), and the fracture toughness (Kc) (Ghadiri and Zhang, 2002; Zhang and Ghadiri, 2002).

$$\eta = \frac{\rho v^2 l H}{K_c^2} \qquad \text{Equation 6}$$

As evident in Equation 6, specific powder properties such as particle size, particle density, hardness, friability, and fracture toughness affect the milling performance. The decision to choose to mill as a particle size reduction mechanism and specific milling method depends on material characteristics such as material hardness. Mohs scale can be used to categorize the material hardness qualitatively in comparison with reference materials (Fig. 1). Moreover, some compounds cannot be milled since milling can lead to

the loss of crystallinity (compaction sensitivity), melting and crystal form conversion (temperature sensitivity), and may also lead to a change in hydration state.

4.1.1. Crystal lattice

A crystalline lattice structure is made from its smallest repeating unit also known as a unit cell. Real crystals are not perfect and possess defects to different degrees. Point defects are classified as vacancies, substitutional, interstitial, and self-interstitial point defects. Vacancy point defects occur where there is a missing unit cell in the crystal lattice. If unit cells are replaced with a different atom, ion, or molecules from the ones forming the crystal, the defect is called substitutional point defect and is classified as chemical impurities. Additional lattice points made from the same, or different atom, ion, or molecules in the crystalline lattice are classified as self-interstitial, or interstitial point defects (Troy, 2005). Some defects in the crystalline lattice structure affects the milling behavior of the solid. For hard crystals, the breakages are predicted to occur at corners and edges, and the "chipping" result in a significant population of fines can lead to bimodal and multimodal particle size distributions.

4.1.2. Morphology

Particle morphology specifically aspect ratio of particles may affect the milling result. For example, milling needles do not lead to significant specific surface area increase since milling leads to breakages along the length of the particles, which only leads to decreased aspect ratio with preservation of the specific surface area.

4.1.3. Density

Solids' densities have a direct relationship with the number of particle–particle or particle–wall collisions as well as the force of the collisions during milling (Bentham et al., 2004). Particles with higher density undergo more extensive particle size reduction.

4.1.4. Melting point

Material with low melting points can present significant challenges during milling. Mechanical milling methods with moving parts are capable of reaching temperatures between 40 – 60 °C (Fisher, 2013). Furthermore, they are usually associated with a lower hardness. Therefore, it will be harder to milling in comparison with material with higher melting point.

4.1.5. Molecular weight

The molecular weight of polymers may influence whether the polymer may be milled without undergoing physical and chemical changes. It is predicted that polymers with larger molecular weights are more susceptible to this types of changes (Gabriel et al., 2010).

4.2. Spray-drying

4.2.1. Formulation

Intrinsic properties of liquid-feed include viscosity, surface tension, and density. Santa-Maria, et al. spray-dried alginate solutions with and without the presence of calcium, as cross-linker, and observed that higher spray solution viscosity resulted in bigger particle sizes. Furthermore, the addition of a surface active agent such as bovine

serum albumin (BSA) addition to the formulation led to smaller particle sizes after spray drying (Santa-Maria et al., 2012, p. -). Furthermore, hollow particles have a lower density in comparison to solid particles and will have smaller aerodynamic diameter compared to their solid counterpart. Fig. 3 depicts a patented example of these particles developed by Nektar Therapeutics. In PulmoSphere® technology, spray-dried particles of drug particles are created by spray-drying an emulsion of perfluorocarbons, water, along with the drug. The sudden removal of low boiling point fluorocarbon causes the perforation of the particles (Miller and Gil, 2012). These particles are low-density and porous with geometric diameters of 3-5 μm; however, their aerodynamic particle size is, and they possess excellent dispersibility compared with carrier-less micronized formulations allowing for high dose delivery of inhalation formulations due to decreased contact and presence of rough surfaces on the particles and they are depicted in Fig. 3 (Dellamary et al., 2000). Corrugation, also known as surface roughness, is attributed to higher dispersibility of spray-dried powders for inhalation is attributed to lower particle cohesion and a reduced total accessible area for adhesion. Weiler et. al. produced spray-dried particles with different morphology and surface corrugation (Weiler et al., 2010).

4.2.2. Melting point

Drug melting point is a key parameter, which dictates whether a material can be spray-dried, or not. Drugs with low melting point may not be processed using spray drying where the outlet temperature of the spray drying processing is greater than the drug's melting point.

4.2.3. Glass transition temperature

Furthermore, it is not advised to conduct spray drying above the glass transition temperature (Tg) for a solid. Doing so may yield solid-like glasses or highly supercooled, viscous liquids. As a plasticizer, moisture content significantly alters the T_g thus altering the processability of the solid (Roos, 2002).

5. Conclusion:

Particle engineering techniques allow for top-down and bottom-up processing of pharmaceutical solids. Additionally, final product's attributes may be affected by the processing technique. Additionally, material's intrinsic properties may limit the feasibility of the utilization of a particular technique.

6. References:

Alhalaweh, A., Velaga, S.P., 2010. Formation of Cocrystals from Stoichiometric Solutions of Incongruently Saturating Systems by Spray Drying. Cryst. Growth Des. 10, 3302–3305. doi:10.1021/cg100451q

Am Ende, D.J., Brenek, S.J., 2004. Strategies to control particle size during crystallization processes. Am Pharm Rev 7, 98–104.

Amidon, G.L., Lennernäs, H., Shah, V.P., Crison, J.R., 1995. A Theoretical Basis for a Biopharmaceutic Drug Classification: The Correlation of in Vitro Drug Product Dissolution and in Vivo Bioavailability. Pharm. Res. 12, 413–420. doi:10.1023/A:1016212804288

Beinborn, N.A., Lirola, H.L., Williams III, R.O., 2012. Effect of process variables on morphology and aerodynamic properties of voriconazole formulations produced by thin film freezing. Int. J. Pharm. 429, 46–57. doi:10.1016/j.ijpharm.2012.03.010

Benson, S.W., Ellis, D.A., 1948. Surface Areas of Proteins. I. Surface Areas and Heats of Absorption1. J. Am. Chem. Soc. 70, 3563–3569.

Bentham, A.C., Kwan, C.C., Boerefijn, R., Ghadiri, M., 2004. Fluidised-bed jet milling of pharmaceutical powders. Powder Technol., Pharmaceutical Particle Formation 141, 233–238. doi:10.1016/j.powtec.2004.01.024

Boldyrev, V.V., 2004. Mechanochemical modification and synthesis of drugs. J. Mater. Sci. 39, 5117–5120. doi:10.1023/B:JMSC.0000039193.69784.1d

Brodka-Pfeiffer, K., Häusler, H., Grass, P., Langguth, P., 2003. Conditioning following powder micronization: influence on particle growth of salbutamol sulfate. Drug Dev. Ind. Pharm. 29, 1077–1084. doi:10.1081/DDC-120025865

Chadwick, K., Davey, R., Cross, W., 2007. How does grinding produce co-crystals? Insights from the case of benzophenone and diphenylamine. CrystEngComm 9, 732–734. doi:10.1039/B709411F

Chen, X., Young, T.J., Sarkari, M., Williams III, R.O., Johnston, K.P., 2002. Preparation of cyclosporine A nanoparticles by evaporative precipitation into aqueous solution. Int. J. Pharm. 242, 3–14. doi:10.1016/S0378-5173(02)00147-3

Clement, S., Purutyan, H., 2002. Narrowing down equipment choices for particle-size reduction. Chem. Eng. Prog. 98, 50–54.

Corrigan, O.I., 1995. Thermal analysis of spray dried products. Thermochim. Acta, Pharmaceuticals and Thermal Analysis 248, 245–258. doi:10.1016/0040-6031(94)01891-J

Dali, M.V., Carstensen, J.T., 1996. Effect of change in shape factor of a single crystal on its dissolution behavior. Pharm. Res. 13, 155–162. doi:10.1023/A:1016010207729

Dellamary, L.A., Tarara, T.E., Smith, D.J., Woelk, C.H., Adractas, A., Costello, M.L., Gill, H., Weers, J.G., 2000. Hollow Porous Particles in Metered Dose Inhalers. Pharm. Res. 17, 168–174. doi:10.1023/A:1007513213292

Descamps, M., Willart, J.F., Dudognon, E., Caron, V., 2007. Transformation of pharmaceutical compounds upon milling and comilling: The role of T-g. J. Pharm. Sci. 96, 1398–1407. doi:10.1002/jps.20939

De Yoreo, J.J., Vekilov, P.G., 2003. Principles of crystal nucleation and growth. Rev. Mineral. Geochem. 54, 57–93.

Dokoumetzidis, A., Macheras, P., 2006. A century of dissolution research: From Noyes and Whitney to the Biopharmaceutics Classification System. Int. J. Pharm. 321, 1–11. doi:10.1016/j.ijpharm.2006.07.011

Drying, Y. improvement I., 1872. Improvement in drying and concentrating liquid substances by atomizing. US125406 A.

Dudognon, E., Willart, J.F., Caron, V., Capet, F., Larsson, T., Descamps, M., 2006. Formation of budesonide/alpha-lactose glass solutions by ball-milling. Solid State Commun. 138, 68–71. doi:10.1016/j.ssc.2006.02.007

Engstrom, J.D., Lai, E.S., Ludher, B.S., Chen, B., Milner, T.E., Williams, R.O., Kitto, G.B., Johnston, K.P., 2008. Formation of Stable Submicron Protein Particles by Thin Film Freezing. Pharm. Res. 25, 1334–1346. doi:10.1007/s11095-008-9540-4

Feeley, J.C., York, P., Sumby, B.S., Dicks, H., 1998. Determination of surface properties and flow characteristics of salbutamol sulphate, before and after micronisation. Int. J. Pharm. 172, 89–96. doi:10.1016/S0378-5173(98)00179-3

Fini, A., Fazio, G., Fernandezhervas, M., Holgado, M., Rabasco, A., 1995. Influence of Crystallization Solvent and Dissolution Behavior for a Diclofenac Salt. Int. J. Pharm. 121, 19–26. doi:10.1016/0378-5173(94)00419-6

Fisher, E.S., 2013. Milling of Active Pharmaceutical Ingredients, in: Encyclopedia of Pharmaceutical Technology, Third Edition. Taylor & Francis, pp. 2339–2351.

Friedrich, A.J., 2001. Size reduction overview : Shear, compression, and impact. Powder Bulk Eng. 15, 19–25.

Frijlink, H.W., de Boer, A.H., 2005. Trends in the technology-driven development of new inhalation devices. Drug Discov. Today Technol. 2, 47–57. doi:10.1016/j.ddtec.2005.05.020

Fusaro, F., Mazzotti, M., Muhrer, G., 2004. Gas Antisolvent Recrystallization of Paracetamol from Acetone Using Compressed Carbon Dioxide as Antisolvent. Cryst. Growth Des. 4, 881–889. doi:10.1021/cg034172u

Gabriel, M.C., Mendes, L.B., Carvalho, B.D.M., Pinheiro, L.A., Capocchi, J.D.T., Kubaski, E.T., Cintho, O.M., 2010. High-Energy Mechanical Milling of Ultra-High Molecular Weight Polyethylene (UHMWPE). Mater. Sci. Forum 660-661, 325–328. doi:10.4028/www.scientific.net/MSF.660-661.325

Ghadiri, M., Zhang, Z., 2002. Impact attrition of particulate solids. Part 1: A theoretical model of chipping. Chem. Eng. Sci. 57, 3659–3669. doi:10.1016/S0009-2509(02)00240-3

Guinot, S., Leveiller, F., 1999. The use of MTDSC to assess the amorphous phase content of a micronised drug substance. Int. J. Pharm. 192, 63–75. doi:10.1016/S0378-5173(99)00273-2

Hinds, W.C., 2012. Aerosol Technology : Properties, Behavior, and Measurement of Airborne Particles, 2nd ed. Wiley, Hoboken.

Hu, J., Johnston, K.P., Williams, R.O., 2004a. Stable amorphous danazol nanostructured powders with rapid dissolution rates produced by spray freezing into liquid. Drug Dev. Ind. Pharm. 30, 695–704. doi:10.1081/DDC-120039212

Hu, J., Johnston, K.P., Williams, R.O., 2004b. Rapid dissolving high potency danazol powders produced by spray freezing into liquid process. Int. J. Pharm. 271, 145–154.

John S., P., 1996. Mechanisms of macromolecule absorption by the lungs. Adv. Drug Deliv. Rev. 19, 3–36. doi:10.1016/0169-409X(95)00113-L

Joshi, V., Dwivedi, S., Ward, G.H., 2002. Increase in the specific surface area of budesonide during storage postmicronization. Pharm. Res. 19, 7–12. doi:10.1023/A:1013690929173

Kayaert, P., Van den Mooter, G., 2012. Is the amorphous fraction of a dried nanosuspension caused by milling or by drying? A case study with Naproxen and Cinnarizine. Eur. J. Pharm. Biopharm. 81, 650–656. doi:10.1016/j.ejpb.2012.04.020

Kulshreshtha, A.K., Singh, O.N., Wall, G.M., 2009. Pharmaceutical Suspensions: From Formulation Development to Manufacturing. Springer Science & Business Media.

Labiris, N.R., Dolovich, M.B., 2003. Pulmonary drug delivery. Part I: Physiological factors affecting therapeutic effectiveness of aerosolized medications. Br. J. Clin. Pharmacol. 56, 588–599. doi:10.1046/j.1365-2125.2003.01892.x

Littringer, E.M., Mescher, A., Eckhard, S., Schröttner, H., Langes, C., Fries, M., Griesser, U., Walzel, P., Urbanetz, N.A., 2012. Spray drying of mannitol as a drug carrier—the impact of process parameters on product properties. Dry. Technol. 30, 114–124.

Maas, S.G., Schaldach, G., Littringer, E.M., Mescher, A., Griesser, U.J., Braun, D.E., Walzel, P.E., Urbanetz, N.A., 2011. The impact of spray drying outlet temperature on the particle morphology of mannitol. Powder Technol. 213, 27–35. doi:10.1016/j.powtec.2011.06.024

Macfhionnghaile, P., Hu, Y., Gniado, K., Curran, S., Mcardle, P., Erxleben, A., 2014. Effects of Ball-Milling and Cryomilling on Sulfamerazine Polymorphs: A Quantitative Study. J. Pharm. Sci. 103, 1766–1778. doi:10.1002/jps.23978

Mackin, L., Zanon, R., Park, J., Foster, K., Opalenik, H., Demonte, M., 2002. Quantification of low levels (< 10%) of amorphous content in micronised active batches using dynamic vapour sorption and isothermal microcalorimetry. Int. J. Pharm. 231, 227–236.

Martin, A., Cocero, M.J., 2008. Micronization processes with supercritical fluids: Fundamentals and mechanisms. Adv. Drug Deliv. Rev. 60, 339–350. doi:10.1016/j.addr.2007.06.019

Masuda, H., Ebooks Corporation, 2006. Powder Technology Handbook. CRC Press, Hoboken.

Matsuda, Y., Kawaguchi, S., Kobayashi, H., Nishijo, J., 1984. Physicochemical characterization of spray-dried phenylbutazone polymorphs. J. Pharm. Sci. 73, 173–179. doi:10.1002/jps.2600730209

Miller, D.A., Gil, M., 2012. Spray-Drying Technology, in: III, R.O.W., Watts, A.B., Miller, D.A. (Eds.), Formulating Poorly Water Soluble Drugs, AAPS Advances in the Pharmaceutical Sciences Series. Springer New York, pp. 363–442.

Muhrer, G., Lin, C., Mazzotti, M., 2002. Modeling the gas antisolvent recrystallization process. Ind. Eng. Chem. Res. 41, 3566–3579. doi:10.1021/ie020070+

Muhrer, G., Mazzotti, M., Muller, M., 2003. Gas antisolvent recrystallization of an organic compound. Tailoring product PSD and scaling-up. J. Supercrit. Fluids 27, 195–203. doi:10.1016/S0896-8446(02)00237-1

Mujumdar, A.S., 2006. Handbook of Industrial Drying, Third Edition. CRC Press.

Muller, M., Meier, U., Kessler, A., Mazzotti, M., 2000. Experimental study of the effect of process parameters in the recrystallization of an organic compound using compressed carbon dioxide as antisolvent. Ind. Eng. Chem. Res. 39, 2260–2268. doi:10.1021/ie990828y

Muller, R.H., Becker, R., Kruss, B., Peters, K., 1999. Pharmaceutical nanosuspensions for medicament administration as systems with increased saturation solubility and rate of solution. US5858410 A.

Mullin, J.W., 2001. Crystallization. Butterworth-Heinemann.

Mullins, M.E., Michaels, L.P., Menon, V., Locke, B., Ranade, M.B., 1992. Effect of geometry on particle adhesion. Aerosol Sci. Technol. 17, 105–118.

Mumenthaler, M., Leuenberger, H., 1991. Atmospheric spray-freeze drying: a suitable alternative in freeze-drying technology. Int. J. Pharm. 72, 97–110.

Nakach, M., Authelin, J.R., Chamayou, A., Dodds, J., 2004. Comparison of various milling technologies for grinding pharmaceutical powders. Int. J. Miner. Process. 74, S173–S181. doi:10.1016/j.minpro.2004.07.039

Nalajala, V.S., Moholkar, V.S., 2011. Investigations in the physical mechanism of sonocrystallization. Ultrason. Sonochem. 18, 345–355. doi:10.1016/j.ultsonch.2010.06.016

Newell, H.E., Buckton, G., Butler, D.A., Thielmann, F., Williams, D.R., 2001. The Use of Inverse Phase Gas Chromatography to Measure the Surface Energy of Crystalline, Amorphous, and Recently Milled Lactose. Pharm. Res. 18, 662–666. doi:10.1023/A:1011089511959

Newman, S.P., Chan, H.-K., 2008. In Vitro/In Vivo Comparisons in Pulmonary Drug Delivery. J. Aerosol Med. Pulm. Drug Deliv. 21, 77–84. doi:10.1089/jamp.2007.0643

Olsson, B., Bondesson, E., Borgström, L., Edsbäcker, S., Eirefelt, S., Ekelund, K., Gustavsson, L., Hegelund-Myrbäck, T., 2011. Pulmonary drug metabolism, clearance, and absorption, in: Smyth, H.D., Hickey, A.J. (Eds.), Controlled Pulmonary Drug Delivery. Springer, pp. 21–50.

Overhoff, K.A., Engstrom, J.D., Chen, B., Scherzer, B.D., Milner, T.E., Johnston, K.P., Williams III, R.O., 2007. Novel ultra-rapid freezing particle engineering process for enhancement of dissolution rates of poorly water-soluble drugs. Eur. J. Pharm. Biopharm. 65, 57–67. doi:10.1016/j.ejpb.2006.07.012

Patton, J.S., Fishburn, C.S., Weers, J.G., 2004. The lungs as a portal of entry for systemic drug delivery. Proc. Am. Thorac. Soc. 1, 338–44. doi:10.1513/pats.200409-049TA

Patton, J.S., Platz, R.M., 1992. (D) Routes of delivery: Case studies: (2) Pulmonary delivery of peptides and proteins for systemic action. Adv. Drug Deliv. Rev., Routes of Drug Delivery: Case studies 8, 179–196. doi:10.1016/0169-409X(92)90002-8

Pérez-Maqueda, L.A., Duran, A., Pérez-Rodríguez, J.L., 2005. Preparation of submicron talc particles by sonication. Appl. Clay Sci., EUROCLAY 2003 28, 245–255. doi:10.1016/j.clay.2004.01.012

Planinšek, O., Zadnik, J., Kunaver, M., Srčič, S., Godec, A., 2010. Structural evolution of indomethacin particles upon milling: Time-resolved quantification and

localization of disordered structure studied by IGC and DSC. J. Pharm. Sci. 99, 1968–1981. doi:10.1002/jps.21986

Puri, V., Dantuluri, A.K., Kumar, M., Karar, N., Bansal, A.K., 2010. Wettability and surface chemistry of crystalline and amorphous forms of a poorly water soluble drug. Eur. J. Pharm. Sci. 40, 84–93. doi:10.1016/j.ejps.2010.03.003

Rasenack, N., Müller, B.W., 2004. Micron-Size Drug Particles: Common and Novel Micronization Techniques. Pharm. Dev. Technol. 9, 1–13. doi:10.1081/PDT-120027417

Roos, Y.H., 2002. Importance of glass transition and water activity to spray drying and stability of dairy powders. Le Lait 82, 10. doi:10.1051/lait:2002025

Rowe, J.M., Johnston, K.P., 2012. Precipitation Technologies for Nanoparticle Production, in: III, R.O.W., Watts, A.B., Miller, D.A. (Eds.), Formulating Poorly Water Soluble Drugs, AAPS Advances in the Pharmaceutical Sciences Series. Springer New York, pp. 501–568.

Sander, J.R.G., Zeiger, B.W., Suslick, K.S., 2014. Sonocrystallization and sonofragmentation. Ultrason. Sonochem. 21, 1908–1915. doi:10.1016/j.ultsonch.2014.02.005

Santa-Maria, M., Scher, H., Jeoh, T., 2012. Microencapsulation of bioactives in cross-linked alginate matrices by spray drying. J. Microencapsul. 29, 286–295. doi:10.3109/02652048.2011.651494

Shakhtshneider, T.P., 1997. Phase transformations and stabilization of metastable states of molecular crystals under mechanical activation. Solid State Ion., International Symposium on the Reactivity of Solids 101–103, Part 2, 851–856. doi:10.1016/S0167-2738(97)00224-5

Sharma, P., Denny, W.A., Garg, S., 2009. Effect of wet milling process on the solid state of indomethacin and simvastatin. Int. J. Pharm. 380, 40–48. doi:10.1016/j.ijpharm.2009.06.029

Shegokar, R., Mueller, R.H., 2010. Nanocrystals: Industrially feasible multifunctional formulation technology for poorly soluble actives. Int. J. Pharm. 399, 129–139. doi:10.1016/j.ijpharm.2010.07.044

Simonell.ap, Mehta, S., Higuchi, W., 1970. Inhibition of Sulfathiazole Crystal Growth by Polyvinylpyrrolidone. J. Pharm. Sci. 59, 633–&. doi:10.1002/jps.2600590512

Steckel, H., Rasenack, N., Villax, P., Müller, B.W., 2003. In vitro characterization of jet-milled and in-situ-micronized fluticasone-17-propionate. Int. J. Pharm. 258, 65–75. doi:10.1016/S0378-5173(03)00153-4

Strydom, S.J., Rose, W.E., Otto, D.P., Liebenberg, W., de Villiers, M.M., 2013. Poly(amidoamine) dendrimer-mediated synthesis and stabilization of silver sulfonamide nanoparticles with increased antibacterial activity. Nanomedicine Nanotechnol. Biol. Med. 9, 85–93. doi:10.1016/j.nano.2012.03.006

Suslick, K., 1989. The Chemical Effects of Ultrasound. Sci. Am. 260, 80–86.

Suslick, K.S., 1990. Sonochemistry. Science 247, 1439–1445. doi:10.1126/science.247.4949.1439

Takagi, T., Ramachandran, C., Bermejo, M., Yamashita, S., Yu, L.X., Amidon, G.L., 2006. A Provisional Biopharmaceutical Classification of the Top 200 Oral Drug Products in the United States, Great Britain, Spain, and Japan. Mol. Pharm. 3, 631–643. doi:10.1021/mp0600182

Telko, M.J., Hickey, A.J., 2005. Dry Powder Inhaler Formulation. Respir. Care 50, 1209–1227.

Ticehurst, M.D., Basford, P.A., Dallman, C.I., Lukas, T.M., Marshall, P.V., Nichols, G., Smith, D., 2000. Characterisation of the influence of micronisation on the crystallinity and physical stability of revatropate hydrobromide. Int. J. Pharm. 193, 247–259.

Troy, D.B., 2005. Remington: The science and practice of pharmacy. Lippincott, Williams & Wilkins, Philadelphia, PA.

Van Oort, M.M., Sacchetti, M., 2007. Spray-drying and supercritical fluid particle generation techniques. LUNG Biol. Health Dis. 221, 307.

Viçosa, A., Letourneau, J.-J., Espitalier, F., Inês Ré, M., 2012. An innovative antisolvent precipitation process as a promising technique to prepare ultrafine rifampicin particles. J. Cryst. Growth, 6th National Congress on Industrial Crystallization (CRISTAL-6) 342, 80–87. doi:10.1016/j.jcrysgro.2011.09.012

Weiler, C., Egen, M., Trunk, M., Langguth, P., 2010. Force control and powder dispersibility of spray dried particles for inhalation. J. Pharm. Sci. 99, 303–316. doi:10.1002/jps.21849

Wildfong, P.L.D., Hancock, B.C., Moore, M.D., Morris, K.R., 2006. Towards an understanding of the structurally based potential for mechanically activated disordering of small molecule organic crystals. J. Pharm. Sci. 95, 2645–2656. doi:10.1002/jps.20672

Williams, R.O., Johnston, K.P., Young, T.J., Rogers, T.L., Barron, M.K., Yu, Z., Hu, J., 2005. Process for production of nanoparticles and microparticles by spray freezing into liquid. US6862890 B2.

Witkin, D.B., Lavernia, E.J., 2006. Synthesis and mechanical behavior of nanostructured materials via cryomilling. Prog. Mater. Sci. 51, 1–60. doi:10.1016/j.pmatsci.2005.04.004

Xu, Z., Hickey, A.J., 2011. The physics of aerosol droplet and particle generation from inhalers, in: Smyth, H.D., Hickey, A.J. (Eds.), Controlled Pulmonary Drug Delivery. Springer, pp. 75–100.

Yang, W., Iii, D.E.O., Iii, R.O.W., 2012. Pharmaceutical Cryogenic Technologies, in: III, R.O.W., Watts, A.B., Miller, D.A. (Eds.), Formulating Poorly Water Soluble Drugs, AAPS Advances in the Pharmaceutical Sciences Series. Springer New York, pp. 443–500.

Yu, L., 2001. Amorphous pharmaceutical solids: preparation, characterization and stabilization. Adv. DRUG Deliv. Rev. 48, 27–42.

Yu, Z., Johnston, K.P., Williams III, R.O., 2006. Spray freezing into liquid versus spray-freeze drying: Influence of atomization on protein aggregation and biological activity. Eur. J. Pharm. Sci. 27, 9–18. doi:10.1016/j.ejps.2005.08.010

Zeiger, B.W., Suslick, K.S., 2011. Sonofragmentation of Molecular Crystals. J. Am. Chem. Soc. 133, 14530–14533. doi:10.1021/ja205867f

Zhang, Z., Ghadiri, M., 2002. Impact attrition of particulate solids. Part 2: Experimental work. Chem. Eng. Sci. 57, 3671–3686. doi:10.1016/S0009-2509(02)00241-5

Zheng, J., 2009. Formulation and Analytical Development for Low-Dose Oral Drug Products. John Wiley & Sons.

Zijlstra, G.S., Rijkeboer, M., Van Drooge, D.J., Sutter, M., Jiskoot, W., Van De Weert, M., Hinrichs, W.L., Frijlink, H.W., 2007. Characterization of a cyclosporine solid dispersion for inhalation. AAPS J. 9, E190–E199.

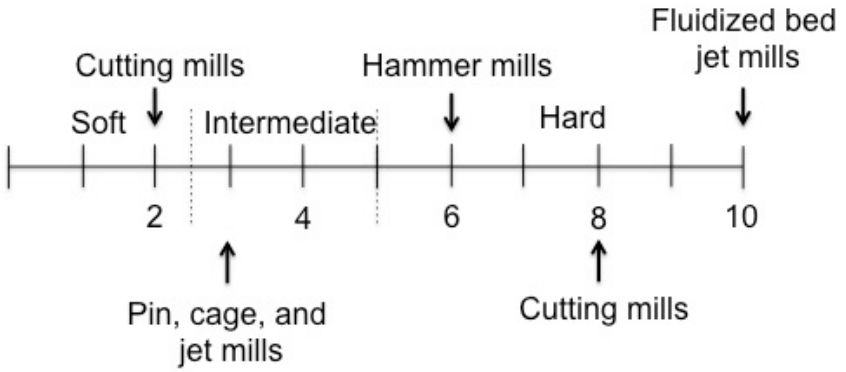

Figure 1.1: The upper limit of material hardness on Mohs hardness scale that different types of dry milling equipment can process

Table 1.1: Approximate particle size obtainable by various milling techniques. Adapted from (Zheng, 2009), with permission of John Wiley & Sons Inc.

	Size (μm)	Hammer mill	Universal and pin mill	Jet mill	Jet mill with internal classifier	Media mill	Toothed rotor-stator	Colloid mill
Type	-	Dry	Dry	Dry	Dry	Wet	Wet	Wet
Very fine	50 - 150	X	X		X		X	
Super fine	10 - 50	X	X	X	X	X	X	X
Ultra fine	< 10		X	X	X	X		X
Colloidal	< 1				X	X		X

CHAPTER II

RESEARCH OBJECTIVES

1. Overall objective

Ibuprofen (IBU) is a non-steroidal anti-inflammatory agent (NSAID) is generally administered orally as tablets and suspensions. It is indicated for pain, fever, and other inflammatory conditions. More recently, a slower rate of respiratory decline is shown in cystic fibrosis (CF) patients on high, oral doses of IBU in comparison to placebo. The use of this treatment modality has not been well adopted or widespread due to high doses, side effects, contraindications, and black box warnings regarding the use of IBU.

Pulmonary delivery may be an attractive alternative to high-dose oral administration in CF since lungs are the desired targets for the anti-inflammatory and antibiotic activities of IBU. Typically with inhaled powders, a binary formulation of a drug with a carrier, such as lactose, significantly improves their performance; however, this strategy is not practical for the delivery of a large drug dose via a dry powder inhaler (DPI). Other inhalation devices such as nebulizers require significantly more time for drug delivery, and metered dose inhalers may be incapable of metering sufficiently large drug doses. Therefore, carrier-free DPIs have been explored for large drug dose delivery.

IBU exists as the stable polymorph I (in its acicular crystal habit), or as the less stable polymorph II. Low melting point (75.85°C), water solubility, and crystal habit of ibuprofen makes its processing challenging. For instance, spray drying could not be used to produce the carrier-free ibuprofen DPI formulation as the smallest particle size

produced using a design of experiment approach with the smallest particle size (D_{50}) between 10 and 20 μm. The overall objective of this dissertation was to develop a carrier-free DPI formulation of IBU with an acceptable flowability and in-vitro aerodynamic performance determined by Next Generation Impactor.

2. Supportive objective

Indomethacin and diclofenac could serve as alternatives to ibuprofen for the development of carrier-free DPI formulation. Supportive objective of this dissertation was to evaluate the feasibility of for the development of carrier-free DPI formulation. Additionally, the stability of the ibuprofen formulation was assessed over the course of 6 month.

CHAPTER III*

Implementation of Design of Experiments Approach for the Micronization of a Drug with a High Brittle-Ductile Transition Particle Diameter

Authors:

Ashkan K. Yazdi[a], Hugh D.C. Smyth[a]

[a] Division of Pharmaceutics, College of Pharmacy, The University of Texas at Austin, PHR 4.214, 2409 University Ave, A1920, Austin TX 78712-1119, USA

Corresponding Author:

Ashkan K. Yazdi

Office: 512 471 4752

Fax: 512 471 7474

Email: ashkan.k.yazdi@utexas.edu

Keywords:

Air-jet milling, Pushing nozzle pressure, Grinding nozzle pressure, Response, Factor

* This chapter has been submitted to the Drug Development and Industrial Pharmacy journal and is in revision. A Yazdi, and H Smyth. "Implementation of Design of Experiments Approach for the Micronization of a Drug with a High Brittle-Ductile Transition Particle Diameter." Drug Development and Industrial Pharmacy.

Abstract

***Objective*:** To optimize air-jet milling conditions of ibuprofen (IBU) using design of experiment (DoE) method, and to test the generalizability of the optimized conditions for the processing of another non-steroidal anti-inflammatory drug (NSAID).

***Methods*:** Bulk IBU was micronized using an Aljet mill according to a circumscribed central composite (CCC) design with grinding and pushing nozzle pressures (GrindP, PushP) varying from 20 to 110 psi. Output variables included yield and particle diameters at the 50^{th} and 90^{th} percentile (D_{50}, D_{90}). Following data analysis, the optimized conditions were identified and tested to produce IBU particles with a minimum size and an acceptable yield. Finally, indomethacin (IND) was milled using the optimized conditions as well as the control.

***Results*:** CCC design included eight successful runs for milling IBU from the ten total runs due to powder "blowback" from the feed hopper. DoE analysis allowed the optimization of the GrindP and PushP at 75 and 65 psi. In subsequent validation experiments using the optimized conditions, the experimental D_{50} and D_{90} values (1.9 and 3.6 μm) corresponded closely with the DoE modeling predicted values. Additionally, the optimized conditions were superior over the control conditions for the micronization of IND where smaller D_{50} and D_{90} values (1.2 and 2.7 μm vs. 1.8 and 4.4 μm) were produced.

***Conclusion*:** The optimization of a single-step air-jet milling of IBU using the DoE approach elucidated the optimal milling conditions, which were used to micronize IND using the optimized milling conditions.

1 Introduction

Successful deep lung deposition for dry powder inhaler (DPI) formulations, is strongly correlated to the percentage of particles with an aerodynamic diameter (D_{ae}) less than 3 μm (Newman and Chan, 2008). As depicted in Equation 1, for spherical, solid particles, the aerodynamic diameter is equal to the geometric diameter (D_{eq}) where particle density (ρ_p) is equal to unit density (ρ_o) and the dynamic shape factor (χ) is equal to one (Telko and Hickey, 2005).

$$D_{ae} = D_{eq}\sqrt{\frac{\rho_p}{\rho_o \chi}} \qquad \textit{(Equation 1)}$$

Microparticles with geometric diameters less than 3 μm can be produced via top-down approaches, such as an air-jet mill, as well as bottom-up approaches, such as a controlled crystallization method (Merisko-Liversidge and Liversidge, 2011; Rasenack et al., 2003). Top-down approaches include: mechanical mills where the milling energy is imparted directly, fluid energy mills where the milling energy is imparted indirectly, and high-pressure homogenizers where the milling energy is imparted both directly and indirectly (Moribe et al., 2013; Naik and Chaudhuri, 2015). An air-jet mill is an example of a fluid energy mill and is composed of a milling chamber where the powder is fed in through a hopper via a pushing nozzle, and particle collisions and fractures are caused by the introduction of one or more milling nozzles (Muller et al., 1996).

Fracture inducing mechanisms can be classified as impaction, compression, or attrition (Naik and Chaudhuri, 2015). During impaction and compression, the fracture

inducing force is applied normal to the surface, leading to the formation of two or more fragments; however, it is applied parallel to the surface during attrition, and it results in the production of extremely fine particles (Parrott, 1974). As opposed to the mechanical mills where impaction, compression, and attrition are all responsible for milling, in an air-jet mill only attrition is responsible for milling.

The extent of milling for a material is dependent on its mechanical properties, initial particle size distribution (PSD) and the milling conditions (Saleem and Smyth, 2010; Vatsaraj et al., 2003). If material experiences plastic deformation before fracture, it is classified as ductile; otherwise, it is classified as brittle. Brittle fracture is a function of temperature, strain rate, stress state, and particle size (Larsson and Kristensen, 2000). The brittle-ductile transition occurs at the critical particle diameter, below which particles undergo a ductile fracture as opposed to a brittle fracture during milling, with an increased energy requirement (Kendall, 1978). The critical diameter characterizing the brittle-ductile transition for ibuprofen (IBU) is reported as 854 μm (Leuenberger, 1982) and more recently between 125 – 355 μm (Larsson and Kristensen, 2000), which makes milling IBU more difficult than other solids with smaller brittle-ductile transition critical diameters (Roberts and Rowe, 1987).

IBU, 2(4-isobutylphenyl)propanoic acid, has a molecular weight (MW) of 206.29 g/mol and is commercially available as a racemic mixture of S(+)-IBU (pharmacologically active) and R(-)-IBU (pharmacologically inactive) (Neupert et al., 1997). IBU exists either as the stable polymorph I with a melting point (MP) of 75.85°C,

or as the less stable polymorph II, with a lower MP of 16.85°C (Dudognon et al., 2008). Previously, micronized IBU has been produced, and companies such as BASF have reported the minimum particle diameters at the 10^{th}, 50^{th}, and 90^{th} percentile (D_{10}, D_{50}, and D_{90}) at around 10, 25, 65 μm respectively (BASF Group, n.d.). Furthermore, Shariare et al. reported air-jet milling of a < 40 μm sieve fraction to a D_{10}, D_{50}, and D_{90} of 0.75, 2.25, and 4.10 μm respectively where the starting particles were needle-shaped with a high degree of crystalline imperfection (Shariare et al., 2012). Even though these materials may eventually be suitable for inhalation, multiple steps of crystallization, drying, sieving, and micronization were required to reach this PSD profile. In addition, the poor flowability of raw materials due to shape and their physical instability due to crystalline imperfections may not enable industrialization of such an approach. Alternatively, the optimization of milling such that appropriate particle sizes can be obtained using a single milling step is highly desirable and can be more easily commercialized.

In this research, we investigated the micronization of a bulk pharmaceutical grade of IBU via air-jet milling, by the application of a design of experiments (DoE) statistical method of optimization, and we increased batch sizes to evaluate its effect on the particle size distribution (PSD). Furthermore, we applied the optimized conditions for the micronization of indomethacin (IND), another non-steroidal anti-inflammatory drug with different physicochemical properties. Our research hypothesis was that the optimized

conditions for the air-jet milling of IBU, a physically difficult material to micronize, could be used to mill IND with different physical and mechanical properties.

2 Methods

IBU, USP, was purchased from Letco Medical (Decatur, Alabama). IND (pharmaceutical grade, Parafarm, Saporiti, Buenos Aires, Argentina) was a generous donation from collaborators in Argentina. Scintillation vials (Wheaton, Millville, NJ) were used for the collection and the storage of the micronized powder. Tween 20, Sodium Lauryl Sulfate (SLS), and hydrochloric acid (HCl) were purchased from Fisher Scientific (Pittsburgh, PA). House deionized water was used for the preparation of suspensions. For scanning electron microscopy (SEM) imaging, standard aluminum stubs were purchased from Electron Microscopy Sciences (Hatfield, PA).

2.1 Air-jet milling

A Model 00 Jet-O-Mizer™ (also known as Aljet mill, Fluid Energy, Telford, PA) was configured according to Figure 3.1, and it was used to micronize IBU and IND. For milling IBU, the milling conditions were varied between 20 and 110 psi for the pushing and grinding nozzle pressures (Vatsaraj et al., 2003). Throughout the DoE runs, the feed rate of 1 g/min and the batch size of 5 g were used. The milled powder samples were collected from the different segments of the jet mill in a desiccator under vacuum. The samples were from the segments illustrated in Figure 3.1: the tube after grinding chamber (bfC), the cyclone (C), the collection vessel adapter (D), the collection bag adapter (E), the collection vessel (G), and the collection bag (H). Following the powder collection, the

yield percentage for each segment as well as the overall yield was calculated according to the Equation 2 where m_R is the recovered mass from the respective segment or the overall recovered mass and m is the total processed mass:

$$Yield = \frac{m_R}{m} \times 100 \qquad \textit{(Equation 2)}$$

The DoE analysis results were used to predict the milling conditions allowing the maximum particle size reduction. For the scale-up experiments and testing the DoE predictions, the milling runs were conducted on IBU batch sizes of 5, 10, and 20 g using the optimized conditions from the DoE. Additionally, two 5 g batches of indomethacin (IND) were milled using the optimized conditions, as well as the worst milling conditions, as determined by the DoE.

2.2 DoE

Circumscribed central composite (CCC) experimental design with two center points was developed in JMP Pro 10 (SAS Institute Inc., Cary, North Carolina) statistical software. In a previous air-jet milling study, authors suggested to maximize attrition between particles, the grinding nozzle pressures could be set at the same pressure level (Vatsaraj et al., 2003). Therefore, both grinding nozzle pressures were grouped together as one variable, and along with the pushing nozzle pressure, were the two studied factors. With a CCC axial value of 1.414 for two factors (*NIST/SEMATECH e-Handbook of Statistical Methods*, n.d.) and the initial factor values ranging between 35 and 95 psi, the experimental design runs were randomized and tabulated, and the factors' values were rounded to multiples of five. The values for grinding and pushing nozzle pressures ranged

from 20 to 110 psi (Table 3.1). The analyzed responses included: the yield, D_{50}, and D_{90} values associated with the PSD for the recovered samples.

2.3 PSD analysis by Laser light diffraction

PSDs were determined using a Sympatec Helos equipped with a Cuvette module (System-Partikel-Technik GmbH, Clausthal-Zellerfeld, Germany). Data were analyzed using the Sympatec WINDOX software. For each measurement per a previously optimized method, about 2 mg of powder was dispersed in 0.5 mL of 0.1 % (w/v) SLS in water and the sample was sonicated for 5 minutes. A reference measurement was performed on the cell filled with 50 mL of 0.005 % (v/v) Tween 20 and 50 μL of 2.5 N HCl in water. After the reference measurement, 50 μL aliquots of the sonicated suspension were added to the cell to achieve optical concentrations of between 10 to 20 % and the total of six measurements were performed on each sample. Analyzed samples included: unprocessed IBU and IND as well as the milled samples from the bfC, C, D, E, G, and H segments for each run. The span value was calculated according to the following formula:

$$Span = \frac{D_{90} - D_{10}}{D_{50}} \qquad \textit{Equation 3}$$

To estimate the overall D_{10}, D_{50}, and D_{90} values for the combined recovered fractions associated with each run, stacked bar charts were graphed and herein are referred to as the yield normalized cumulative PSDs. Each stacked bar corresponded to a particle size bin and its height corresponded to the volume density distributions' weighted

averages by the yield for each segment of the jet mill. The D_{10}, D_{50}, and D_{90} values for the normalized cumulative PSDs were the particle sizes corresponding to the 10, 50, and 90 % area of the stacked bar chart respectively. This method was validated through the calculation of these values for a single PSD using this method and their comparison with the calculated values using the Sympatec WINDOX software.

2.4 Scanning Electron Microscopy (SEM)

Samples were mounted on standard aluminum SEM stubs, were sputter coated with 15 nm platinum/palladium (Pt/Pd) using a Cressington sputter coater 208 HR (Cressington Scientific Instruments Ltd., Watford, UK) and were imaged using a Zeiss Supra 40VP SEM (Carl Zeiss Microscopy GmbH, Jena, Germany).

3 Results

3.1 Air-jet milling

The 4^{th} and 10^{th} runs were unsuccessful due to powder "blowback," where grinding nozzle pressures were significantly larger than the push nozzle pressure (65 vs. 20 psi and 95 vs. 35 psi). Due to the adhesion of IBU throughout the interior surface of the jet mill downstream from the milling chamber (Figure 3.1), milled samples from the different segments were collected individually. The overall yields ranged from 64.5 to 85.5 % for the DoE runs. The collection bag yield percentage ranged from 5.7 to 17.3 % (Figure 3.2).

3.2 DoE analysis

The primary goals of the DoE analysis were to minimize the D_{50} and D_{90} values of the PSDs and to maximize the collection bag yield percentage. Since the PSDs for the collection bag fraction were associated with the smallest D_{50} and D_{90} values, they were utilized for the DoE analysis. For the collection bag fraction, the D_{50} values ranged from 3.2 to 11.9 μm, and the D_{90} values ranged from 8.1 to 92.4 μm (Figure 3.3). Following the DoE analysis, it was determined that the grinding and pushing nozzle pressures have a significant effect on D_{90} ($p = 0.0046^{*}$, 0.0090^{*}) and the grinding nozzle pressure had a second-degree effect on D_{90} ($p = 0.0064^{*}$). The D_{50} and D_{90} values for the yield normalized cumulative PSDs ranged from 6.4 to 12.5 μm for D_{50} and 13.2 to 27.2 μm for D_{90} (Figure 3.4).

The prediction profiler graphs were generated by the JMP software (Figures 3.5 - 3.8) and predicted the collection bag yield, D_{50}, and D_{90} values as a function of the grinding and pushing nozzle pressures. To test the DoE analysis, the optimal collection bag yield and the PSD parameters were predicted for the grinding nozzle pressure of 75 psi and the pushing nozzle pressure of 65 psi. Specifically, Figure 3.5 illustrates the prediction profiler for the overall and the collection bag yields. Likewise, Figures 3.6 – 3.8 illustrate the prediction profiler graphs for the D_{50} and D_{90} values for the PSDs associated with: the cyclone fraction (Figure 3.6), the collection bag fraction (Figure 3.7), and the yield normalized cumulative PSD (Figure 3.8).

3.3 DoE testing and batch size

The DoE predictions were tested through milling a 5 g batch of IBU with a grinding nozzle pressure of 75 psi and a pushing nozzle pressure of 65 psi. The yield percentages, PSDs, and yield normalized cumulative PSD from the different segments of the air-jet mill are presented in Figures 3.10 and 3.11. Furthermore, milling was conducted on 10 and 20 g batches of IBU as well as 5 g batches of IND. The collection bag yield, D_{50}, D_{90}, and span values are presented in Table 3.3.

3.4 Scanning Electron Microscopy (SEM)

The unprocessed IBU particles had a smooth acicular morphology with an approximate length of 150 μm and an approximate cross section of 20 x 20 μm. The milled IBU particles from the collection bag sizes ranged from 1 μm to greater than 5 μm with at least one smooth dimension and one or more rough dimensions. As opposed to the unprocessed IBU particles, the milled IBU particles existed as particle agglomerates of at least 20 to 30 μm (Figure 3.12).

4 Discussion

The DoE method allowed for the IBU milling conditions optimization and led to a PSD with the D_{50} and D_{90} values significantly bellow the brittle-ductile transition critical diameter of IBU where dry milling below this size is more difficult (Shariare et al., 2012). At the grinding nozzle pressure of 75 psi and the pushing nozzle pressure of 65 psi, the prediction profilers (Figures 3.5 – 3.8) predicted the maximal yield for the collection bag fraction, the smallest D_{50} value for the cyclone and the collection bag

fraction PSD, and the smallest D_{50} and D_{90} value for the yield normalized cumulative PSD. The collection bag and the overall yields from the DoE testing experiment corresponded closely with the yields predicted by the prediction profilers (Figure 3.5 and 10, 16 vs. 16.7 %, and 79.4 vs. 80.3 %). On the other hand, the D_{50} and D_{90} values for the collection bag fraction from the DoE testing experiment were less than the D_{50} and D_{90} values predicted by the prediction profiler (Figure 3.7 and Table 3.3, 1.9 vs. 4.36 μm and 3.6 vs. 5.48 μm). As depicted in Table 3.3, the collection bag fraction D_{50} and D_{90} values increased with increasing batch sizes. The D_{50} and D_{90} values for the 20 g batch agreed more closely with the predicted values using the prediction profiler. Batch size independent processing conditions are advantageous during scale up in the pharmaceutical industry.

During milling using the optimized conditions, the collection jar and the collection bag fractions had a left-shifted PSD in comparison with the other fractions (Figure 3.11). This shift was responsible for the formation of a bimodal distribution in the yield normalized cumulative PSD (Figure 3.10). Fine IBU aggregates deposition in the collection jar versus fine IBU particles deposition in the collection bag could explain similar PSDs for these two fractions. In contrast with the D_{90} values of the collection bag fractions, the yield normalized cumulative PSDs D_{90} values did not exceed 30 μm (Figure 3.3 – 3.4). Since the collection bag yields were about 10 %, the larger particles effects on the yield normalized cumulative PSDs D_{90} values became smaller (Figure 3.2).

For each DoE run, a pressure index (PI) value (Equation 4) was calculated where P_0 was set to 1 psi; these values are tabulated in Table 3.2. Similar pressure ratios have been previously calculated (Magee et al., 2008).

$$Pressure\ Index = \log \frac{Grinding\ nozzle\ pressure^2}{Pushing\ nozzle\ pressure \cdot P_0} \qquad \textit{Equation 4}$$

There was a good correlation ($R^2 = 0.83$) between the cyclone yield and the PI values (Figure 3.9). A decrease in the PI value was associated with an increase in the flow level through the cyclone, thereby increasing the likelihood to impact and to trap the largest particles on the cyclone wall. The two largest PI values (2.32 & 2.41) were associated with the 4th and 10th runs (Table 3.2), which were terminated due to powder blowback. These PI values were followed by the PI value for the 1st run (2.27), which was conducted successfully. Accordingly, the powder blowback inducing PI value lies between 2.27 and 2.32.

Furthermore, there was a good correlation ($R^2 = 0.71$) between the collection bag fraction D_{90} and the PI values. Previously, it was reported that the pushing nozzle pressure does not influence the particle size as significantly as the grinding nozzle pressure (Saleem and Smyth, 2010; Vatsaraj et al., 2003). Low grinding and high pushing nozzle pressures correspond with low PI values and were associated with the collection bag D_{90} values close to the unprocessed material (Figure 3.3). Decreasing the grinding nozzle pressure reduced the frequencies of the particle-particle and the particle-wall collisions and decreased the milling efficiency (Teng et al., 2009). Moreover, an increase

in the pushing nozzle pressure is associated with a less efficient particle size reduction caused by a shorter sample residence time in the grinding chamber (Muller et al., 1996).

The overall yields for the DoE runs were greater than 80 % except for the first run. Additionally, the collection bag yield improved over the coordinates of the design space (maximum of 16.1 %). However, the collection bag yield was greater than 15 % only for the central points (Figure 3.2). For the DoE optimized parameters, increasing batch sizes from 5 to 20 g improved the yield from 16.1 to 29 % (Table 3.3). The low collection bag yields were due to IBU's tendency to adhere to the walls of processing equipments. Furthermore, we observed different deposition patterns on the air-jet mill segments over the design space where the particle sizes associated with each segment was different from others. The low collection bag yields are permissible since IBU is a low-cost API. The critical output variables are the D_{50} and D_{90} here and it is expected that the collection bag yield would improve further with the batch size increase. Additionally, bulk IBU with different starting particle sizes and double milling could be used to increase the collection bag yield (Clark et al., 1998; Xu et al., 2010).

In comparison with the IBU milling using the optimized conditions, the IND milling yielded smaller particles, where the D_{90} value was less than 3 μm and the D_{50} value was about 1 μm. Moreover, the least favorable milling conditions based on the DoE led to the micronization of IND; however, the micronization was not as efficient as the optimized conditions and the PSD possessed a larger span. IND would less likely undergo the ductile mode of fracture due to a higher strength of crystal lattice than IBU

with an MP of 158 °C, which is almost twice the MP for IBU (Jansook et al., 2010; Katritzky et al., 2001). Furthermore, IND has a more brittle crystalline structure than IBU since it underwent a higher degree of comminution than IBU. This observation is supported by a smaller predicted brittle-ductile transition critical diameter for IND in comparison with IBU. At particle sizes above this diameter, IND undergoes the brittle mode of fracture, whereas IBU undergoes the ductile mode of fracture (Troy, 2005). However, the smaller initial D_{50} and D_{90} values for IND could be a contributory factor for the smaller final D_{50} and D_{90} values for IND in comparison with IBU.

5 Conclusion

Being a soft solid with a low MP, IBU has a large brittle-ductile transition critical diameter. IBU showed to be a good model drug for the optimization of a single-step air-jet milling. The DoE method allowed for the optimization of the milling conditions, which were used for the micronization of IBU and IND. Furthermore, the calculated PI values predicted failed runs as well as particle trapping in the cyclone for the Aljet mill. Increasing IBU batch sizes improved the collection bag fraction yield with the relative preservation of PSD. In future studies, the *in vitro* aerodynamic performance and the stability of the micronized IBU will be investigated to develop a carrier-free, high-dose DPI formulation with the potential to reach the deep lung regions upon successful aerosolization.

6 Acknowledgements

Authors would like to thank Nazareth Eliana Ceschan and Dr. María Verónica Ramírez-Rigo for the generous donation of indomethacin. Furthermore, authors would like to thank Dr. Kristin Fathe for assistance in editing and reviewing this manuscript.

7 Declaration of Interest

Hugh D.C. Smyth is a consultant to Respira Therapeutics. The terms of this arrangement have been reviewed and approved by the University of Texas at Austin in accordance with its policy on objectivity in research.

8 References

BASF Group, n.d. Ibuprofen.

Clark, A.R., Hsu, C.C., Walsh, A.J., 1998. Preparation of sodium chloride aerosol formulations. US5747002 A.

Dudognon, E., Danède, F., Descamps, M., Correia, N.T., 2008. Evidence for a new crystalline phase of racemic Ibuprofen. Pharm. Res. 25, 2853–2858. doi:10.1007/s11095-008-9655-7

Jansook, P., Kurkov, S.V., Loftsson, T., 2010. Cyclodextrins as solubilizers: Formation of complex aggregates. J. Pharm. Sci. 99, 719–729. doi:10.1002/jps.21861

Katritzky, A.R., Jain, R., Lomaka, A., Petrukhin, R., Maran, U., Karelson, M., 2001. Perspective on the Relationship between Melting Points and Chemical Structure. Cryst. Growth Des. 1, 261–265. doi:10.1021/cg010009s

Kendall, K., 1978. The impossibility of comminuting small particles by compression. Nature 272, 710–711. doi:10.1038/272710a0

Larsson, I., Kristensen, H.G., 2000. Comminution of a brittle/ductile material in a Micros Ring Mill. Powder Technol. 107, 175–178. doi:10.1016/S0032-5910(99)00184-9

Leuenberger, H., 1982. The compressibility and compactibility of powder systems. Int. J. Pharm. 12, 41–55. doi:10.1016/0378-5173(82)90132-6

Magee, G., Vaughan, C., Smith, J., Kraus, D., 2008. Proposing a Design Space – A Case Study Using Design of Experiments and Jet Milling, in: Respiratory Drug Delivery. CRC Press Boca Raton, pp. 259–270.

Merisko-Liversidge, E., Liversidge, G.G., 2011. Nanosizing for oral and parenteral drug delivery: A perspective on formulating poorly-water soluble compounds using wet media milling technology. Adv. Drug Deliv. Rev. 63, 427–440. doi:10.1016/j.addr.2010.12.007

Moribe, K., Ueda, K., Limwikrant, W., Higashi, K., Yamamoto, K., 2013. Nano-Sized Crystalline Drug Production by Milling Technology. Curr. Pharm. Des. 19, 6246–6258.

Muller, F., Polke, R., Schadel, G., 1996. Spiral jet mills: Hold up and scale up. Int. J. Miner. Process. 44-5, 315–326. doi:10.1016/0301-7516(95)00042-9

Naik, S., Chaudhuri, B., 2015. Quantifying Dry Milling in Pharmaceutical Processing: A Review on Experimental and Modeling Approaches. J. Pharm. Sci. 104, 2401–2413. doi:10.1002/jps.24512

Neupert, W., Brugger, R., Euchenhofer, C., Brune, K., Geisslinger, G., 1997. Effects of ibuprofen enantiomers and its coenzyme A thioesters on human prostaglandin endoperoxide synthases. Br. J. Pharmacol. 122, 487–492. doi:10.1038/sj.bjp.0701415

Newman, S.P., Chan, H.-K., 2008. In Vitro/In Vivo Comparisons in Pulmonary Drug Delivery. J. Aerosol Med. Pulm. Drug Deliv. 21, 77–84. doi:10.1089/jamp.2007.0643

NIST/SEMATECH e-Handbook of Statistical Methods, n.d.

Parrott, E., 1974. Milling of Pharmaceutical Solids. J. Pharm. Sci. 63, 813–829. doi:10.1002/jps.2600630603

Rasenack, N., Steckel, H., Muller, B.W., 2003. Micronization of anti-inflammatory drugs for pulmonary delivery by a controlled crystallization process. J. Pharm. Sci. 92, 35–44. doi:10.1002/jps.10274

Roberts, R.J., Rowe, R.C., 1987. Brittle/ductile behaviour in pharmaceutical materials used in tabletting. Int. J. Pharm. 36, 205–209. doi:10.1016/0378-5173(87)90157-8

Saleem, I.Y., Smyth, H.D.C., 2010. Micronization of a Soft Material: Air-Jet and Micro-Ball Milling. AAPS PharmSciTech 11, 1642–1649. doi:10.1208/s12249-010-9542-5

Shariare, M.H., Blagden, N., de Matas, M., Leusen, F.J.J., York, P., 2012. Influence of solvent on the morphology and subsequent comminution of ibuprofen crystals by air jet milling. J. Pharm. Sci. 101, 1108–1119. doi:10.1002/jps.23003

Telko, M.J., Hickey, A.J., 2005. Dry Powder Inhaler Formulation. Respir. Care 50, 1209–1227.

Teng, S., Wang, P., Zhu, L., Young, M.-W., Gogos, C.G., 2009. Experimental and numerical analysis of a lab-scale fluid energy mill. Powder Technol. 195, 31–39. doi:10.1016/j.powtec.2009.05.013

Troy, D.B., 2005. Remington: The science and practice of pharmacy. Lippincott, Williams & Wilkins, Philadelphia, PA.

Vatsaraj, N.B., Gao, D., Kowalski, D.L., 2003. Optimization of the operating conditions of a lab scale Aljet mill using lactose and sucrose: A technical note. AAPS PharmSciTech 4, 141–146. doi:10.1208/pt040227

Xu, Z., Mansour, H.M., Mulder, T., McLean, R., Langridge, J., Hickey, A.J., 2010. Dry powder aerosols generated by standardized entrainment tubes from drug blends with lactose monohydrate: 2. Ipratropium bromide monohydrate and fluticasone propionate. J. Pharm. Sci. 99, 3415–3429. doi:10.1002/jps.22100

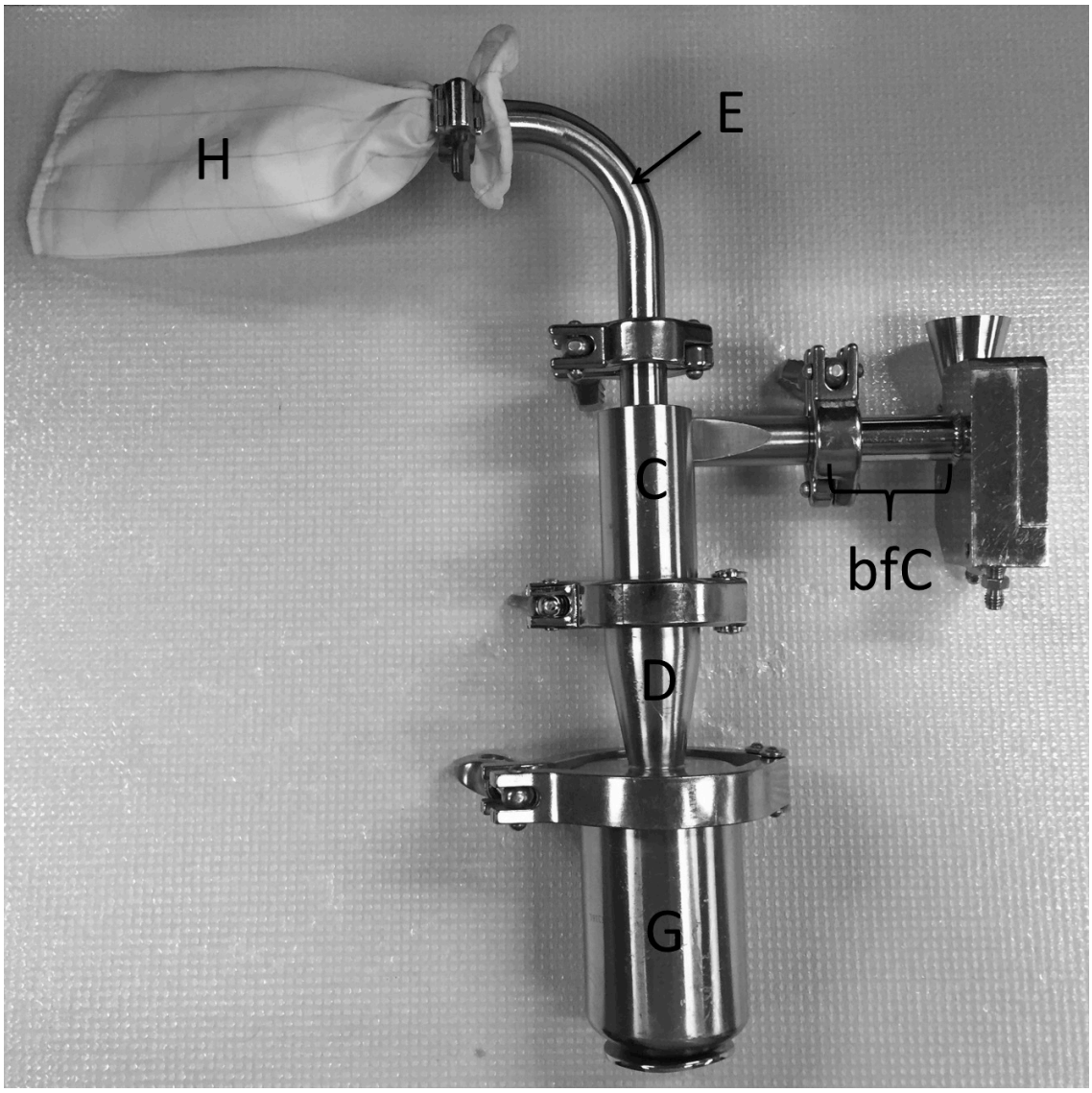

Figure 3.1: The Aljet mill configuration: the tube after grinding chamber (bfC), the cyclone (C), the collection vessel adapter (D), the collection bag adapter (E), the collection vessel (G), and the collection bag (H).

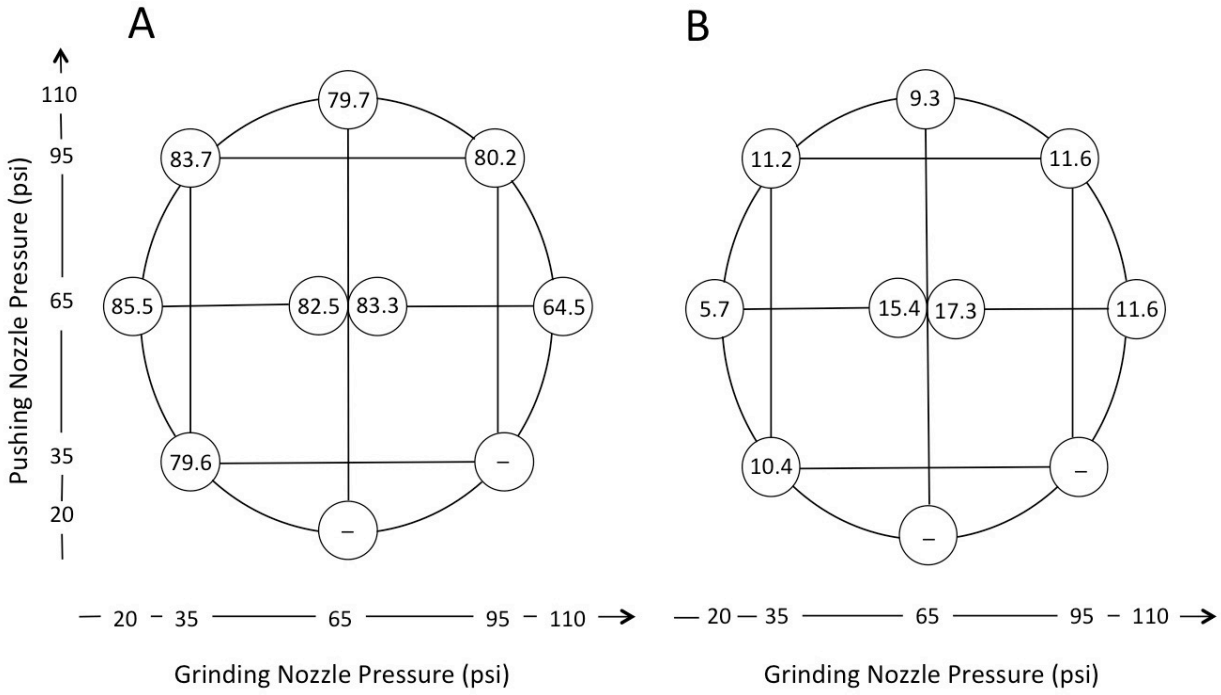

Figure 3.2: The (A) overall and (B) collection bag yields and the corresponding pushing and grinding nozzle pressures (psi) for the air-jet milling of ibuprofen.

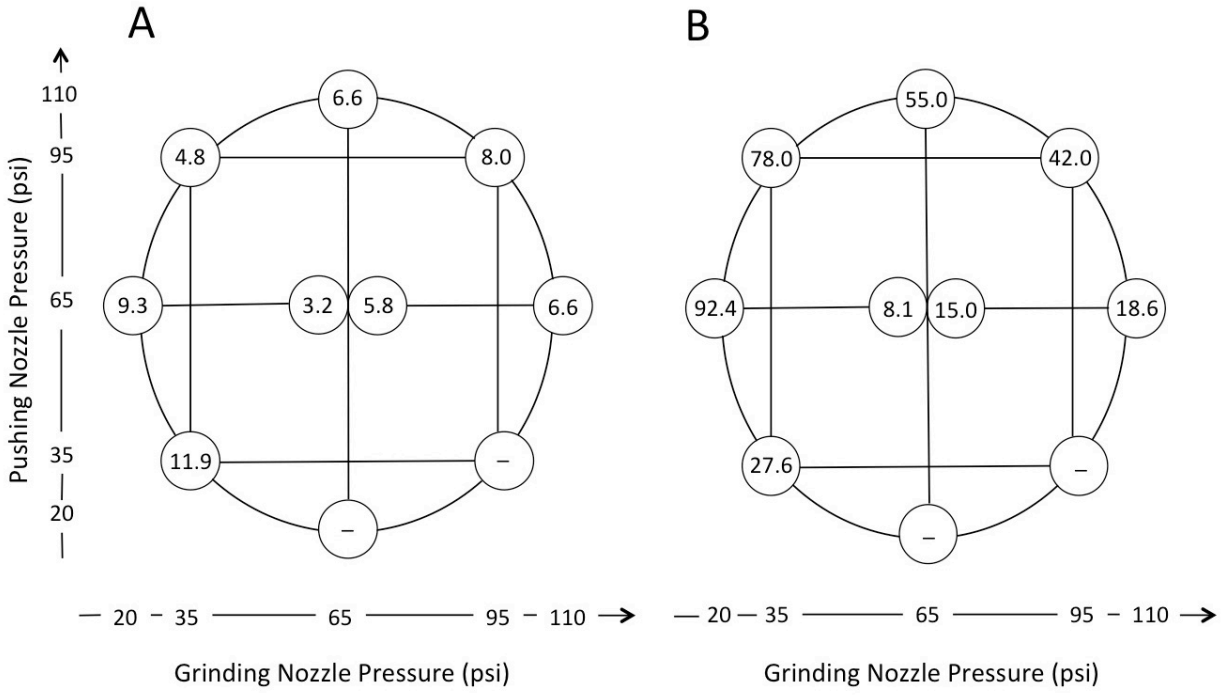

Figure 3.3: The (A) D_{50} (µm) and (B) D_{90} (µm) for the collection bag particle size distribution and the corresponding pushing and grinding nozzle pressures (psi) for the air-jet milling of ibuprofen.

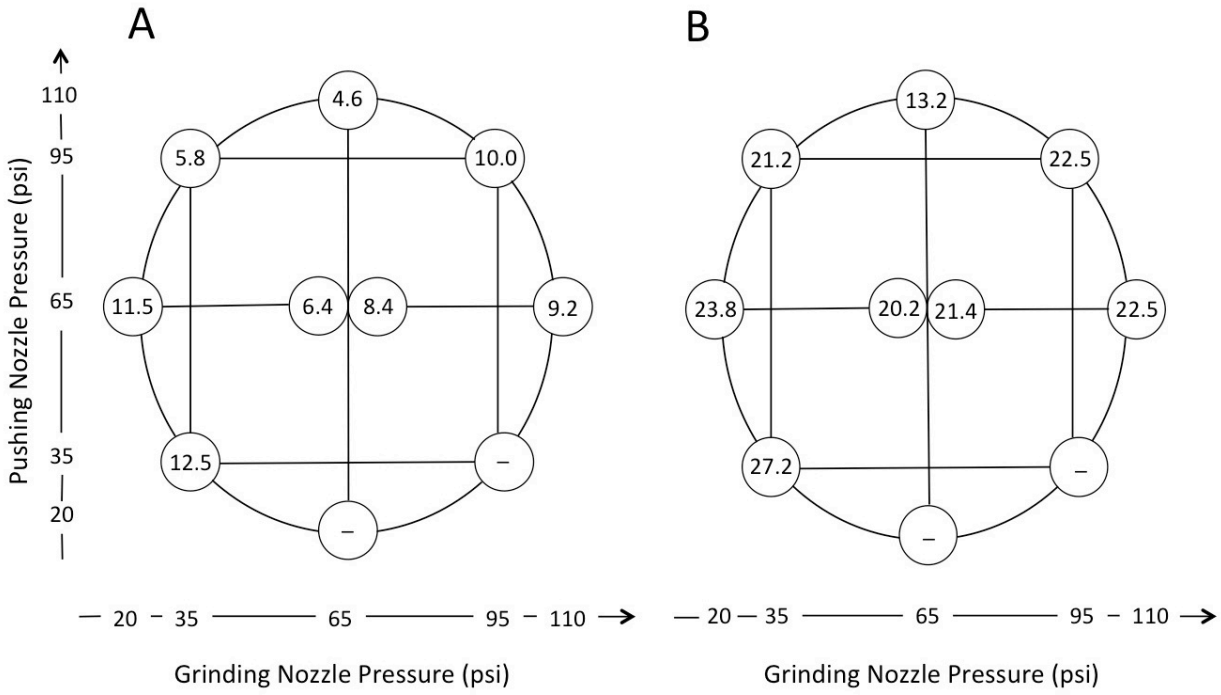

Figure 3.4: The (A) D_{50} (μm) and (B) D_{90} (μm) for the yield normalized cumulative particle size distribution and the corresponding pushing and grinding nozzle pressures (psi) for the air-jet milling of ibuprofen.

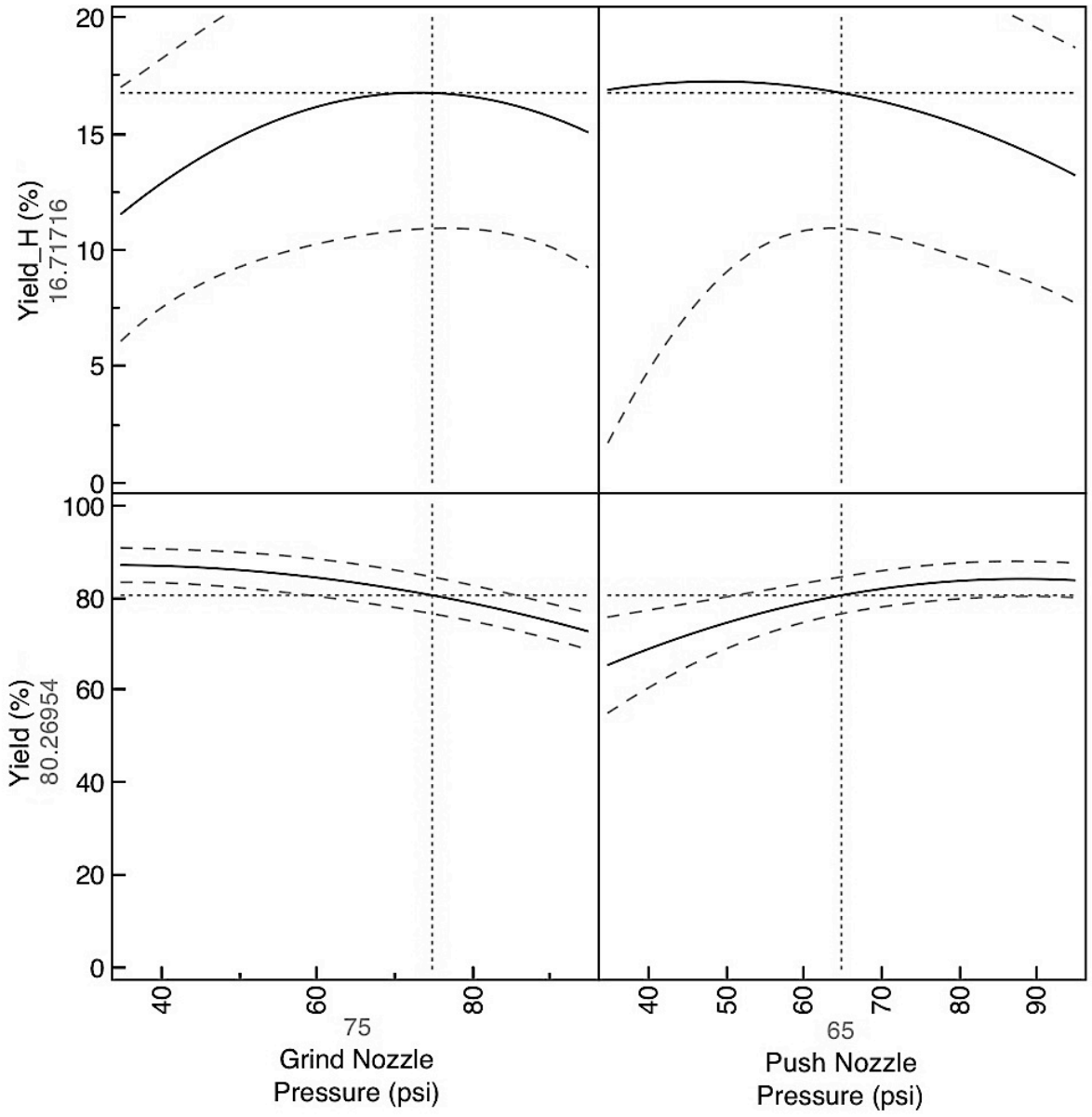

Figure 3.5: The prediction profilers for the collection bag (Yield_H) and the overall yields (%) as functions of the grinding and the pushing nozzle pressures (psi).

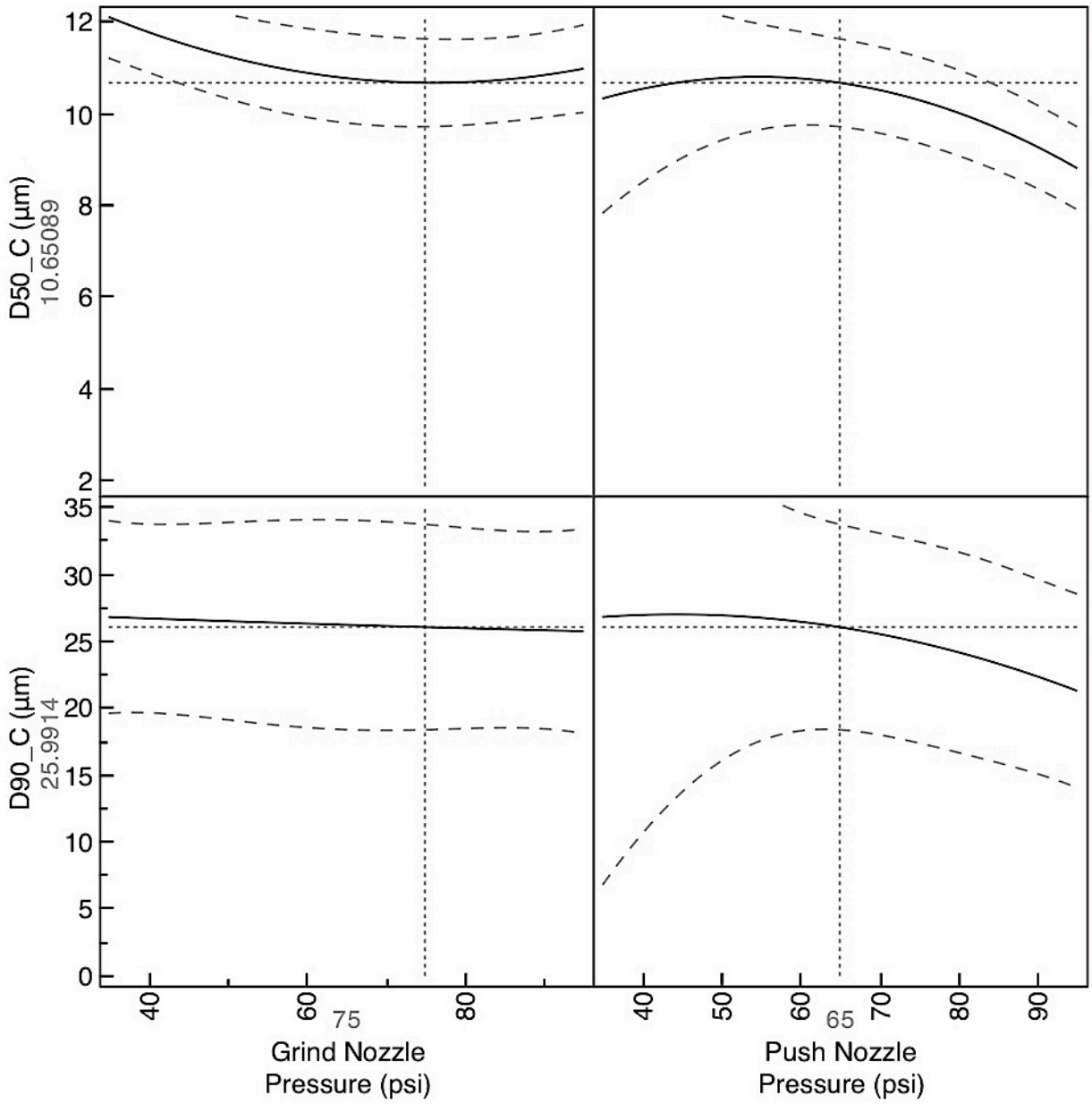

Figure 3.6: The prediction profilers for the D_{50} (µm) and D_{90} (µm) of the cyclone particle size distribution as functions of the grinding and the pushing nozzle pressures (psi).

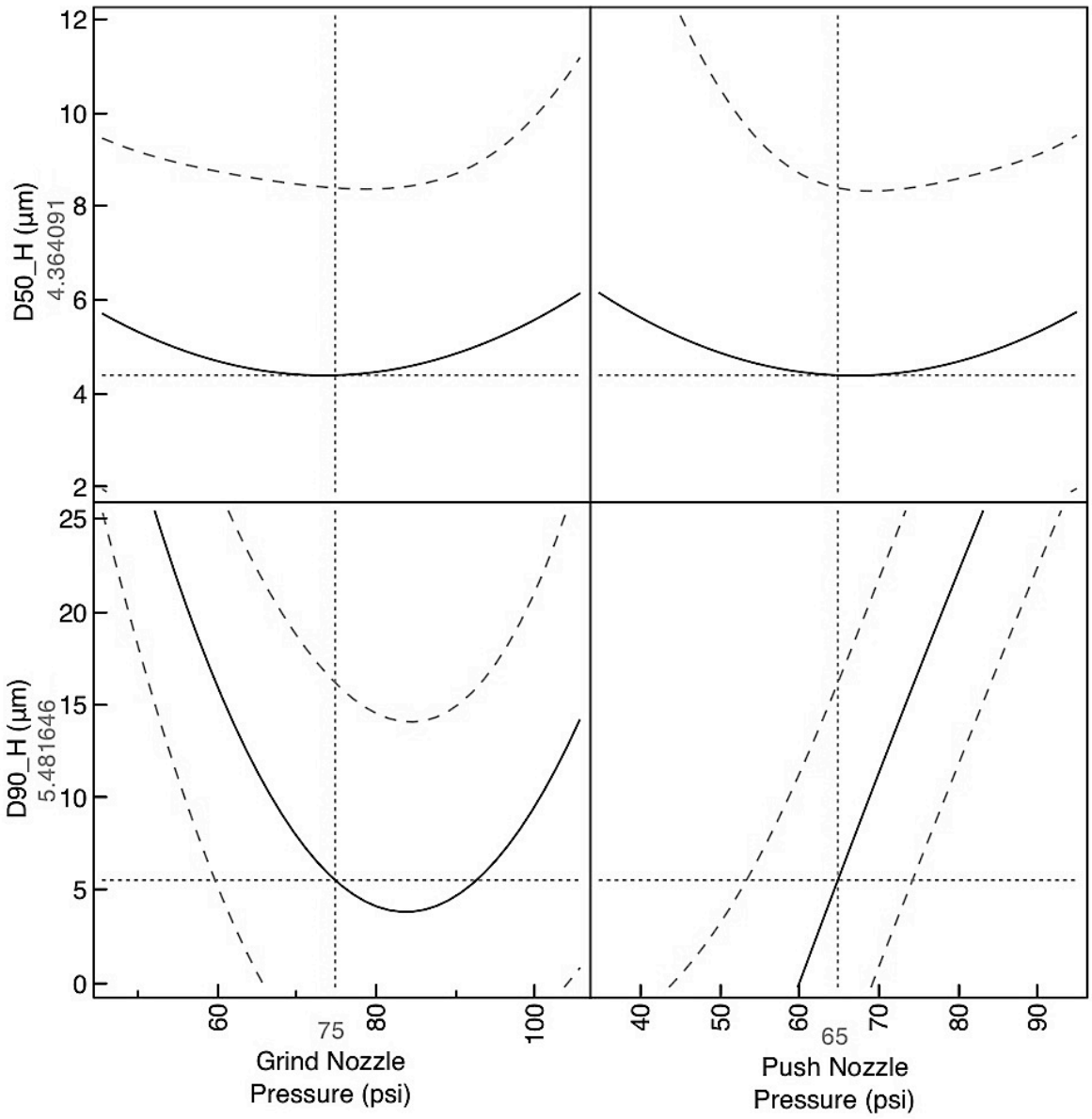

Figure 3.7: The prediction profilers for the D_{50} (µm) and D_{90} (µm) of the collection bag particle size distribution as functions of the grinding and the pushing nozzle pressures (psi).

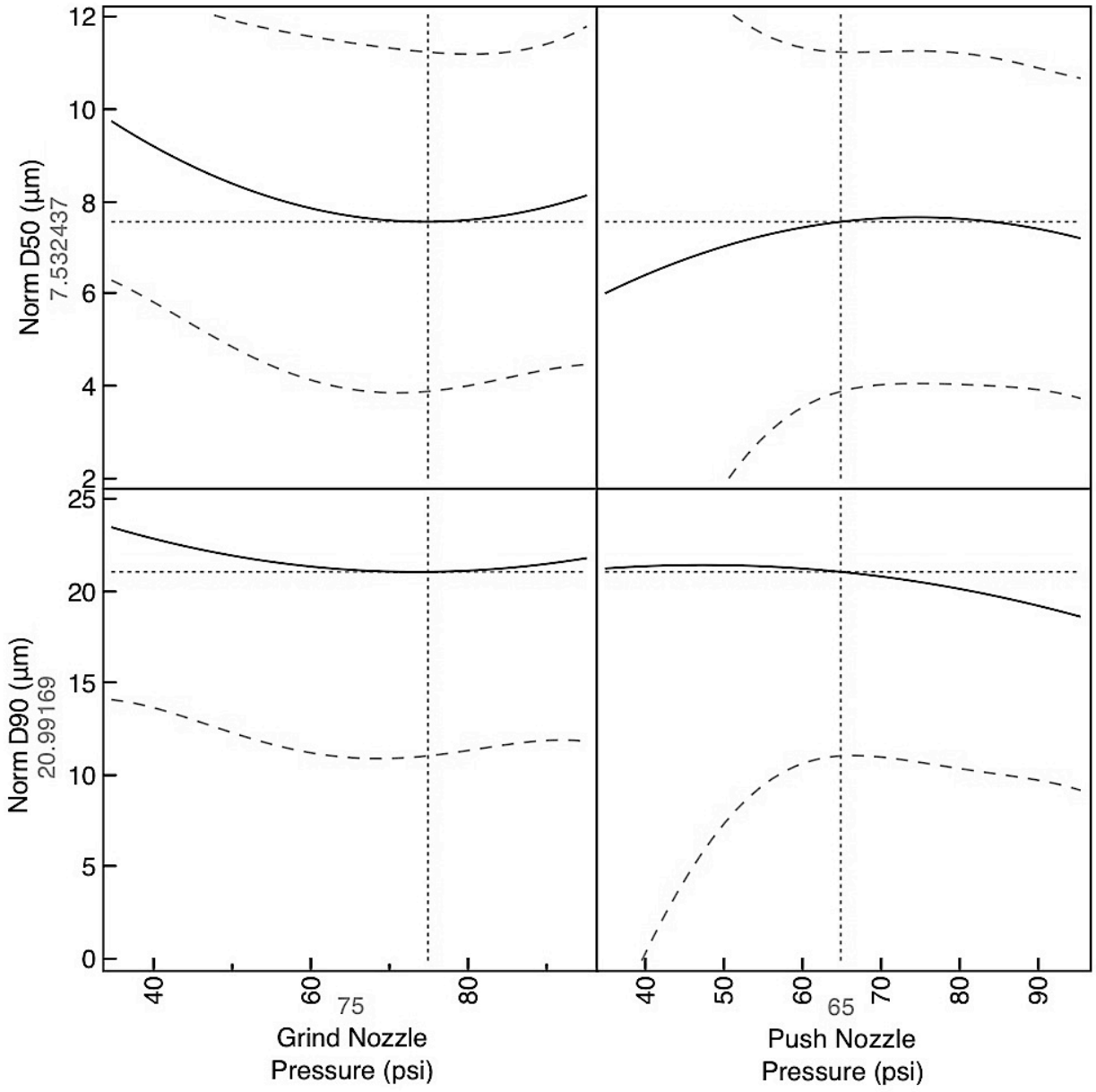

Figure 3.8: The prediction profilers for the D_{50} (µm) and D_{90} (µm) of the yield normalized cumulative particle size distribution as functions of the grinding and the pushing nozzle pressures (psi).

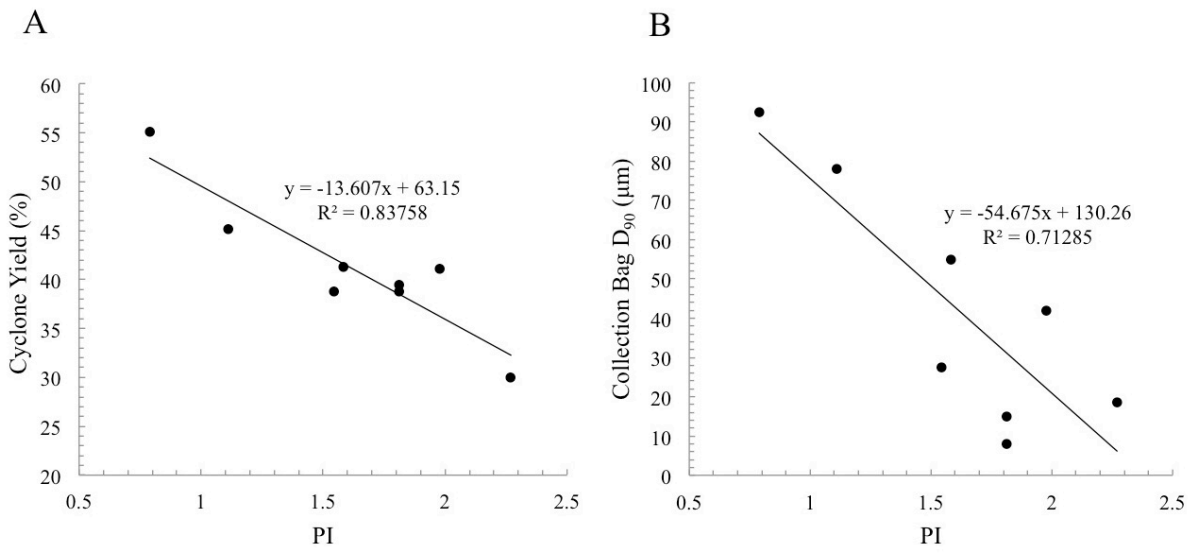

Figure 3.9: (A) The cyclone yield (%) and (B) the collection bag D_{90} (μm) values as a function of the pressure index (PI), where PI = log (Grinding nozzle pressure^2/Pushing nozzle pressure x P_0), and P_0 = 1 psi.

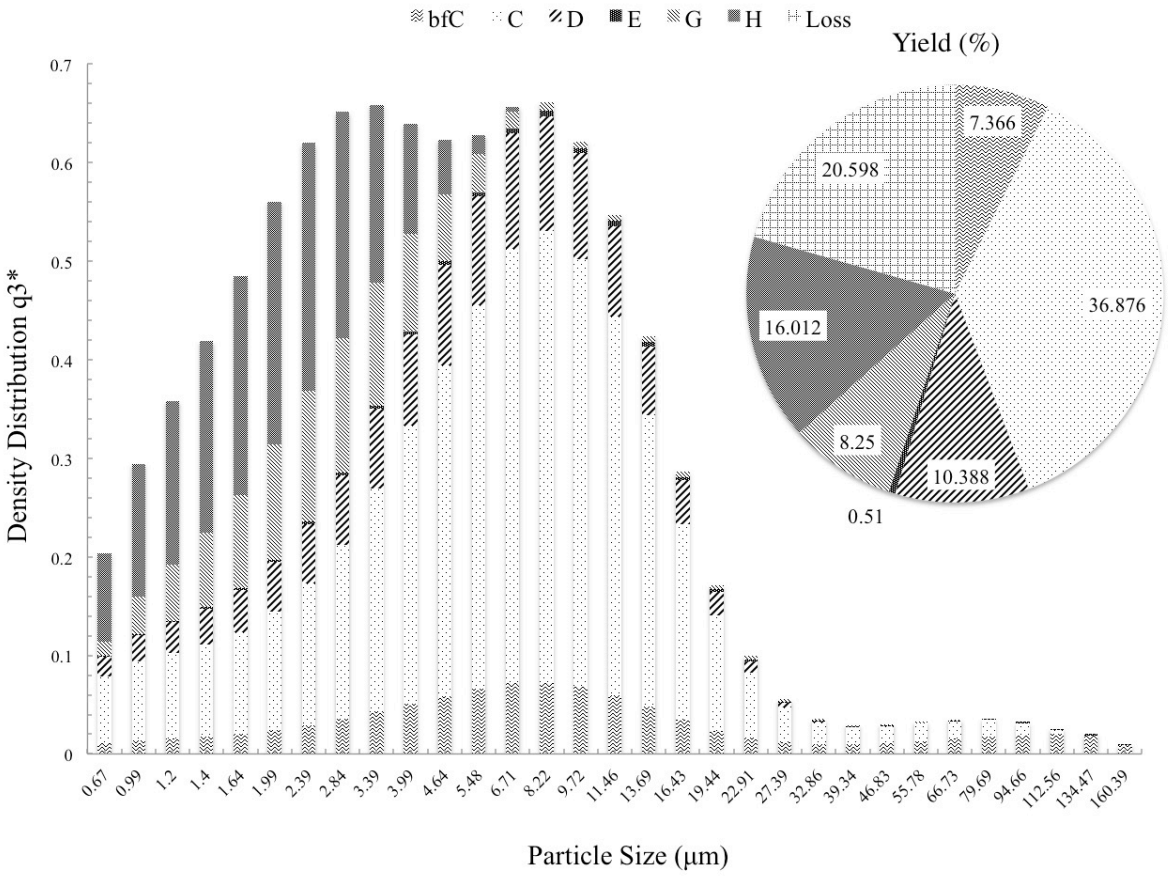

Figure 3.10: The yield normalized cumulative particle size distribution of the jet-milled ibuprofen and the associated yields (%) from the different segments of the jet mill including: the tube after grinding chamber (bfC), the cyclone (C), the collection vessel adapter (D), the collection bag adapter (E), the collection vessel (G), and the collection bag (H).

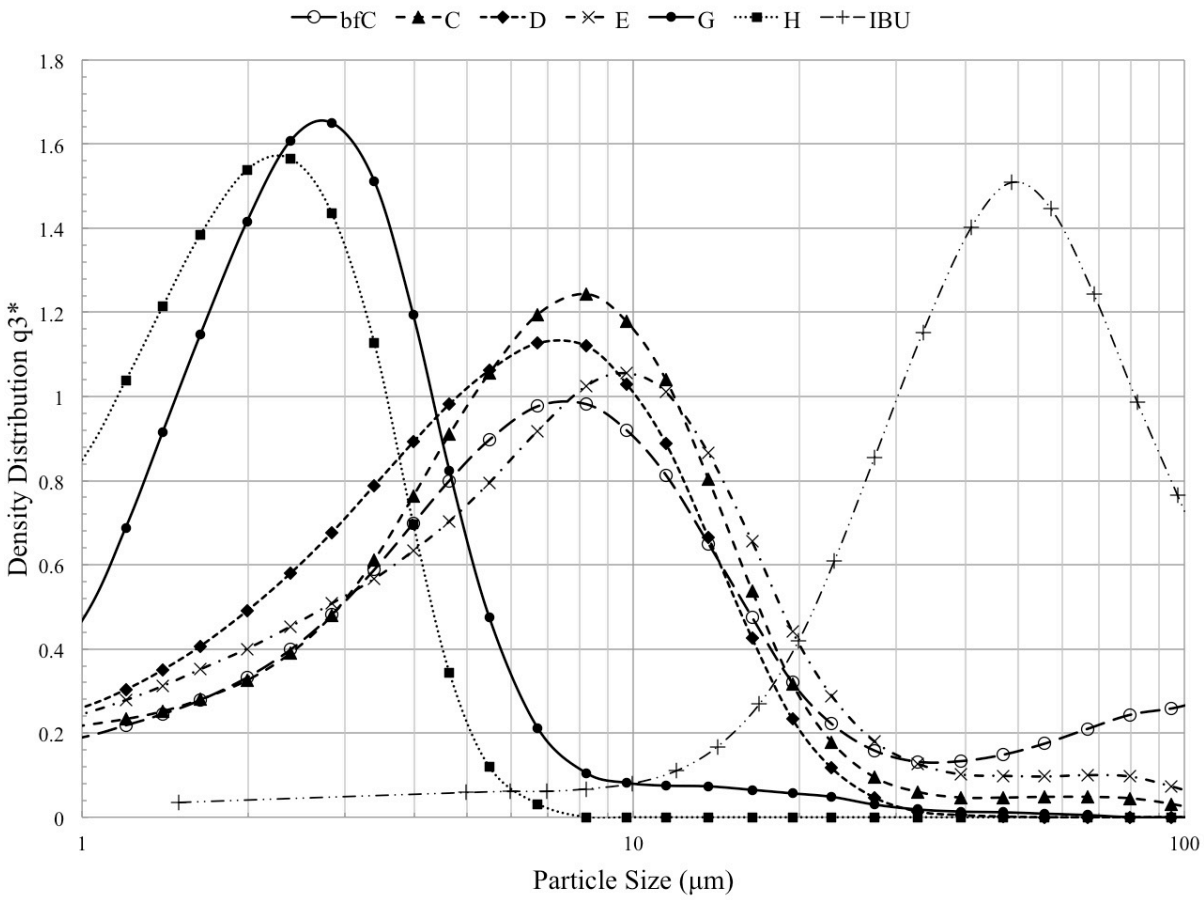

Figure 3.11: The particle size distributions of the unprocessed ibuprofen (IBU) and the IBU samples from the different segments of the jet mill including: the tube after grinding chamber (bfC), the cyclone (C), the collection vessel adapter (D), the collection bag adapter (E), the collection vessel (G), and the collection bag (H).

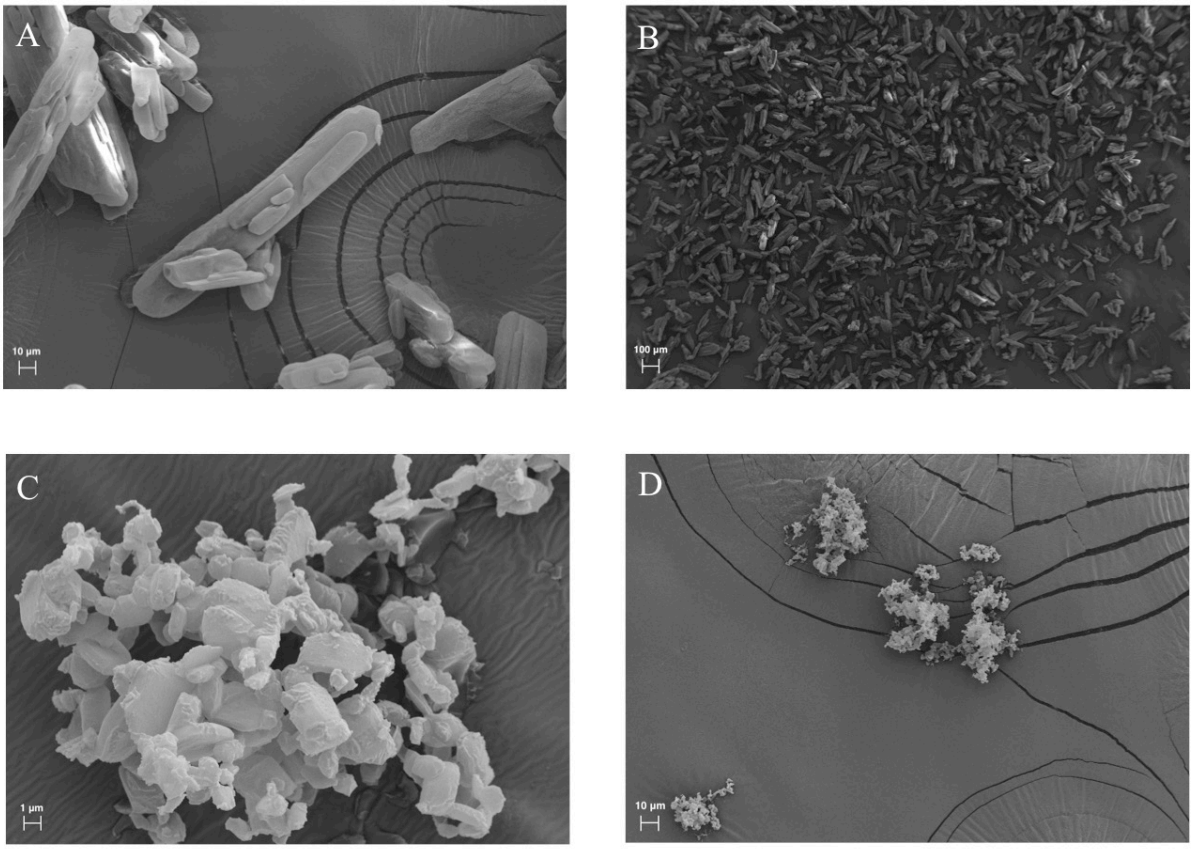

Figure 3.12: The scanning electron microscopy images of: A, B) the unprocessed ibuprofen; C, D) the jet-milled ibuprofen.

Table 3.1: The circumscribed central composite experimental design with two center points

Run #	Grinding Nozzle Pressure (psi)	Pushing nozzle Pressure (psi)
1	110	65
2	65	110
3	35	95
4	**65**	**20**
5	35	35
6	95	95
7	65	65
8	20	65
9	65	65
10	**95**	**35**

Table 3.2: The Circumscribed central composite experimental design with two center points with the Pressure Index (PI) calculation for each run where PI = log (Grinding nozzle pressure^2/Pushing nozzle pressure x P_0), and P_0 = 1 psi.

Run #	Grinding Nozzle Pressure (psi)	Pushing nozzle Pressure (psi)	PI
1	110	65	2.27
2	65	110	1.58
3	35	95	1.11
4	**65**	**20**	**2.32**
5	35	35	1.54
6	95	95	1.98
7	65	65	1.81
8	20	65	0.79
9	65	65	1.81
10	**95**	**35**	**2.41**

Table 3.3: The collection bag yield, the D_{50}, the D_{90}, and the span values for 5, 10, 20 g batches of the jet-milled ibuprofen (IBU) and indomethacin (IND)

Name	GrindP (psi)	PushP (psi)	Yield (%)	D_{50} (μm)	D_{90} (μm)	Span
Stock IBU	-	-	-	48.0	106.7	1.8
IBU 5g	75	65	16.1	1.9	3.6	1.5
IBU 10g	75	65	17.4	2.2	4.2	1.5
IBU 20g	75	65	29.0	2.7	6.0	1.8
Stock IND	-	-	-	26.3	64.8	2.3
IND+ 5g	75	65	2.3	1.2	2.7	1.7
IND- 5g	35	35	2.7	1.8	4.4	2.1

CHAPTER IV*

Carrier-free high-dose dry powder inhaler formulation of ibuprofen: Physicochemical characterization and *in vitro* aerodynamic performance

Authors:

Ashkan K. Yazdi[a], Hugh D. C. Smyth[a]

[a] Division of Pharmaceutics, College of Pharmacy, The University of Texas at Austin, PHR 4.214, 2409 University Ave, A1920, Austin TX 78712-1119, USA

Corresponding Author:

Hugh D. C. Smyth

Office: 512 471 3383

Fax: 512 471 7474

Email: hugh.smyth@austin.utexas.edu

Keywords:

Air-jet milling, Next generation impactor, Capsule fill weight, Storage temperature, Conditioning period

* This chapter has been published in the International Journal of Pharmaceutics and may be cited as: Yazdi, A.K., Smyth, H.D.C., 2016. Carrier-free high-dose dry powder inhaler formulation of ibuprofen: Physicochemical characterization and in vitro aerodynamic performance. International Journal of Pharmaceutics 511, 403–414. doi:10.1016/j.ijpharm.2016.06.061

Abstract:

Objective: To investigate influences of capsule fill weight, batch size, and storage conditions on *in vitro* aerodynamic performance of jet-milled ibuprofen (IBU) carrier-free, dry powder inhaler formulations.

Materials and methods: Milled and unmilled IBU samples were characterized thermally and spectroscopically. Physicochemical characterization was performed by quantifying specific surface area, density, and angle of repose. Performance testing was conducted on IBU formulations in combination with a high resistance Monodose RS01 using Next Generation Impactor.

Results and discussion: There were no detectable differences between IBU samples thermally and spectroscopically. The milled IBU sample exhibited improved powder flow in comparison with the unmilled sample. The milled IBU powders possessed surprisingly high *in vitro* aerodynamic performance with a fine particle fraction percentage between 67 and 85 %, and a minimum respirable fraction percentage of 49 %. The capsule fill weights, from 10 to 50 mg, and milling batch sizes did not significantly influence performance. The importance of powder conditioning following milling was illustrated as the storage duration and temperature negatively affected performance.

Conclusion: *In vitro* aerodynamic performance of IBU is independent of capsule fill weight and batch size; however, some period of powder conditioning is recommended to reduce variability in formulation performance.

1 Introduction

Ibuprofen (IBU) is a non-steroidal anti-inflammatory agent (NSAID) indicated for pain, fever, and other inflammatory conditions such as osteoarthritis, rheumatoid arthritis, and pericarditis (Lexi-Comp, 2015). Additionally, a slower rate of respiratory decline is shown in cystic fibrosis (CF) patients on high, oral doses of IBU in comparison to placebo (Konstan et al., 1995; Lands et al., 2007). More recently, Shah et al. showed that IBU acts synergistically with other antibiotics, and may play a multifunctional role in the treatment of CF lung infections (Shah et al., 2015). Even though IBU holds promise in the management of CF, the use of this treatment modality has not been well-adopted or widespread. From 1995 to 2005, the frequency of use of oral, high-dose IBU remained low (3.6 vs. 3.3 %) according to an epidemiologic study of CF patients (Konstan et al., 2010). High doses, side effects, contraindications, and black box warnings regarding the use of IBU in patients with a moderate to severe renal impairment, or with an increased risk of upper gastrointestinal (GI) bleeding (Bhala et al., 2013; Lexi-Comp, 2015), may be responsible for this apparent under-prescribing and underuse in this patient population.

Pulmonary delivery may be an attractive alternative to high-dose oral administration in CF (Konstan et al., 1995) since lungs are the desired targets for the anti-inflammatory and antibiotic activities of IBU and inhalation therapy is already well accepted in CF patients (Agent and Parrott, 2015). Inhalation route is well-known to be associated with pharmacokinetic advantages, requiring a decreased administered dose for an equivalent pharmacological effect in the lungs compared to oral or systemic routes

(Smyth et al., 2007). In comparison with oral and systemic administrations, inhalation administration can provide a dosing advantage between 10 and 24 fold and may be able to minimize the systemic risks related to conventional high-dose IBU therapy (Bhala et al., 2013; Smyth et al., 2007; Telko and Hickey, 2007). Pulmonary delivery of IBU will minimize GI adverse drug reactions by eliminating direct GI toxicity (Matsui et al., 2011). Typically with inhaled powders, a binary formulation of a drug with a carrier, such as lactose, significantly improves their performance (Hickey et al., 2007; Hira et al., 2010; Steckel and Bolzen, 2004). However, this strategy is not practical for the delivery of a large drug dose via a dry powder inhaler (DPI). Other inhalation devices such as nebulizers require significantly more time for drug delivery (Geller et al., 2011), and metered dose inhalers may be incapable of metering sufficiently large drug doses (Smyth, 2005). Therefore, carrier-free DPIs have been explored for large drug dose delivery (Healy et al., 2014).

In this study, we explored the potential for delivering IBU in a carrier-free system. Jet-milled IBU samples were characterized, and effects of capsule fill weight (i.e. loaded dose), air-jet milling batch size, and formulation aging/conditioning on the *in vitro* aerodynamic performance of carrier-free, high-dose DPI formulations of IBU were investigated. For simplicity in these studies, a capsule-based DPI was used. Capsule-based inhalation systems require individual capsules to have adequate powder loading to avoid multiple administrations and to decrease administration burden for high-dose DPI delivery. Previously, it has been shown that capsule-based DPI device air flow resistance

is dependent on the capsule fill weight (Yazdi and Smyth, 2015). However, the effect of capsule fill weight on *in vitro* aerodynamic performance has not been reported despite the knowledge that *in vitro* aerodynamic performance is affected by changes in device resistance (Adams et al., 2012). Air-jet milling is considered a batch manufacturing process where batch size and batch-to-batch variability may significantly influence physicochemical characteristics of milled powders (Lee et al., 2015). Additionally, powder handling may affect these characteristics within a single batch (Marek et al., 2011). Even though these changes may not be detectable with standard characterization methods, they may affect performance of DPIs during formulations (Ticehurst et al., 1994). Finally, milling disturbs integrity of crystalline material, and post-milling storage alters particle size through "surface re-crystallization" and "stress relaxation" (Ward and Schultz, 1995). Surface re-crystallization of amorphous domains on adjacent particles and resultant interparticulate bridges increase effective particle size (Brodka-Pfeiffer et al., 2003). Conversely, stress relaxation of milled material decreases particle size through introduction of new fractures and subsequent reorientation of molecules in crystalline structure (Joshi et al., 2002). Both phenomena alter DPI performance, and their degree of presence should be evaluated during post-milling storage. Our research hypothesis is that the *in vitro* aerodynamic performance, and thereby the expected *in vivo* performance, of carrier-free, high-dose DPI formulations may be affected by capsule fill weight, air-jet milling batch size, and formulation aging.

2 Materials and methods

Unprocessed IBU, USP (Letco Medical, Decatur, Alabama) served as a control in the physicochemical characterization. IBU samples were micronized via air-jet milling (Model 00 Jet-O-Mizer^{TM} also known as Aljet mill, Fluid Energy, Telford, PA, USA). The samples included the milled IBU from 5, 10, and 20 g batches (IBU5, IBU10.1, IBU10.2, IBU20) as depicted in Table 4.1. The particle size distribution (PSD) D_{10}, D_{50}, and D_{90} values for each sample were defined as particle diameters at the 10th, 50th, and 90th percentile and the span value was calculated according to Equation 1:

$$Span = \frac{D_{90} - D_{10}}{D_{50}} \quad (1)$$

2.1 Scanning electron microscopy (SEM)

The milled samples (IBU5, IBU10.1, IBU10.2, and IBU20) were mounted on standard aluminum SEM stubs, were sputter coated with 15 nm platinum/palladium (Pt/Pd) using a Cressington sputter coater 208 HR (Cressington Scientific Instruments Ltd., Watford, UK) and were imaged using a Zeiss Supra 40VP SEM (Carl Zeiss Microscopy GmbH, Jena, Germany).

2.2 X-Ray powder diffraction (XRD)

Two-dimensional X-Ray diffractograms for the milled samples (IBU5, IBU10.1, IBU10.2, and IBU20) were obtained using an automatic R-Axis Spider (Rigaku Corporation, Tokyo, Japan), an X-ray single crystal diffractometer controlled by RINT Rapid software with target radiation of Copper at 40 KV voltage and 40mA current. The samples were suspended in light mineral oil and were loaded on loops epoxied to

conventional goniometer bases. Additionally, a background X-Ray diffractogram of light mineral oil loaded on the loops was subtracted from sample diffractograms, one-dimensional 2θ diffractograms were generated, and .txt files were saved using 2DP Software (Ragaku Corporation, Tokyo, Japan). To analyze the one-dimensional diffractograms using Jade (Ragaku Corporation, Tokyo, Japan), .raw files were generated from .txt files using the ConvX.exe (Mark Bowden, Industrial Research Ltd., Lower Hutt, New Zealand).

2.3 Differential scanning calorimetry (DSC)

For the sample IBU20 and unmilled IBU, thermograms were obtained using an Auto Q20 (TA Instruments-Waters LLC, New Castle, DE, USA) differential scanning calorimeter controlled by the TA Advantage Software (TA Instruments-Waters LLC, New Castle, DE, USA) and equipped with a RCS40 (TA Instruments-Waters LLC, New Castle, DE, USA) refrigerated cooling system with nitrogen purge of 50 mL/min. About 4 mg of each sample were loaded in standard DSC pans (DSC Consumables Inc., Austin, MN, USA) and were crimped using a Tzero sample press (TA Instruments-Waters LLC, New Castle, DE, USA). Samples were heated at the rate of 10° C/min from 30°C to 100°C.

2.4 Fourier transform infrared spectroscopy (FT-IR)

For the sample IBU20 and unmilled IBU, FT-IR spectra were obtained using a Nicolet™ iS™50 FT-IR Spectrometer (Thermo Fisher Scientific Inc., Madison, WI,

USA) equipped with a germanium Attenuated Total Reflection (ATR) accessory and a pressure tower.

2.5 Powder characterization

Physicochemical characterization was conducted on the sample IBU20, as a representation of the other milled samples, as well as the unmilled IBU by quantifying specific surface area (SSA), density, and angle of repose. IBU20 was chosen for this purpose as it possessed similar particle size distribution in comparison with the two other batch sizes while making available the largest quantity of powder for analysis.

2.5.1 Brunauer-Emmett-Teller

Surface area (SA) was evaluated via a single-point BET method using a Monosorb® surface area analyzer (Quantrachrome Instruments; FL, USA) following 24 h outgassing with helium at room temperature (RT) before each measurement in triplicate on a known powder mass (m). SSA was calculated using Equation 2:

$$SSA = \frac{SA}{m} \quad (2)$$

2.5.2 Helium pycnometry

True densities were measured using an MVP-D160-E multipycnometer (Quantrachrome Instruments; FL, USA) equipped with the micro cell and adapter. Measurements were conducted in triplicate. Before pressure measurements, the multipycnometer was purged with helium gas according to the manufacturer's recommendations.

2.5.3 Angle of repose

Angles of repose were measured in triplicate according to the United States Pharmacopoeia (USP) method (USP General Chapter, 2015a). Images of the powder mounds were taken using a digital camera and were analyzed using the ImageJ software (Wayne Rasband, Research Services Branch, National Institute of Mental Health, Bethesda, MD, USA).

2.5.4 Bulk and tapped density

The bulk density (ρ_B) and tapped density (ρ_T) calculations were performed using a tapped density tester (Agilent Technologies, Santa Clara, CA, USA) for a small mass of powder using a modified USP method (USP General Chapter, 2015b). In this modified method, a 10 mL graduated cylinder fitted with a molded adapter substituted the 100 mL graduated cylinder in the tapped density tester. The compressibility index (CI) and Hausner ratio (HR) calculations were performed according to the following formulas (USP General Chapter, 2015a):

$$CI = 100 \times \frac{\rho_T - \rho_B}{\rho_B} \quad (3)$$

$$HR = \frac{\rho_B}{\rho_T} \quad (4)$$

2.6 *In vitro* aerodynamic performance testing

For the *in vitro* aerodynamic performance testing, the DPI device was a high-resistance monodose RS01, a gift from Plastiape S.p.a. (Osnago, Italy). Vcaps No. 3 hydroxypropyl methylcellulose (HPMC) capsules were provided by Capsugel Inc.

(Morristwon, New Jersey, USA). The *in vitro* aerodynamic performance of carrier-free, high-dose DPI formulations were assessed using the Next Generation Impactor (NGI) (MSP Corporation, MN, USA) attached sequentially to a Whatman® HEPA filter (GE Healthcare Bio-Sciences, Pittsburg, PA, USA), a volumetric digital flow meter (TSI 4000 Series, TSI Performance Measurement Tools, Shoreview, MN, USA), a two-way solenoid valve timer, and a high-capacity vacuum pump (HCP5, Copley Scientific Limited, Nottingham, UK).

For these studies, the DPI device was loaded with an HPMC capsule containing 10, 25, or 50 mg of IBU5 or 25 mg of IBU10.1, IBU10.2, or IBU20. Capsule filling was conducted manually using a micro-spatula and an analytical balance where capsule fill weight did not include the capsule shell weight. To minimize the drug burden on patients due to high dosage requirement of ibuprofen, it is important to use the largest capsule fill weight where the performance is not affected by it. No. 3 capsules can be filled with a maximum capsule fill weight of 50 mg. 10 and 25 mg capsule fill weights were selected to represent the low- and mid- values for the capsule fill weights. Table 4.2 describes the formulations for *in vitro* aerodynamic performance studies with addition of the unprocessed IBU as negative control. Before testing, the preseparator was loaded with 15 mL of ethanol, and the NGI stages were coated with silicon oil via application of 1 % (v/v) of silicon oil in hexane. The temperature and relative humidity were measured using an SRH77A thermo-hygrometer by Cooper-Atkins Instrument Corporation (Middlefield, CT, USA). The *in vitro* aerodynamic performance of formulations were evaluated at a

flow rate of 58.8 L/min creating a 4 kPa pressure drop across the DPI device (Yazdi and Smyth, 2015) for 4.08 s for a total volume of 4 L per Chapter 601 of the USP, apparatus 5 for inhalation powders in triplicate (USP General Chapter, 2015c). The capsule, the inhaler base, the mouthpiece, the adapter, the induction port, the preseparator, the stages 1 – 7, and the micro-orifice collector (MOC) were each washed twice with 5 mL of ethanol and their UV-absorbance were analyzed at the wavelength of 265 nm using a Tecan® Infinite® 200 PRO multimode microplate reader (Tecan Systems, Inc. San Jose, CA, USA).

Drug mass in each fraction was quantified. Emitted dose percentage (ED) was calculated as the percentage of the entire dose depositing downstream from the mouthpiece of the DPI where the entire dose is the total recovered drug mass in all the fractions. Respirable fraction percentage (RF) was calculated as the percentage of the entire dose deposited on stages two through seven plus the MOC. Fine particle fraction percentage (FPF) was calculated as the percentage of the emitted dose deposited on the stages two through seven plus the MOC. Fine particle (< 5 μm) fraction percentage (FPF5μm), fine particle (< 3 μm) fraction percentage (FPF3μm), and fine particle (< 1 μm) fraction percentage (FPF1μm) corresponded to the percentage of the emitted dose predicted to have the aerodynamic diameter below 5, 3, and 1 μm respectively. The FPF5μm, FPF3μm, and FPF1μm values were interpolated from a graph with the cumulative percentage of the emitted dose deposited downstream from an NGI stage as the ordinate and the particle cutoff size of that stage as the abscissa.

2.7 PSD analysis by laser light diffraction

PSDs were determined using a Sympatec Helos equipped with a Cuvette module (System-Partikel-Technik GmbH, Clausthal-Zellerfeld, Germany). Data were analyzed using the Sympatec WINDOX software. For each measurement, per a previously optimized method, about 2 mg of powder was dispersed in 0.5 mL of 0.1% (w/v) sodium dodecyl sulfate in water and the sample was sonicated for 5 min. A reference measurement was performed on the cell filled with 50 mL of 0.005% (v/v) Tween 20 and 50 μL of 2.5 N hydrochloric acid in water. After the reference measurement, 50 μL aliquots of the sonicated suspension were added to the cell to achieve optical concentrations between 10 to 20 % and the total of six measurements were performed on each sample. Formulations were analyzed immediately following air-jet milling (25IBU10.1, 25IBU10.2) and after 6 months (25IBU10.1**, 25IBU10.2**) stored at RT (IBU10.1), or at -80°C (IBU10.2).

3 Results

3.1 SEM

As depicted in Figure 4.1, the samples IBU5, IBU10.1, IBU10.2, and IBU20 consisted of micronized particles with plate-like morphology as agglomerates of 10 to 30 μm. There were no morphological differences between the milled IBU batches.

3.2 XRD

XRD spectra from the unmilled IBU and the samples IBU5, IBU10.1, IBU10.2, and IBU20 overlapped (Figure 4.2) and peaks corresponded closely with the peaks from

the solved XRD diffractogram of racemic IBU (McConnell, 1974), which is listed in Cambridge Structural Database (refcode: IBPRAC).

3.3 DSC

DSC thermograms for the sample IBU20 and unmilled IBU (Figure 4.3) possessed endotherms at 77.78°C and 77.18°C corresponding to the melting point of IBU. There were no other endotherms, exotherms, or phase transitions in the thermograms.

3.4 FT-IR

Peaks associated with the FT-IR spectra for the sample IBU20 and unmilled IBU overlapped (Figure 4.4). The 1712.43 cm^{-1} sharp peaks corresponded with the carbonyl group of the carboxylic acid functionality of the IBU molecule. The group of peaks surrounding 2955.20 cm^{-1} corresponded with the sp^2 carbon-hydrogen bond stretches of the aromatic ring superimposed on the carboxylic acid oxygen-hydrogen bond stretch. Finally, 779.99 cm^{-1} corresponds with para substitution on the aromatic ring of IBU.

3.5 Powder characterization

Table 4.3 summarizes the powder characterization for the sample IBU20 and unmilled IBU. There was a six-fold difference in SSA between the two samples (2.02 vs. 0.36 m^2/g); however, the true density measurements were the same. The calculated CI and HR based on the density measurements were as follows: 45.00 vs. 39.19 and 1.82 vs. 1.64. According to the USP, calculated CI greater than 25 and HR greater than 1.34 are indicative of poor flowability; however, the angle of repose improved from 62.6 ± 2.9°

for the unmilled IBU to 37.8 ± 5° for the sample IBU20. IBU was transformed from a powder with almost very, very poor flow to one with almost good flow according to angle of repose testing (USP General Chapter, 2015a).

3.6 *In vitro* aerodynamic performance testing

Testing was conducted at relative humidity levels between 28 and 51 % and RT of 23 and 25° C. Formulations 10IBU5, 25IBU5, and 50IBU5 performances were compared to evaluate the capsule fill weight effect (Figure 4.5). Formulations 25IBU5, 25IBU10.1, 25IBU10.2, and IBU20 performances were compared to investigate the batch size effect (Figure 4.6). Capsule fill weight and batch size did not significantly affect the performance. Formulations 25IBU20, 25IBU20*, 25IBU10.1, 25IBU10.1** performances were compared to evaluate the formulation performance effect on aging (Figure 4.7). Formulations 25IBU10.1, 25IBU10.1', and 25IBU10.1" performances were compared to evaluate the storage temperature effect (Figure 4.8). An increased storage duration and temperature affected the performance negatively. Finally, formulations 25IBU10.1, 25IBU10.1**, 25IBU10.2, and 25IBU10.2** performances were compared to evaluate the storage temperature effect on aging (Figure 4.9). Decreased storage temperature was associated with improved performance.

3.7 PSD analysis

The PSDs for formulations 25IBU10.1, 25IBU10.1**, 25IBU10.2, and 25IBU10.2** are reported in Figure 4.10. The D_{50} and D_{90} values for the sample

increased at RT after a six-month storage (2.19 & 4.23 μm vs. 3.00 & 13.23 μm). However, the D_{50} and D_{90} values for the sample did not change at -80°C after a six-month storage (2.74 & 7.56 μm vs. 2.43 & 4.77 μm). The appearance of a secondary peak in the PSD after a six-month storage at RT was responsible for this increase.

4 Discussion

The jet-milled samples possessed a plate-like morphology according to the SEM micrographs (Figure 4.1) and were crystalline as determined by XRD (Figure 4.2). The crystalline structure corresponded with the conventional phase (phase I) of IBU (Dudognon et al., 2008). The DSC thermogram and FT-IR spectrum for sample IBU20, representative of all milled samples, corresponded to the thermogram and spectrum for the unmilled IBU (Nokhodchi et al., 2015). The melting point drop following air-jet milling, from 77.78 to 77.18° C, was due to the smaller particle size of the milled sample in comparison with the unmilled sample (Révész, 2005). The true density measurements by helium pyncometry matched the literature reported value (Ostrowska et al., 2015).

Powder flow is critical in pharmaceutical processing including capsule filling for DPIs (Shah et al., 2008). Sample IBU20 showed an improved powder flow, signified by a smaller angle of repose, in comparison with the unmilled IBU (Table 4.3). However, this observation was in contrast with the calculated CI and HR values and the notion that air-jet milling leads to poor powder flow due an increase in adhesive and cohesive forces where Van der Waals forces become greater than gravitational forces (Hickey, 2003). As

evident in the SEM micrographs, the milled IBU particles formed agglomerates, which likely behaved as granules and resulted in a smaller angle of repose.

The SSA and the PSD parameters for sample IBU20 indicate formation of reversible agglomerates as opposed to irreversible agglomerates. The D_{10}, D_{50}, D_{90} values for sample IBU20 were associated with individual particles, as agglomerates were disintegrated upon dispersion before sizing. Moreover, the theoretical particle size (D_{theo} = 2.88 μm) was calculated based on SSA and ρ according to Equation 5 (Lowell et al., 2004). The calculated D_{theo} value for sample IBU20 corresponded to the measured D_{50} value for the PSD, which implies the surface area for individual particles contributed to SSA. However, irreversible agglomerates would be associated with a smaller SSA and larger D_{theo} value in comparison with reversible agglomerates. Moreover, superior *in vitro* aerodynamic performance data (Figures 4.5 – 4.9) may imply that IBU particles form loose agglomerates.

$$D_{theo} = \frac{6}{SSA \times \rho} \quad (5)$$

As depicted in Figure 4.5, the ED values were about 70 % regardless of the capsule fill weight. The RF values decreased slightly; however, the FPF values decreased when the capsule fill weight increased from 10 to 50 mg. The observed drops were the most significant for the FPF1μm value for formulation 50IBU5 with a relative drop of 25 % in comparison with formulation 10IBU5. It has been previously shown that the monodose RS01 device resistance decreases with the increasing capsule fill weight for

the high resistance monodose RS01 device (Yazdi and Smyth, 2015). A decreased device resistance is associated with a decreased deagglomeration efficiency at similar flow rates (de Boer et al., 2012; Hassoun et al., 2015). The decreased RF and FPF values can be explained by the decreased degree of deagglomeration due to the resistance drop. Even though the performance was negatively affected by increasing capsule fill weight, the decrease is not clinically significant since at least half of the dose per capsule can be delivered in practice.

A closer inspection of the breakdown of the deposition percentage for the different capsule fill weights showed an increasing recovery percentage of the dose from the capsule walls with a decreasing capsule fill weight; however, the recovered IBU mass was about 1 mg across all capsule fill weights. Conversely, significantly larger IBU mass was recovered from the inhaler for 50IBU5 in comparison with 10IBU5 (27 vs. 20 %, 14 vs. 2 mg). Accordingly, similar ED values were achieved for different capsule fill weights. Decreased FPF values were due to increased deposition levels in the induction port and the preseparator because of reduced deagglomeration efficiency with increasing capsule fill weights.

The RF values for formulations of different samples ranged from 49 to 55 % and were not significantly different (Figure 4.6). Except formulation 25IBU10.2, the ED value remained at about 70 % for other formulations (25IBU5, 25IBU10.1, 25IBU20); however, formulation 25IBU10.2 possessed the highest FPF values at 1, 3, and 5 μm. The deposition percentage breakdown showed the highest deposition in the capsule, inhaler

base, mouthpiece, and stages four through seven and the lowest deposition in the induction port and preseparator for formulation 25IBU10.2. This deposition pattern implies that sample IBU10.2 contained the highest percentage of fine particles in comparison with the other milled samples. Fine particles adhere to the interior of the capsule, inhaler base, and mouthpiece; however, large particles are trapped in the induction port and preseparator during *in vitro* aerodynamic performance testing for DPI formulations.

There was a significant drop in the RF value from 52 to 43 % for the formulation 25IBU20 analyzed immediately following air-jet milling and after a 21-day storage in a desiccator under vacuum at RT (Figure 4.7). Additionally, there was a similar drop in the RF value from 49 to 40 % for formulation 25IBU10.1 analyzed immediately following air-jet milling and after a six-month storage at the same conditions (Figure 4.9). For both formulations, the ED values improved from 72 to 81 %; however, the FPF, FPF5μm, and FPF3μm values dramatically dropped by 20 % and the FPF1μm values decreased by 50 %. Specifically, the deposited IBU mass in the inhaler base and mouthpiece decreased, and the deposited IBU mass in the induction port and preseparator increased. This observation was attributed to IBU particle size growth and the formation of irreversible agglomerates within 21 days. However, there were no further changes from 21 days to six months of storage.

Upon storage at RT, a secondary peak upstream of the primary peak appeared in the PSD corresponding with the irreversible aggregates, which did not break apart upon

dispersion before sizing (Figure 4.10). As it was previously discussed in the introduction, amorphous domains could be created during air-jet milling of crystalline material due to high energy input (Ward and Schultz, 1995). Techniques such as DSC and XRD utilized in this paper to assess amorphous content did not possess the required resolution to make this assessment and detect these domains. Bridges could form between neighboring microparticles upon the crystallization of these domains and reversible agglomerates transform into irreversible agglomerates (Brodka-Pfeiffer et al., 2003).

The *in vitro* aerodynamic performance following a 24-hour purge with helium at 30° C versus RT yielded similar results, whereas an increased temperature accelerated this transformation to under 24 h (Figure 4.8). The *in vitro* aerodynamic performance immediately after air-jet milling and after six months at -80° C for formulation 25IBU10.2 was compared with the *in vitro* aerodynamic performance at RT for formulation 25IBU10.1 (Figure 4.9). Sample storage at -80° C limited the formation extent of irreversible aggregates and preserved the RF value at 51 % following six-month storage. The secondary peak, corresponding with the irreversible aggregates, was absent in the PSD upon storage at -80° C in comparison with storage at RT (Figure 4.10).

The *in vitro* aerodynamic performance data, following storage at RT and -80° C (Figures 4.7 & 4.9), suggest the need for a conditioning period immediately after air-jet milling and before further processing. The conditioning period could constitute, at least, a 21-day storage at RT, following which performance would stabilize after an initial drop. The performance following this conditioning period is acceptable since it is limited to a

20 % relative drop and is superior in comparison with most commercial DPI formulations (Donovan, 2015). Alternatively, the conditioning temperature could be reduced down to -80° C, during which the formation extent of irreversible aggregates is limited. However, this conditioning period is associated with an increased cost due to the temperature requirements.

The current study is the first report of *in vitro* aerodynamic performance data for a carrier-free, high-dose formulation of IBU. The RF values were at least about 50 % for all formulations immediately after air-jet milling. With a minimum FPF3μm and ED values of 55.8 and 72.6 % for formulation 25IBU10.2, 40 % of the dose is predicted to reach the deep lung with an aerodynamic diameter below 3 μm. These values are significantly larger than most commercial DPI formulations (Donovan, 2015). To achieve the estimated maximum 300 mg/day dose requirement for CF via pulmonary delivery, based on an approximate maximum 3 g/day oral dose, six capsules with 50 mg capsule fill weight are required to be administered every twelve hours assuming RF of 50 %. Further experiments are warranted to evaluate other performance considerations (e.g. flow rate dependency, 2 kPa pressure drop, etc.) for the carrier-free, high-dose IBU formulation in combination with the high-resistance monodose RS01 inhaler.

5 Conclusion

The *in vitro* aerodynamic performances of the carrier-free, high-dose DPI formulations of IBU were tested for the first time. The formulations exhibited superior performance with predicted lung delivery of at least 40 % of the dose regardless of

capsule fill weight, batch size and storage conditions. It is likely that some loose crystalline agglomerates in the carrier-free formulation transformed into irreversible agglomerates upon aging at RT within one month; however, there were no further changes by six months. This transformation is temperature dependent; it occurred within 24 h at 30° C and did not occur at -80° C during a six-month period. The performance was minimally influenced by capsule fill weight and batch size.

6 Acknowledgements

Authors would like to thank Dr. Kristin Fathe for assistance in editing and reviewing this manuscript.

7 References

Adams, W.P., Lee, S.L., Plourde, R., Lionberger, R.A., Bertha, C.M., Doub, W.H., Bovet, J.-M., Hickey, A.J., 2012. Effects of device and formulation on in vitro performance of dry powder inhalers. Aaps J. 14, 400–409. doi:10.1208/s12248-012-9352-7

Agent, P., Parrott, H., 2015. Inhaled therapy in cystic fibrosis: agents, devices and regimens. Breathe 11, 111–118. doi:10.1183/20734735.021014

Bhala, N., Emberson, J., Merhi, A., Abramson, S., Arber, N., Baron, J.A., Bombardier, C., Cannon, C., Farkouh, M.E., FitzGerald, G.A., Goss, P., Halls, H., Hawk, E., Hawkey, C., Hennekens, C., Hochberg, M., Holland, L.E., Kearney, P.M., Laine, L., Lanas, A., Lance, P., Laupacis, A., Oates, J., Patrono, C., Schnitzer, T.J., Solomon, S., Tugwell, P., Wilson, K., Wittes, J., Baigent, C., 2013. Vascular and upper gastrointestinal effects of non-steroidal anti-inflammatory drugs: meta-analyses of individual participant data from randomised trials. Lancet Lond. Engl. 382, 769–79. doi:10.1016/S0140-6736(13)60900-9

Brodka-Pfeiffer, K., Häusler, H., Grass, P., Langguth, P., 2003. Conditioning following powder micronization: influence on particle growth of salbutamol sulfate. Drug Dev. Ind. Pharm. 29, 1077–1084. doi:10.1081/DDC-120025865

de Boer, A.H., Chan, H.K., Price, R., 2012. A critical view on lactose-based drug formulation and device studies for dry powder inhalation: Which are relevant and

what interactions to expect? Adv. Drug Deliv. Rev., Lactose as a carrier for inhalation products 64, 257–274. doi:10.1016/j.addr.2011.04.004

Donovan, M.J., 2015. Influence of carrier particle size and surface roughness on the aerosol performance of DPI formulations (Thesis).

Dudognon, E., Danède, F., Descamps, M., Correia, N.T., 2008. Evidence for a new crystalline phase of racemic Ibuprofen. Pharm. Res. 25, 2853–2858. doi:10.1007/s11095-008-9655-7

Geller, D.E., Weers, J., Heuerding, S., 2011. Development of an inhaled dry-powder formulation of tobramycin using PulmoSphere™ technology. J. Aerosol Med. Pulm. Drug Deliv. 24, 175–182. doi:10.1089/jamp.2010.0855

Hassoun, M., Ho, S., Muddle, J., Buttini, F., Parry, M., Hammond, M., Forbes, B., 2015. Formulating powder-device combinations for salmeterol xinafoate dry powder inhalers. Int. J. Pharm. 490, 360–367. doi:10.1016/j.ijpharm.2015.05.028

Healy, A.M., Amaro, M.I., Paluch, K.J., Tajber, L., 2014. Dry powders for oral inhalation free of lactose carrier particles. Adv. Drug Deliv. Rev. 75, 32–52. doi:10.1016/j.addr.2014.04.005

Hickey, A.J., 2003. Pharmaceutical Inhalation Aerosol Technology, 2nd ed. Informa Healthcare, New York.

Hickey, A.J., Mansour, H.M., Telko, M.J., Xu, Z., Smyth, H.D.C., Mulder, T., McLean, R., Langridge, J., Papadopoulos, D., 2007. Physical characterization of

component particles included in dry powder inhalers. II. Dynamic characteristics. J. Pharm. Sci. 96, 1302–1319. doi:10.1002/jps.20943

Hira, D., Okuda, T., Kito, D., Ishizeki, K., Okada, T., Okamoto, H., 2010. Inhalation performance of physically mixed dry powders evaluated with a simple simulator for human inspiratory flow patterns. Pharm. Res. 27, 2131–2140. doi:10.1007/s11095-010-0215-6

Joshi, V., Dwivedi, S., Ward, G.H., 2002. Increase in the specific surface area of budesonide during storage postmicronization. Pharm. Res. 19, 7–12. doi:10.1023/A:1013690929173

Konstan, M.W., Byard, P.J., Hoppel, C.L., Davis, P.B., 1995. Effect of high-dose ibuprofen in patients with cystic fibrosis. N. Engl. J. Med. 332, 848–854. doi:10.1056/NEJM199503303321303

Konstan, M.W., VanDevanter, D.R., Rasouliyan, L., Pasta, D.J., Yegin, A., Morgan, W.J., Wagener, J.S., 2010. Trends in the use of routine therapies in cystic fibrosis: 1995–2005. Pediatr. Pulmonol. 45, 1167–1172. doi:10.1002/ppul.21315

Lands, L.C., Milner, R., Cantin, A.M., Manson, D., Corey, M., 2007. High-dose ibuprofen in cystic fibrosis: Canadian safety and effectiveness trial. J. Pediatr. 151, 249–254. doi:10.1016/j.jpeds.2007.04.009

Lee, S.L., O'Connor, T.F., Yang, X., Cruz, C.N., Chatterjee, S., Madurawe, R.D., Moore, C.M.V., Yu, L.X., Woodcock, J., 2015. Modernizing Pharmaceutical

Manufacturing: from Batch to Continuous Production. J. Pharm. Innov. 10, 191–199. doi:10.1007/s12247-015-9215-8

Lexi-Comp, 2015. Ibuprofen [WWW Document]. URL http://online.lexi.com.ezproxy.lib.utexas.edu/lco/action/doc/retrieve/docid/patch_f/7066#f_dosages (accessed 8.28.15).

Lowell, S., Shields, J.E., Thomas, M.A., Thommes, M., 2004. Characterization of Porous Solids and Powders: Surface Area, Pore Size and Density, Particle Technology Series. Springer Netherlands.

Marek, S.R., Donovan, M.J., Smyth, H.D.C., 2011. Effects of mild processing pressures on the performance of dry powder inhaler formulations for inhalation therapy (1): Budesonide and lactose. Eur. J. Pharm. Biopharm. 78, 97–106. doi:10.1016/j.ejpb.2010.12.020

Matsui, H., Shimokawa, O., Kaneko, T., Nagano, Y., Rai, K., Hyodo, I., 2011. The pathophysiology of non-steroidal anti-inflammatory drug (NSAID)-induced mucosal injuries in stomach and small intestine. J. Clin. Biochem. Nutr. 48, 107–111. doi:10.3164/jcbn.10-79

McConnell, J.F., 1974. 2-(4-Isobutylphenyl) propionic acid. Cryst Struct Commun 3, 73–75.

Nokhodchi, A., Homayouni, A., Araya, R., Kaialy, W., Obeidat, W., Asare-Addo, K., 2015. Crystal engineering of ibuprofen using starch derivatives in crystallization

medium to produce promising ibuprofen with improved pharmaceutical performance. RSC Adv. 5, 46119–46131. doi:10.1039/C5RA06183K

Ostrowska, K., Kropidłowska, M., Katrusiak, A., 2015. High-pressure crystallization and structural transformations in compressed R, S-Ibuprofen. Cryst. Growth Des. 15, 1512–1517. doi:10.1021/cg5018888

Révész, Á., 2005. Melting behavior and origin of strain in ball-milled nanocrystalline Al powders. J. Mater. Sci. 40, 1643–1646. doi:10.1007/s10853-005-0664-1

Shah, P.N., Marshall-Batty, K.R., Panzer, M.J., Smolen, J.A., Tagaev, J.A., Rodesney, C.A., Le, H.H., Gordon, V.D., Greenberg, D.E., Youngs, W.J., Cannon, C.L., 2015. Antimicrobial and synergistic effects of ibuprofen against resistant cystic fibrosis pathogens. Presented at the 115th General Meeting of American Society of Microbiology.

Shah, R.B., Tawakkul, M.A., Khan, M.A., 2008. Comparative evaluation of flow for pharmaceutical powders and granules. AAPS PharmSciTech 9, 250–258. doi:10.1208/s12249-008-9046-8

Smyth, H.D.C., 2005. Propellant-driven metered-dose inhalers for pulmonary drug delivery. Expert Opin. Drug Deliv. 2, 53–74. doi:10.1517/17425247.2.1.53

Smyth, H.D., Saleem, I., Donovan, M., Verschraegen, C.F., 2007. Pulmonary delivery of anti-cancer agents, in: Advanced Drug Formulation Design to Optimize Therapeutic Outcomes. p. 81.

Steckel, H., Bolzen, N., 2004. Alternative sugars as potential carriers for dry powder inhalations. Int. J. Pharm. 270, 297–306. doi:10.1016/j.ijpharm.2003.10.039

Telko, M., Hickey, A., 2007. Critical assessment of inverse gas chromatography as means of assessing surface free energy and acid-base interaction of pharmaceutical powders. J. Pharm. Sci. 96, 2647–2654. doi:10.1002/jps.20897

Ticehurst, M.D., Rowe, R.C., York, P., 1994. Determination of the surface properties of two batches of salbutamol sulphate by inverse gas chromatography. Int. J. Pharm. 111, 241–249. doi:10.1016/0378-5173(94)90347-6

USP General Chapter, 2015a. <1174> Powder flow, in: US Pharmacopeial Convention, Rockville, MD, USA. pp. 1326–30.

USP General Chapter, 2015b. <616> Bulk density and tapped density of powders, in: US Pharmacopeial Convention, Rockville, MD, USA. pp. 7059–63.

USP General Chapter, 2015c. <601> Inhalation and nasal drug products: aerosols, sprays, and powders - performance quality tests, in: US Pharmacopeial Convention, Rockville, MD, USA. pp. 388–414.

Ward, G.H., Schultz, R.K., 1995. Process-induced crystallinity changes in albuterol sulfate and Its effect on powder physical stability. Pharm. Res. 12, 773–779. doi:10.1023/A:1016232230638

Yazdi, A.K., Smyth, H.D.C., 2015. Effect of capsule fill weight on device resistance in dry powder inhalers, in: Respiratory Drug Delivery. CRC Press Boca Raton, pp. 523–528.

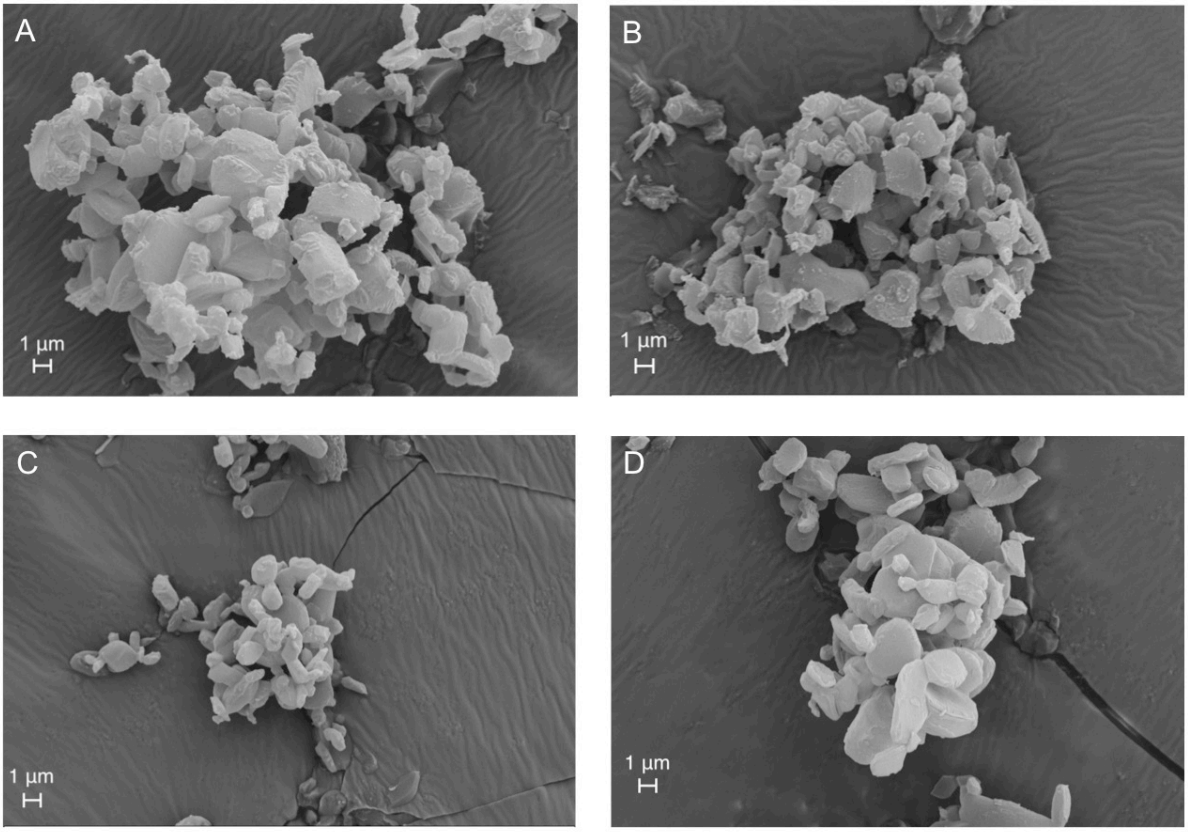

Figure 4.1: The scanning electron microscopy images of jet-milled ibuprofen batches: (A) 5 g batch (IBU5), (B) 10 g Batch (IBU10.1), (C) 10 g Batch (IBU10.2), and (D) 20 g Batch (IBU20).

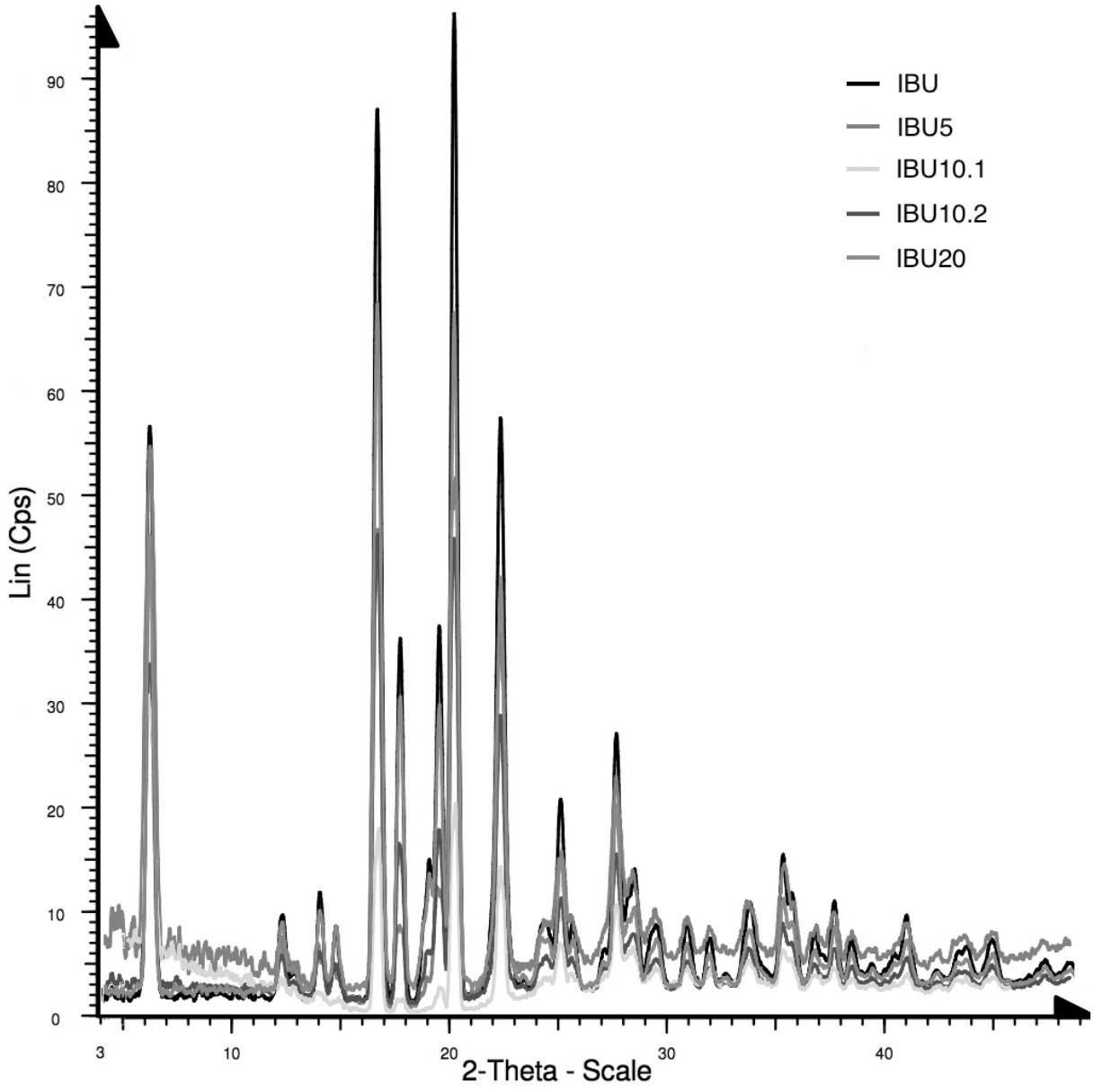

Figure 4.2: The one-dimensional diffractograms for unmilled ibuprofen (IBU) and 5, 10, and 20 g batches of jet-milled IBU (IBU5, IBU10.1, IBU10.2, IBU20).

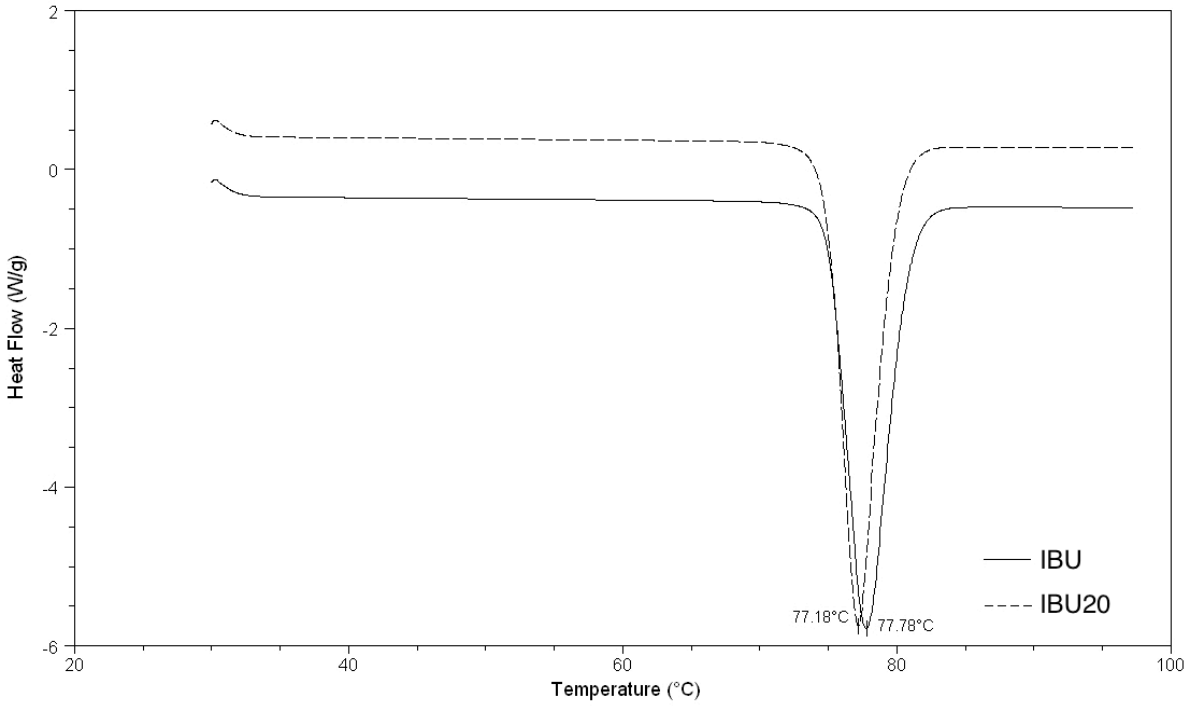

Figure 4.3: The differential scanning calorimetry thermograms for unmilled ibuprofen (IBU) and the 20 g batch of jet-milled ibuprofen (IBU20).

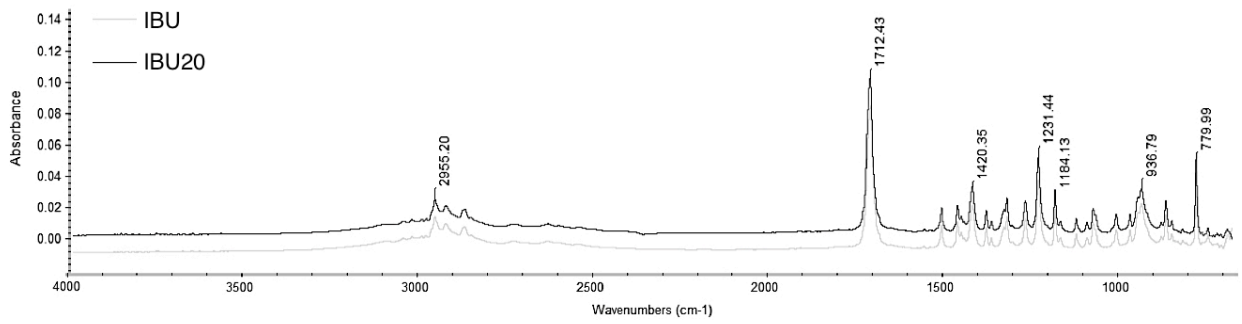

Figure 4.4: The Fourier transform infrared spectra for unmilled ibuprofen (IBU) and the 20 g batch of jet-milled ibuprofen (IBU20).

Formulation	RF (%)	ED (%)	FPF (%)	FPF5μm (%)	FPF3μm (%)	FPF1μm (%)	MMAD (μm)	GSD
10IBU5	55.8 ± 2.0	70.0 ± 3.1	79.7 ± 0.6	80.1 ± 0.6	68.9 ± 1.0	19.7 ± 1.1	2.6 ± 0.1	1.9 ± 0.0
25IBU5	55.3 ± 0.8	72.3 ± 1.8	76.5 ± 1.6	76.8 ± 1.6	64.6 ± 1.9	16.0 ± 0.4	2.8 ± 0.0	1.8 ± 0.0
50IBU5	50.5 ± 1.2	69.3 ± 0.7	72.9 ± 1.1	73.3 ± 1.1	61.0 ± 0.5	14.8 ± 0.6	2.9 ± 0.0	1.8 ± 0.0

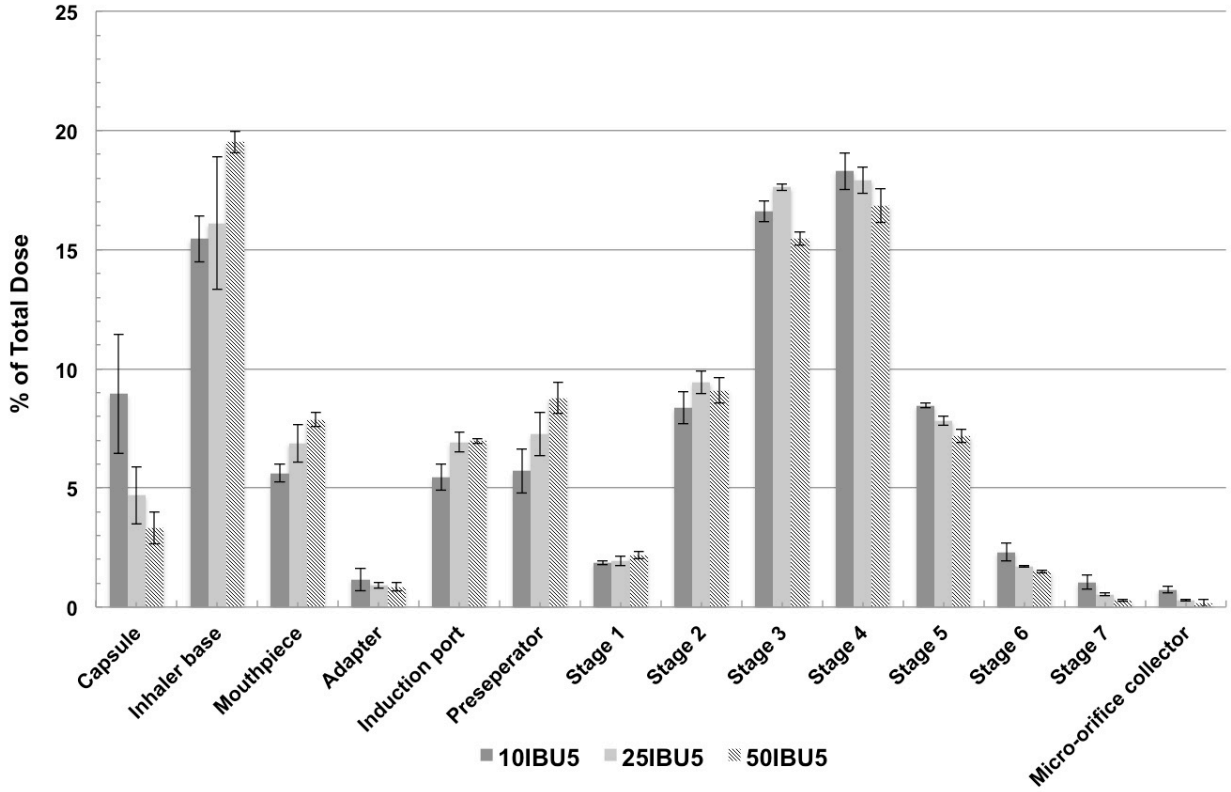

Figure 4.5: The *in vitro* aerodynamic performance of jet-milled ibuprofen formulations with 10, 25, 50 mg capsule fill weight (10IBU5, 25IBU5, 50IBU5) in combination with the high-resistance Monodose RS01 at 4 kPa pressure drop (N=3). respirable fraction percentage (RF), emitted dose percentage (ED), fine particle fraction percentage (FPF), fine particle (< 5 μm) fraction percentage (FPF5μm), fine particle (< 3 μm) fraction percentage (FPF3μm), fine particle (< 1 μm) fraction percentage (FPF1μm), mass median aerodynamic diameter (MMAD), geometric standard deviation (GSD).

Formulation	RF (%)	ED (%)	FPF (%)	FPF5μm (%)	FPF3μm (%)	FPF1μm (%)	MMAD (μm)	GSD
25IBU5	55.3 ± 0.8	72.3 ± 1.8	76.5 ± 1.6	76.8 ± 1.6	64.6 ± 1.9	16.0 ± 0.4	2.8 ± 0.0	1.8 ± 0.0
25IBU10.1	48.8 ± 2.9	72.6 ± 1.7	67.2 ± 4.5	67.6 ± 4.5	55.8 ± 3.8	13.0 ± 1.2	2.9 ± 0.0	1.8 ± 0.0
25IBU10.2	51.5 ± 4.3	60.7 ± 4.7	84.8 ± 0.6	85.0 ± 0.6	78.5 ± 0.8	23.1 ± 1.1	2.3 ± 0.0	1.8 ± 0.0
25IBU20	52.2 ± 0.8	71.5 ± 2.3	73.2 ± 3.2	73.6 ± 3.2	59.2 ± 3.3	13.5 ± 0.9	2.9 ± 0.1	1.8 ± 0.0

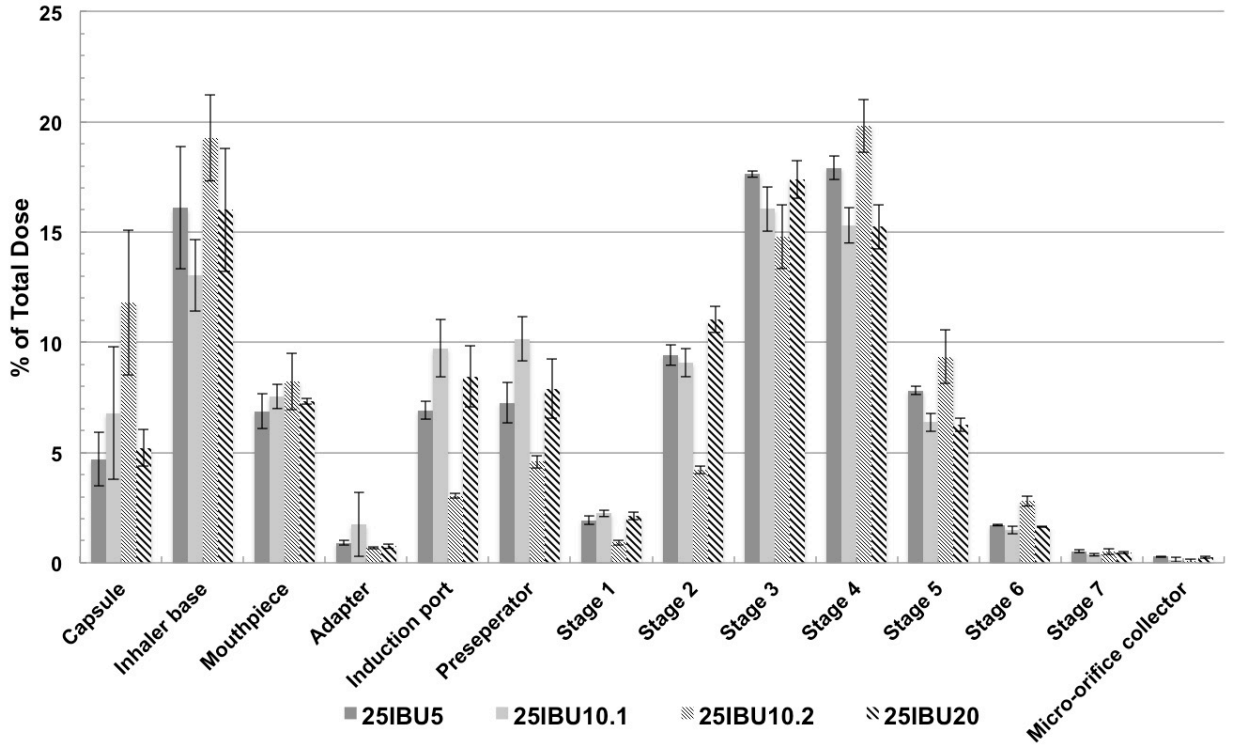

Figure 4.6: The *in vitro* aerodynamic performance of jet-milled ibuprofen formulations (25IBU5, 25IBU10.1, 25IBU10.2, 25IBU20) from 5, 10, and 20 g batches in combination with the high-resistance Monodose RS01 at 4 kPa pressure drop (N=3). respirable fraction percentage (RF), emitted dose percentage (ED), fine particle fraction percentage (FPF), fine particle (< 5 μm) fraction percentage (FPF5μm), fine particle (< 3 μm) fraction percentage (FPF3μm), fine particle (< 1 μm) fraction percentage (FPF1μm), mass median aerodynamic diameter (MMAD), geometric standard deviation (GSD).

Formulation	RF (%)	ED (%)	FPF (%)	FPF5μm (%)	FPF3μm (%)	FPF1μm (%)	MMAD (μm)	GSD
25IBU20	52.2 ± 0.8	71.5 ± 2.3	73.2 ± 3.2	73.6 ± 3.2	59.2 ± 3.3	13.5 ± 0.9	2.9 ± 0.1	1.8 ± 0.0
25IBU20*	43.3 ± 1.3	81.1 ± 1.8	53.4 ± 2.1	53.9 ± 2.1	39.2 ± 1.3	6.8 ± 0.3	3.4 ± 0.1	2.0 ± 0.0
25IBU10.1	48.8 ± 2.9	72.6 ± 1.7	67.2 ± 4.5	67.6 ± 4.5	55.8 ± 3.8	13.0 ± 1.2	2.9 ± 0.0	1.8 ± 0.0
25IBU10.1**	39.9 ± 4.9	81.2 ± 3.4	49.1 ± 4.6	49.6 ± 4.6	37.8 ± 3.2	7.0 ± 0.2	3.3 ± 0.1	1.9 ± 0.0

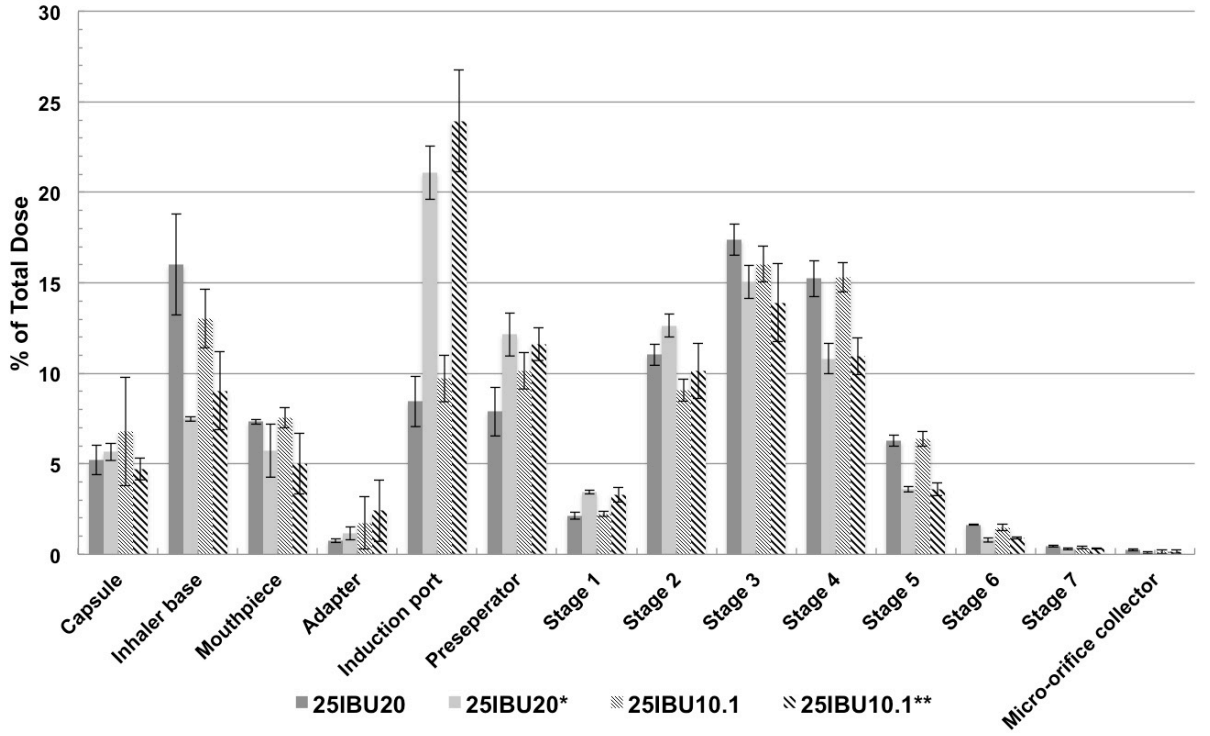

Figure 4.7: The *in vitro* aerodynamic performance of jet-milled ibuprofen formulations (25IBU20, 25IBU20*, 25IBU10.1, 25IBU10.1**) after air-jet milling and after 21 days (*) or 6 months (**) stored at room temperature in combination with the high-resistance Monodose RS01 at 4 kPa pressure drop (N=3). respirable fraction percentage (RF), emitted dose percentage (ED), fine particle fraction percentage (FPF), fine particle (< 5 μm) fraction percentage (FPF5μm), fine particle (< 3 μm) fraction percentage (FPF3μm), fine particle (< 1 μm) fraction percentage (FPF1μm), mass median aerodynamic diameter (MMAD), geometric standard deviation (GSD).

Formulation	RF (%)	ED (%)	FPF (%)	FPF5μm (%)	FPF3μm (%)	FPF1μm (%)	MMAD (μm)	GSD
IBU10.1	48.8 ± 2.9	72.6 ± 1.7	67.2 ± 4.5	67.6 ± 4.5	55.8 ± 3.8	13.0 ± 1.2	2.9 ± 0.0	1.8 ± 0.0
IBU10.1'	49.6 ± 1.1	75.4 ± 1.1	65.7 ± 2.4	66.3 ± 2.4	52.1 ± 1.1	12.5 ± 0.7	3.0 ± 0.0	1.9 ± 0.0
IBU10.1"	39.7 ± 4.7	72.1 ± 0.8	55.0 ± 6.1	55.5 ± 6.1	44.9 ± 4.1	10.7 ± 0.8	3.0 ± 0.1	1.9 ± 0.0

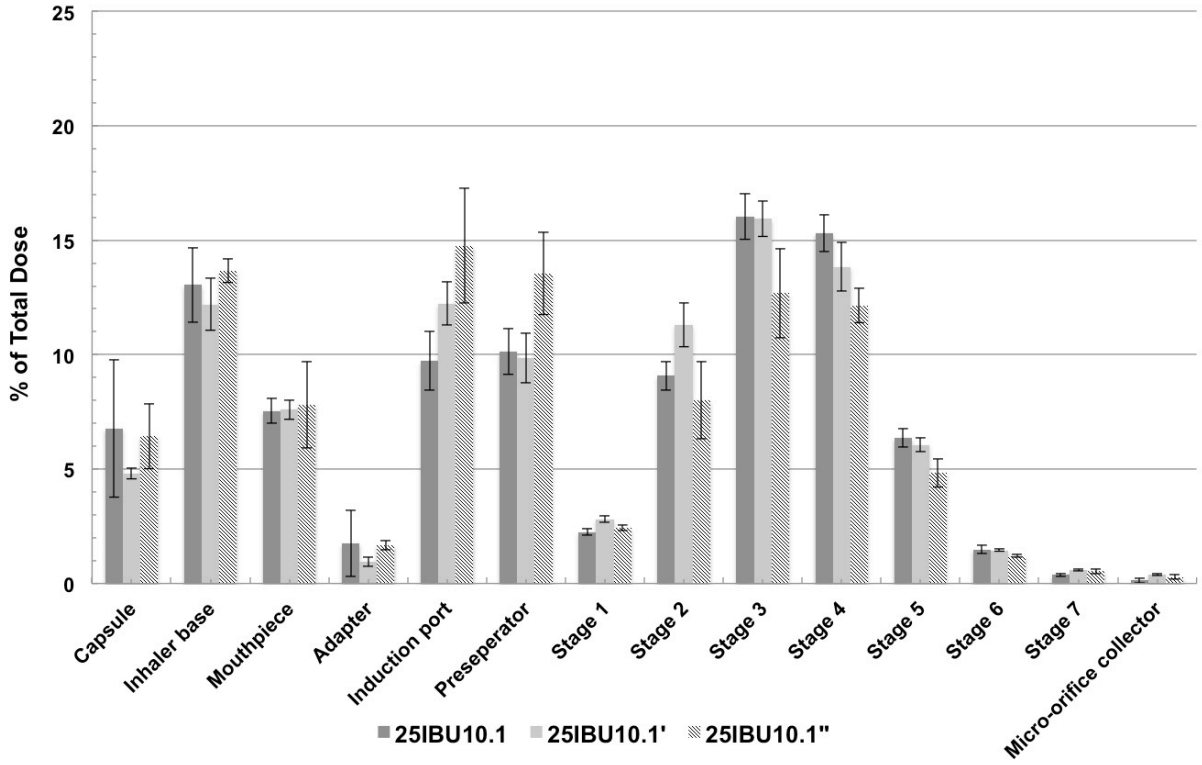

Figure 4.8: The *in vitro* aerodynamic performance of jet-milled ibuprofen formulations (25IBU10, 25IBU10', 25IBU10.1") after air-jet milling and after 24 hours outgassing with helium at room temperature (') or 30°C (") in combination with the high-resistance Monodose RS01 at 4 kPa pressure drop (N=3). respirable fraction percentage (RF), emitted dose percentage (ED), fine particle fraction percentage (FPF), fine particle (< 5 μm) fraction percentage (FPF5μm), fine particle (< 3 μm) fraction percentage (FPF3μm), fine particle (< 1 μm) fraction percentage (FPF1μm), mass median aerodynamic diameter (MMAD), geometric standard deviation (GSD).

Formulation	RF (%)	ED (%)	FPF (%)	FPF5μm (%)	FPF3μm (%)	FPF1μm (%)	MMAD (μm)	GSD
25IBU10.1	48.8 ± 2.9	72.6 ± 1.7	67.2 ± 4.5	67.6 ± 4.5	55.8 ± 3.8	13.0 ± 1.2	2.9 ± 0.0	1.8 ± 0.0
25IBU10.1**	39.9 ± 4.9	81.2 ± 3.4	49.1 ± 4.6	49.6 ± 4.6	37.8 ± 3.2	7.0 ± 0.2	3.3 ± 0.1	1.9 ± 0.0
25IBU10.2	51.5 ± 4.3	60.7 ± 4.7	84.8 ± 0.6	85.0 ± 0.6	78.5 ± 0.8	23.1 ± 1.1	2.3 ± 0.0	1.8 ± 0.0
25IBU10.2**	51.2 ± 3.4	65.9 ± 5.1	77.8 ± 0.9	78.2 ± 0.9	66.8 ± 1.9	17.0 ± 1.0	2.7 ± 0.1	1.8 ± 0.0

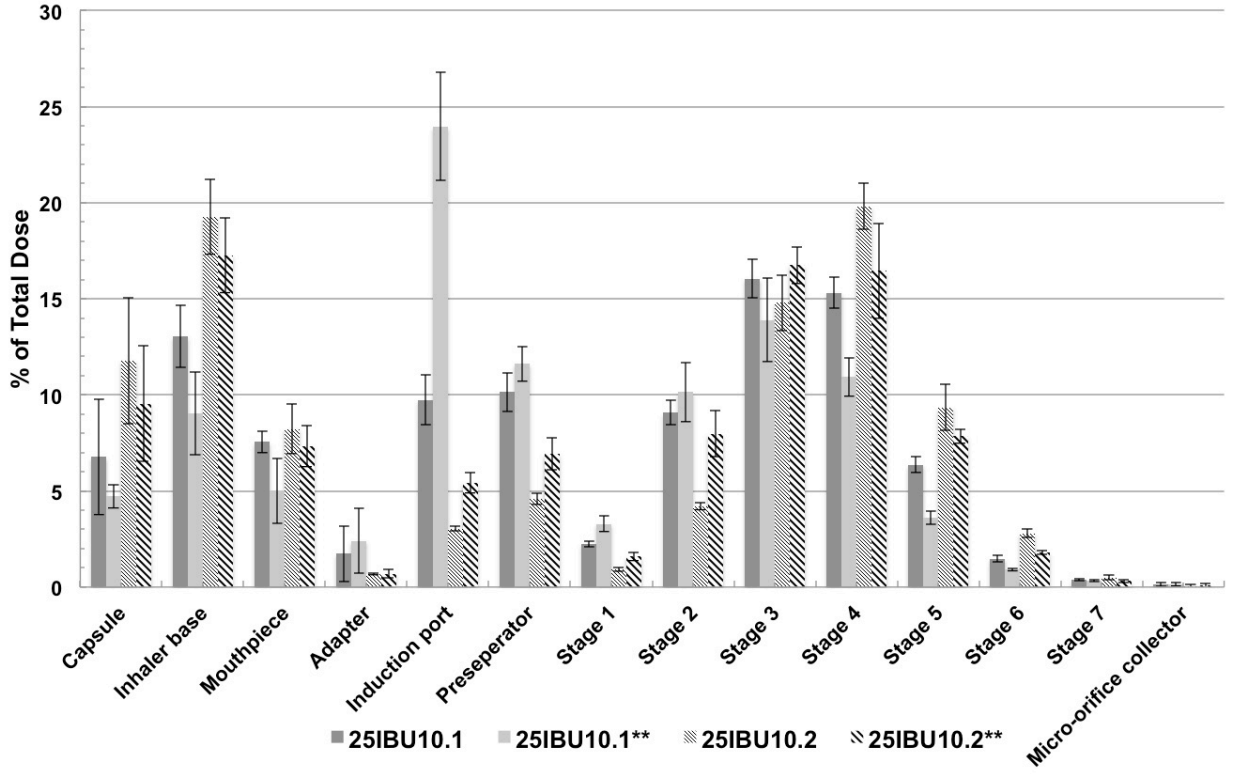

Figure 4.9: The *in vitro* aerodynamic performance of jet-milled ibuprofen formulations after air-jet milling (25IBU10.1, 25IBU10.2) and after 6 months (25IBU10.1**, 25IBU10.2**) stored at room temperature (IBU10.1), or at -80°C (IBU10.2) in combination with the high-resistance Monodose RS01 at 4 kPa pressure drop (N=3). respirable fraction percentage (RF), emitted dose percentage (ED), fine particle fraction percentage (FPF), fine particle (< 5 μm) fraction percentage (FPF5μm), fine particle (< 3 μm) fraction percentage (FPF3μm), fine particle (< 1 μm) fraction percentage (FPF1μm), mass median aerodynamic diameter (MMAD), geometric standard deviation (GSD).

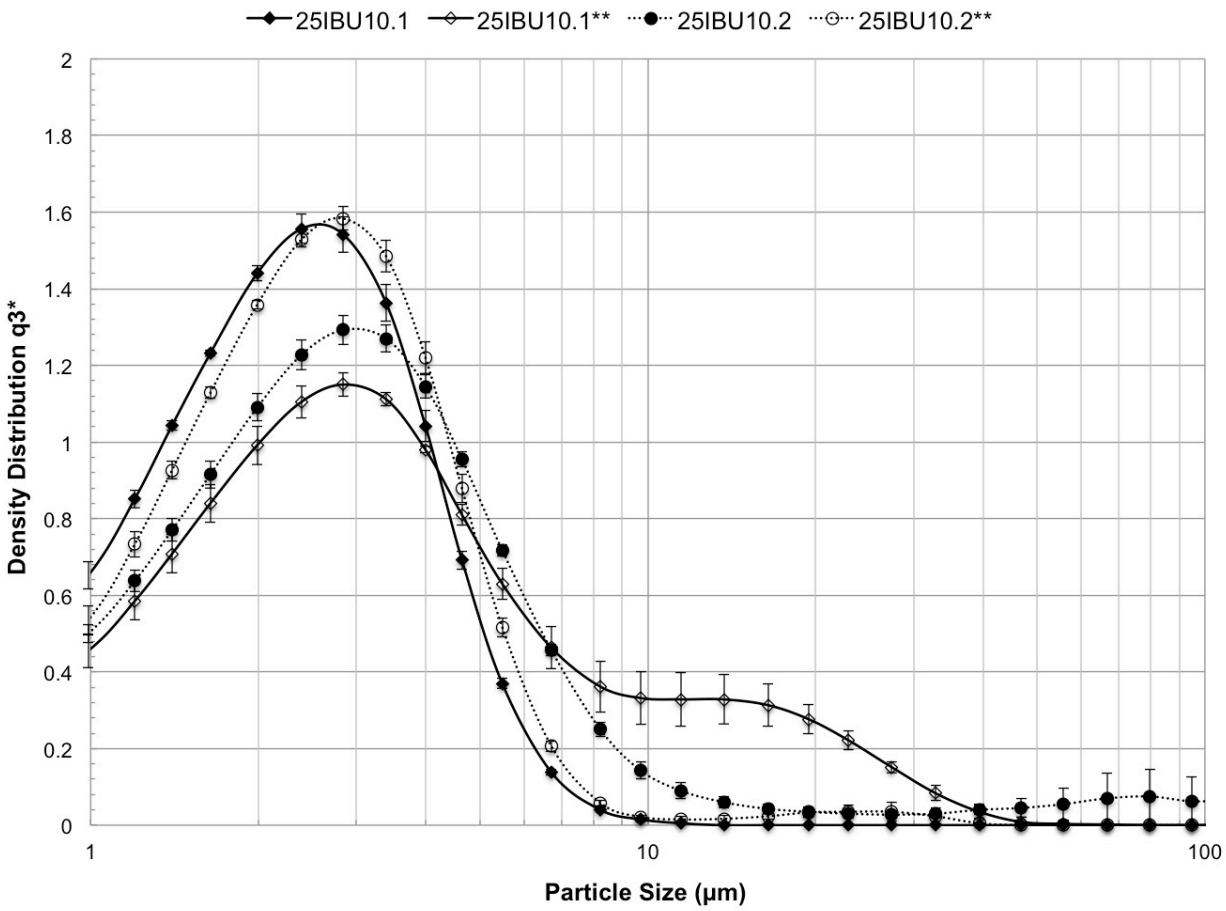

Figure 4.10: The particle size distributions of formulations after air-jet milling (25IBU10.1, 25IBU10.2) and after 6 months (25IBU10.1**, 25IBU10.2**) stored at room temperature (IBU10.1), or at -80°C (IBU10.2).

Table 4.1: The D_{10}, D_{50}, D_{90}, and span values for 5, 10, and 20 g batches of jet-milled ibuprofen (IBU5, IBU10.1, IBU10.2, IBU20).

Notation	Batch (g)	D_{10} (μm)	D_{50} (μm)	D_{90} (μm)	Span
IBU5	5	0.8	1.9	3.6	1.5
IBU10.1	10	0.9	2.2	4.2	1.5
IBU10.2	10	1.0	2.7	7.6	2.4
IBU20	20	1.1	2.7	6.0	1.8

Table 4.2: Dry powder inhaler capsule fill weights and experimental conditions for 5, 10, and 20 g batches of jet-milled ibuprofen (IBU5, IBU10.1, IBU10.2, IBU20) for the *in vitro* aerodynamic performance analysis studies.

Capsule fill weight	10 mg	25 mg	50 mg
IBU5	10IBU5	25IBU5	50IBU5
IBU10.1	-	25IBU10.1, 25IBU10.1** 25IBU10.1', 25IBU10.1"	-
IBU10.2		25IBU10.2, 25IBU10.2**	
IBU20	-	25IBU20, 25IBU20*	-

*/** Formulations were stored in a desiccator under vacuum for 21 days (*), or 6 months (**) at room temperature (IBU10.1, IBU20), or at -80° C (IBU10.2).

'/" Formulations were purged with helium for 24 h at room temperature ('), or at 30°C (").

Table 4.3: Sample characterization for the unmilled ibuprofen (IBU) and the 20 g batch of jet-milled ibuprofen (IBU20)

Sample	SSA (m^2/g)[a]	ρ (g/cm^3)[a]	ρ_B (g/cm^3)	ρ_T (g/cm^3)	HR	CI	Angle of Repose (°)[a]
Unmilled IBU	0.36 ± 0.01	1.14 ± 0.00	0.27	0.44	1.64	39.19	62.6 ± 2.9
IBU20	2.02 ± 0.20	1.15 ± 0.01	0.12	0.21	1.82	45.00	37.8 ± 5.0

[a] N=3, specific surface area (SSA), bulk density (ρ_B), tapped density (ρ_T), true density (ρ), compressibility index (CI) and Hausner ratio (HR)

CHAPTER V*

Hollow Crystalline Straws of Diclofenac for High-Dose and Carrier-Free Dry Powder Inhaler Formulations

Authors:

Ashkan K. Yazdi[a], Hugh D. Smyth[a]

[a] Division of Pharmaceutics, College of Pharmacy, The University of Texas at Austin, PHR 4.214, 2409 University Ave Stop A1920, Austin TX 78712-1119

Corresponding Author:

Ashkan K. Yazdi

Office: 512 471 4752

Fax: 512 471 7474

Email: ashkan.k.yazdi@utexas.edu

Keywords:

Air-jet milling, Precipitation, Diclofenac sodium, Diclofenac, Next generation impactor, Dry powder Inhaler

* This chapter has been published in the International Journal of Pharmaceutics and may be cited as: Yazdi, A.K., Smyth, H.D.C., 2016. Hollow crystalline straws of diclofenac for high-dose and carrier-free dry powder inhaler formulations. International Journal of Pharmaceutics 502, 170–180. doi:10.1016/j.ijpharm.2016.02.030

Abstract:

Objective: To crystallize diclofenac (DF) from diclofenac sodium (DFNa), to micronize DF and DFNa, and to evaluate *in vitro* aerodynamic performance of the jet-milled formulations

Material and methods: From the acidic titration of aqueous DFNa, DF crystals were formed and were identified using thermal analysis, spectroscopy, and X-ray powder diffraction. Following the micronization of the DF and DFNa powders, the recovered samples were imaged, and their particle size distributions were evaluated. Samples before and after jet millings were characterized, and *in vitro* aerodynamic performance testing was performed on the DF sample before jet milling and the DF and DFNa samples following jet milling.

Results and discussion: Hollow needles of DF were precipitated. With similar particle size distributions, the jet-milled DFNa sample from the collection bag, and the DF sample from the cyclone were used for further characterization. Despite different deposition patterns in the Next Generation Impactor, the DF hollow needles had a comparable respirable fraction percentage to the jet-milled DF and DFNa particles. However, the jet-milled DF formulation had the best *in vitro* aerodynamic performance.

Conclusions: Hollow, crystalline needles of DF were formed and possessed promising aerosol performance in comparison with the jet-milled powders.

1 Introduction

Diclofenac (DF) is a non-steroidal anti-inflammatory agent (NSAID) indicated for analgesia, osteoarthritis, rheumatoid arthritis, migraine, and other inflammatory disorders. It has been commonly formulated as its sodium and potassium salts, i.e. diclofenac sodium (DFNa) and diclofenac potassium. The DF salts are marketed as tablets, capsules, or solutions for oral administration, solutions for intravenous administration, solutions for ophthalmic administration, and as creams, gels, patches and solutions for topical administration (Lexi-Comp Inc., 2015).

Despite the availability of NSAIDs as over-the-counter (OTC) medications, there are multiple contraindications, black-boxed warnings, and general warnings regarding their use (Lexi-Comp Inc., 2015). Gastrointestinal adverse drug reactions (ADRs) such as an increased risk of upper gastrointestinal bleeding associated with the use of NSAIDs is well documented (Rodriguez and Jick, 1994). Two primary contraindications for the use of NSAIDs are the treatment of perioperative pain following coronary artery bypass graft surgery and the use in patients with moderate to severe renal impairment (Murray and Brater, 1993). Recently, the United States' Food and Drug Administration (FDA) strengthened their warning about the risk of NSAIDs causing heart attacks or stroke (Center for Drug Evaluation and Research, 2015). The risk of heart attacks and strokes is increased as early as the first few weeks of NSAID use, and risk level is drug-, dose- and duration-dependent. Finally, there is an increased risk of heart failure with NSAID use (Center for Drug Evaluation and Research, 2015).

Delivery via the lung represents a unique opportunity to circumvent the prostaglandin (PG) independent mucosal injury associated with the oral administration of NSAIDs, as it eliminates the direct GI exposures to these drugs (Islam and Gladki, 2008; Matsui et al., 2011). Furthermore, the pulmonary drug delivery route usually decreases the dose requirements by ten to twenty fold, especially for drugs acting locally on the lung (Labiris and Dolovich, 2003). Similarly to the topical delivery, reducing the systemic exposure via pulmonary drug delivery, allows for the minimization of the cardiovascular risks as well as the systemic PG-dependent, GI adverse effects associated with NSAIDs (Klinge and Sawyer, 2013; Wallace, 2008). Finally, the rapid onset times that are seen with pulmonary drug delivery for both local and systemic effects (Boss et al., 2012) are ideal for the patients, to whom NSAIDs are prescribed.

Typically with inhaled powders, such as inhaled corticosteroids and β adrenergic agonists, it has been found that the binary blends of micronized drug with a lactose carrier system significantly improve their performance (Hickey et al., 2007; Hira et al., 2010; Steckel and Bolzen, 2004). This type of formulation approach may not be feasible for inhaled NSAIDs. Despite the ten to twenty fold total dose reduction facilitated by local lung delivery of DF, the required doses will still be in the milligram range, greater than the upper limit for common binary dry powder inhaler formulations (Telko and Hickey, 2005). An example of a carrier-free inhaled product is the Tobi® Podhaler™, containing low-density spray dried particles, which are highly engineered (Novartis, 2013; Wilson et al., 2013). Particle engineering is the primary technique for improving

the aerosol performance of carrier-free dry powder inhaler (DPI) formulations, through the reduction of aerodynamic diameter. Equation 1 describes the relationship between the aerodynamic diameter (D_{ae}), the diameter of equivalent volume sphere (D_{eq}), the particle density (ρ_p), the unit density (ρ_o), and the dynamic shape factor (χ) (Telko and Hickey, 2005).

$$D_{ae} = D_{eq}\sqrt{\frac{\rho_p}{\rho_o \chi}} \qquad \textit{(Equation 1)}$$

Developed and patented by Nektar Therapeutics, PulmoSphere® particles are highly porous spherical particles with a geometric particle size of less than 5 μm. These particles, developed by spray-drying, are characterized by an aerodynamic particle size that is much lower than their geometric size, due to their low particle density (Vehring, 2008). DPI formulations were shown to possess a high lung deposition in patients, as measured by gamma scintigraphy (Newhouse et al., 2003). The Tobramycin PulmoSphere formulation was approved by the FDA in 2013, for the use with the Podhaler inhaler (Novartis, 2013). Additionally, a ciprofloxacin PulmoSphere formulation is in Phase III clinical trials under development by Bayer Schering Pharma AG and Novartis Pharmaceutical Corp. for use in non-cystic fibrosis bronchiectasis (Wilson et al., 2013).

Another potential particle property that could be utilized to improve the lung deposition is particle shape. As shown in Equation 1, needle shaped particles, where the χ value is greater than one (Hinds, 2012), possess smaller aerodynamic diameters in

comparison with particles of similar mass. However, they are associated with a poor flow and further formulation strategies such as a loose aggregate formation are needed to improve manufacturability (Ikegami et al., 2003).

In this study, we attempt to combine the benefits of hollow, low-density particles, with the advantages of needle-shaped particles, for the development of a high dose, carrier free formulation of DF. Our research hypothesis is that hollow, needle particles of DF, with a high aspect ratio, would have a comparable *in vitro* aerodynamic performance to micronized particles of DF and DFNa. This research investigated the particle morphology of DF in the forms of DF free acid and DFNa salt, as a carrier-free dry powder inhaler formulation for lung delivery. DF was prepared from DFNa utilizing the pH-dependent aqueous solubility of DF. Micronized formulations were produced via the jet milling of DF and DFNa, and their *in vitro* aerodynamic performances were evaluated using a Next Generation Impactor (NGI).

2 Materials and Methods

2.1 Formation of DF free acid from DFNa

For DF free acid formation experiments, hydrochloric acid (HCl) was purchased from Fisher Scientific (Pittsburgh, PA, USA) and the house dH_2O was used for preparing the solutions. A solution of 5.376 g of DFNa (Letco Medical, Decatur, Alabama, USA) was prepared in 1 L dH_2O to get a 0.5 % (w/v) concentration of DF in water. Using a burette, 2.5 N aqueous HCl was added to the DFNa solution dropwise, and the solution pH was obtained using an Accumet® Basic AB/15+ (Fisher Scientific, Pittsburgh, PA,

USA). Titration of the conjugate base of DF was continued until the solution reached a pH of 2.0. The precipitate was vacuum filtered and was dried overnight in a 40°C oven.

2.2 Jet milling of DF and DFNa

Model 00 Jet-O-Mizer™ (also known as Aljet mill, Fluid Energy, Telford, PA, USA) was used to micronize DF and DFNa. Aljet mill was configured according to the schematic in Figure 5.1. Jet milling parameters were optimized in unpublished work and were previously disclosed in a patent application pertaining to carrier-free high-dose formulations of non-steroidal anti-inflammatory agents. The jet-milling parameters are as followed: the feed pressure of 65 psi, the grind pressure of 75 psi, the feed rate of 1 g/min, and the batch size of 5 g. Jet-milled powder samples were collected in scintillation vials and were stored in a desiccator under vacuum from different sections of the jet mill (Figure 5.1) including: the tube after grinding chamber (bfC), the cyclone (C), the collection vessel adapter (D), the collection bag adapter (E), the collection vessel (G), and the collection bag (H). Following powder collection and weighing of scintillation vials with known tare weights, total yield, and individual recovery percentages were calculated. Temperature and relative humidity were measured using a SRH77A thermo-hygrometer by Cooper-Atkins Instrument Corporation (Middlefield, CT, USA).

2.3 Scanning Electron Microscopy (SEM)

Samples were mounted on standard aluminum SEM stubs, were sputter coated with 15 nm platinum/palladium (Pt/Pd) using a Cressington sputter coater 208 HR

(Cressington Scientific Instruments Ltd., Watford, UK) and were imaged using a Zeiss Supra 40VP SEM (Carl Zeiss Microscopy GmbH, Jena, Germany).

2.4 Particle size distribution (PSD) analysis by Laser light diffraction

PSDs of DF and DFNa samples from the bfC, C, D, E, G, and H segments were analyzed before and after jet milling using a Sympatec HELOS, equipped with a CUVETTE module (System-Partikel-Technik GmbH, Clausthal-Zellerfeld, Germany). Tween 20 and Sodium Lauryl Sulfate (SLS) were purchased from Fisher Scientific (Fisher Scientific, Pittsburgh, PA, USA), and house dH_2O was used for preparing solutions. For DF, about 2 mg of DF was dispersed in 0.5 mL of 0.1 % (w/v) SLS in water and the sample was sonicated for 5 minutes. Reference measurement was done on acidified 50 mL of 0.005 % (v/v) Tween 20 in water with 50 μL of 2.5 N HCl in water. For DFNa, about 2 mg of DFNa was dispersed in 0.5 mL of 0.1 % (v/v) Span 85 in light mineral oil and the dispersion was sonicated for 5 minutes. A reference measurement was done in 0.1 % (v/v) Span 85 in light mineral oil. After a reference measurement, aliquots of 50 μL of sonicated suspension were added to achieve optical concentrations of 10 – 20 % for a total of six measurements.

Furthermore, D_{10}, D_{50}, and D_{90} values were defined as 10 %, 50 %, and 90 % of the particle size below the respective values. Span was calculated according to the following formula:

$$Span = \frac{D_{90} - D_{10}}{D_{50}} \qquad \textit{(Equation 2)}$$

Normalized cumulative PSDs were composed of yield-normalized distributions, where they were depicted as stacked bar charts. D_{90}, D_{50}, and D_{10} values for normalized cumulative PSDs were calculated by approximating particle sizes associated with 90 %, 50 %, and 10 % area of the stacked bar chart. The approximated values from this method were validated with the D_{90}, the D_{50}, and the D_{10} values for a single distribution by the Sympatec software.

2.5 Thermal analysis

Thermograms were obtained using an Auto Q20 (TA Instruments-Waters LLC, New Castle, DE, USA) differential scanning calorimeter (DSC) controlled by TA Advantage Software (TA Instruments-Waters LLC, New Castle, DE, USA) and equipped with a RCS40 (TA Instruments-Waters LLC, New Castle, DE, USA) refrigerated cooling system with nitrogen purge of 50 mL/min. About 4 mg of samples were loaded in standard DSC pans (DSC Consumables Inc., Austin, MN, USA) and were crimped using a Tzero sample press (TA Instruments-Waters LLC, New Castle, DE, USA). Samples were heated at the rate of 10°C/min from 30°C to 300°C.

2.6 Fourier transform infrared spectroscopy (FT-IR)

FT-IR spectra were obtained using a Nicolet™ iS™50 FT-IR Spectrometer (Thermo Fisher Scientific Inc., Madison, WI, USA) equipped with a germanium Attenuated Total Reflection (ATR) accessory and a pressure tower for the stock and jet-milled powder.

2.7 X-Ray Powder Diffraction (XRD)

Two-dimensional X-Ray diffractograms of DF and DFNa before jet milling were obtained using an automatic R-Axis Spider (Rigaku Corporation, Tokyo, Japan), an X-ray single crystal diffractometer controlled by RINT Rapid software with the target radiation of Copper at 40 KV voltage and 40mA current. Samples for analysis were suspended in light mineral oil and were loaded on loops epoxied to conventional goniometer bases. Additionally, a background X-Ray diffractogram of light mineral oil loaded on a loop was subtracted from the samples' diffractograms, one-dimensional 2θ diffractograms were generated, and .txt files were saved using 2DP Software (Ragaku Corporation, Tokyo, Japan). To analyze the one-dimensional diffractograms using Jade (Ragaku Corporation, Tokyo, Japan), .raw files were generated from .txt files using ConvX.exe (Mark Bowden, Industrial Research Ltd., Lower Hutt, New Zealand).

2.8 Powder Characterization

2.8.1 Brunauer-Emmett-Teller (BET) specific surface area measurements

Specific surface areas were evaluated via a single-point BET method using a Monosorb® surface area analyzer (Quantrachrome Instruments; FL, USA) following 24 hours outgassing with helium at room temperature before each measurement in triplicates. Samples weighed at least 50 mg for the jet-milled powders depending on availability and 500 mg for the stock samples.

$$Specific\ surface\ area = \frac{surface\ area}{mass} \qquad \textit{(Equation 3)}$$

2.8.2 Helium pycnometry

True densities were measured using a MVP-D160-E multipycnometer (Quantrachrome Instruments; FL, USA). For density measurements, the micro cell and the micro cell adapter were used, and samples weighed at least 0.1 g for jet-milled powders depending on availability and at least 0.6 g for the stocks samples.

2.8.3 Angle of repose

The angle of repose measurements were done triplicate according to the United States Pharmacopoeia (USP) method (USP Chapter <1174>, 2014). Images of the powder mounds were taken using a digital camera and were analyzed using the ImageJ software (Wayne Rasband, Research Services Branch, National Institute of Mental Health, Bethesda, MD, USA).

2.8.4 Bulk and tapped density measurements

The tapped density (ρ_T) calculations were performed using a tapped density tester (Agilent Technologies, Santa Clara, CA, USA) with a modified method from the USP (USP Chapter <1174>, 2014) for a small mass of powder. In this modified method, a 10 mL graduated cylinder fitted with a molded adapter substituted the 100 mL graduated cylinder for the calculations of the bulk density (ρ_B) and the use in the tapped density tester. The compressibility index (CI) and the Hausner ratio (HR) calculations were performed according to the following formulas:

$$CI = 100 \times \frac{\rho_T - \rho_B}{\rho_B} \qquad \textit{(Equation 4)}$$

$$HR = \frac{\rho_B}{\rho_T} \qquad \textit{(Equation 5)}$$

2.8.5 Karl-Fischer moisture analysis

The Moisture content of stock powder and jet-milled powders were measured in triplicates using a Photovolt Aquatest™ 2010a Moisture Analyser (a.k.a. The CSC Aquapal III, CSC Scientific Inc., Fairfax, VA, USA). Powder moisture contents were calculated by subtracting the moisture content in 1 mL of anhydrous methanol (Fisher Scientific, Pittsburgh, PA, USA) from the moisture content reading from 5 mg powder dissolved in 1 mL of anhydrous methanol.

2.9 Quantitative sample analysis by ultraviolet-visible spectroscopy

Ultraviolet absorbance was measured using a Tecan® Infinite® 200 PRO multimode microplate reader (Tecan Systems, Inc. San Jose, CA, USA) using either a cuvette or Costar® Corning® 96-well UV-transparent plate. Ultraviolet-visible absorbance scans were performed at wavelengths of 230 – 1000 nm at the resolution of 2 nm. Additionally, absorbance scans were performed at similar ranges for an ethanol blank, and absorbance differences were plotted against the wavelength and in the Microsoft Excel®. Standard concentration curves were prepared for DF and DFNa. Wavelength with maximum absorbance was used for such measurements. Regression lines were forced through zero, and the R^2 values were evaluated.

2.10 *In vitro* aerodynamic performance testing

For the *in vitro* aerodynamic performance testing, the dry powder inhaler device was a high resistance monodose RS01, a generous gift from Plastiape S.p.a., (Osnago,

Italy). Vcaps No. 3 HPMC capsules were generous donations from Capsugel Inc. (Morristwon, New Jersey, USA). *In vitro* aerodynamic performance of jet-milled powder was assessed using the NGI (MSP Corporation, MN, USA) attached sequentially to a Whatman® HEPA filter (GE Healthcare Bio-Sciences, Pittsburg, PA, USA), a volumetric digital flow meter (TSI 4000 Series, TSI Performance Measurement Tools, Shoreview, MN, USA), a home-built two-way solenoid valve timer box, and a high capacity vacuum pump (HCP5, Copley Scientific Limited, Nottingham, UK). For these studies, a high-resistance Monodose RS01 dry powder inhaler device was loaded with an HPMC capsule containing 10 mg of micronized powder. Prior to impactions, the pre-separator was loaded with 15 mL of ethanol and the NGI stages were coated with 5 mL of 1 % (v/v) of silicon oil in hexane and a silicon oil coat was formed on the stages with hexane evaporation. Furthermore, the device resistance was calculated using a dosage unit sampling apparatus according to an abbreviated Apparatus B from USP Chapter 601 (Yazdi and Smyth, 2015) and based on the calculated device resistance, flow rate creating a 4 KPa pressure drop across the dry powder inhaler was calculated. Temperature and relative humidity were measured using an SRH77A thermo-hygrometer by Cooper-Atkins Instrument Corporation (Middlefield, CT, USA). *In vitro* aerodynamic performance of carrier free formulations were evaluated at the calculated flow rate for a total volume of 4 L per USP Chapter 601, Apparatus 5 for Inhalation Powders in triplicates (USP General Chapter <601>, 2009). The dry powder inhaler capsule, the inhaler base, the mouthpiece, and the adapter were each washed twice with 5 mL of

ethanol, and the 10 mL washes from each were stored in 15 mL centrifuge tubes for quantitative sample analysis. Accordingly, the induction port, the stages 1 – 7, and the micro-orifice collector (MOC) were each washed twice with 5 mL of ethanol and the 10 mL washes were collected as described. Finally, the pre-separator was washed with 10 mL of ethanol, and a total of 25 mL wash was collected.

Following the quantification of the drug mass in each fraction, the emitted dose percentage (ED%) is defined as the percentage of the entire dose depositing downstream from the mouthpiece of the dry powder inhaler where the entire dose is the total recovered drug mass in all the fractions. The respirable fraction percentage (RF%) is defined as the percentage of the entire dose deposited on stages two through seven plus the MOC. The fine particle fraction percentage (FPF%) is defined as the percentage of the emitted dose deposited on the stages two through seven plus the MOC. Fine particle fraction (< 5 μm) percentage (FPF5μm %), fine particle fraction (< 3 μm) percentage (FPF3μm %), and fine particle fraction (< 1 μm) percentage (FPF1μm %) are calculated from the cumulative % of the emitted dose deposited downstream of the NGI stage versus the particle cutoff size of the stage graph and correspond to the percentage of the emitted dose predicted to have the aerodynamic diameter below 5, 3, and 1 μm respectively.

3 Results

3.1 Formation of DF free acid from DFNa

With the addition of less than 1 mL of 2.5 N HCl to the aqueous solution of DFNa, a white precipitate of DF was formed. Vacuum filtration and overnight drying in the oven yielded a soft cake of white powder. Physicochemical characterization confirmed the presence of the DF free acid.

3.2 Jet milling of DF and DFNa

Jet milling was conducted at relative humidity levels between 48-55 % and temperatures of around 24°C. Following the jet milling of 5g batches, recovery percentages from various sections of the jet mill was determined and are shown in Table 5.1. There was a 70.6% total recovery associated with DFNa and a 63.6% total recovery associated with DF, with the majority of particles deposited in the primary cyclone. When comparing DF and DFNa deposition on the different components of the jet mill, there were noticeable differences in the percentage recovery from the cyclone, the collection vessel, and the collection bag.

3.3 Scanning Electron Microscopy (SEM)

Un-micronized DFNa was composed of relatively irregularly shaped particles with surface adhered fine particles. Precipitated DF particles were hollow needles with smooth surfaces and cross-sections below 5μm, thicknesses of 0.5 μm and an average length of 20 μm. The Jet-milled DFNa and DF particles were more similar concerning their PSD, as they both were composed of fine particles no larger than 3μm. However,

the jet-milled DF particles had a smoother surface than the jet-milled DFNa particles (5. 3).

3.4 PSD analysis

Powders collected from different sections of the jet mill were associated with different PSD (Figure 5.3). In 5. 2, D_{10}, D_{50}, D_{90}, and span values are compared for: the normalized cumulative particle size distribution of the jet-milled DFNa versus DF, the stock DFNa versus DF, as well as the collection bag fraction of jet-milled DFNa versus the cyclone fraction of jet-milled DF. The D_{50} and the span (2.36 μm and 1.41) associated with the cumulative particle size distribution for the jet-milled DF were smaller than the D_{50} and the span (3.25 μm and 1.61) for the jet-milled DFNa (Figure 5.4). Due to the comparable median particle size for the collection bag fraction from the jet milling of DFNa, and the cyclone fraction from the jet milling of DF (2.72 μm vs. 2.61 μm), these fractions were chosen for further characterization and *in vitro* performance analysis, and will be referred as jet-milled DFNa and jet-milled DF hereinafter.

3.5 Thermal analysis

DSC thermograms of the DFNa and the jet-milled DFNa powders (Figure 5.5) possessed two endotherms at 286.66°C and 293.88°C. DSC thermograms of the DF and the jet-milled DF powder possess a single endotherm at 181.73°C, corresponding to the melting point of DF.

3.6 FT-IR

Peaks associated with the FT-IR spectra of DF and jet-milled DF, as well as DFNa and jet-milled DFNa, overlapped. In the DFNa spectrum, the 1557.57 cm^{-1} and the 1574.88 cm^{-1} peaks were associated with the carboxylate group stretching; however, the 1690.81 cm^{-1} peak in the DF spectrum was associated with a carboxylic acid stretching. Furthermore, the DF spectrum contained a 938.39 cm^{-1} peak corresponding to the O – H bending and the ~3320 cm^{-1} peak associated with the O – H stretching, both absent in DFNa spectrum (Figure 5.6).

3.7 XRD

Background subtracted X-ray diffractograms for DF and DFNa were associated with different peaks and did not overlap.

3.8 Powder characterization

Table 5.3 summarizes the bulk, the tapped, and the true density as well as the BET SSA, the angle of repose, and the moisture content determined by Karl-Fischer titration. Following jet milling, HR and CI calculations of flow showed no significant changes in flow for DF (1.88 and 46.67 vs. 2.08 and 51.85); however, they showed improved flow from very, very poor to fair flow for DFNa (1.83 and 45.24 vs. 1.22 and 18.18). The angle of repose improved from 48.7 ± 5.5 to 26.3 ± 1.7 following jet milling for DFNa, improving the flow property of the powder from poor to excellent according to the USP. On the other hand, the angle of repose remained good according to the USP

classification (34.5 ± 2.3 vs. 31.2 ± 1.2) following jet milling for DF (USP Chapter <1174>, 2014).

3.9 *In vitro* aerodynamic performance testing

Device resistance calculations were performed previously (Yazdi and Smyth, 2015) on a high-resistance Monodose RS01 dry powder inhaler for the device alone, the device loaded with an empty capsule and 10 mg powder mass and device resistances were 0.0393, 0.0348, 0.0347 $kPa^{0.5}$x min/L. The resistance of 0.034 $kPa^{0.5}$x min/L was used to calculate the flow rate of 58.8 L/min that creates a 4 KPa pressure drop. Duration of 4.08 s at the flow rate of 58.8 L/min corresponded to 4 L air required per USP for the *in vitro* testing of formulations and inhalers. *In vitro* aerodynamic performance NGI testing was conducted at relative humidity and temperature of 52% and 24°C for jet-milled DFNa; 41% and 23.7°C for jet-milled DF; and 40% and 24°C for DF. The quantitative sample analysis of DF and DFNa were performed at the maximum UV absorbance of 282 nm for DFNa and the maximum UV absorbance of 278 nm for DF. Percent depositions of the total dose for the different stages of the NGI are shown in Figure 5.7, and key parameters for performance evaluation are shown in Table 5.4.

4 Discussion

In the current study, DF free acid was precipitated due to its pH-dependent solubility from an aqueous solution of DFNa according to the following formulas:

$$Diclofenac\ sodium \rightarrow Diclofenac^{-}(aq) + Na^{+} \quad \textit{(Equation 6)}$$

$$HCl \rightarrow H^{+} + Cl^{-} \quad \textit{(Equation 7)}$$

$$Diclofenac^{-}(aq) + H^{+} \rightarrow Diclofenac(s) \quad \textit{(Equation 8)}$$

SEM revealed the tubular (i.e. hollow acicular, hollow needle) crystal habit of DF free acid. Previously, Beck et al. employed a similar technique to prepare the free acid of DF; however, following precipitation, DF was recrystallized from a 1:1 ethanol/water solution (Beck et al., 2008). To the best of our knowledge, the current study is the first report on DF crystals with hollow needle morphology and the first report for the formation of these crystals using a single solvent system where tubular crystals are formed only by changing pH. There are other reports of this crystal habit in the literature for other drug substances (Eddleston and Jones, 2010; Ulrich et al., 2013; Xiao et al., 2005). Eddleston and Jones reported the conditions required for the formation of tubular crystal habit for caffeine, carbamazepine, carbamazepine dihydrate and theophylline monohydrate. The formation of the cavities is attributed to the diffusion limited conditions at the center of the growing needle crystal, "where crystal growth is more rapid than the diffusion of molecules to the most rapidly growing face of the crystal" (Eddleston and Jones, 2010).

The DSC, the FT-IR, and the XRD data confirm the identity of DF free acid. In Figure 5.5A, the DSC thermogram of DFNa possesses two endotherms at 286.66°C and 293.88°C, which correspond to a literature value of 284.3°C. On the other hand, in Figure 5.5B, the DSC thermogram of DF possesses a single endotherm at 181.73°C with no evidence of DFNa endotherm corresponding to the reported melting point of DF (Llinàs et al., 2007). In the FT-IR spectrum of DFNa (Figure 5.6A), the 1557.57 cm^{-1} and the 1574.88 cm^{-1} peaks are associated with the carboxylate group stretching; however, the 1690.81 cm^{-1} peak in the DF spectrum (Figure 5.6B) was associated with the carboxylic acid stretching. Furthermore, DF spectrum is associated with the 938.39 cm^{-1} peak corresponding to the O – H bending and the ~3320 cm^{-1} peak associated with the O – H stretching, a bond present in the free acid, but not the sodium salt, thereby confirming the formation of DF free acid from DFNa (Beck et al., 2008; Cabaniss and McVey, 1995). Finally, the X-ray diffractogram for DF is compared with the literature, and its identity is verified as the free acid (Llinàs et al., 2007).

Through micronization, DFNa went through a six-fold particle size reduction (19.5 to 3.25 μm); however, DF went through an only three-fold particle size reduction (6.98 to 2.36 μm). Differences in crystal strength and brittleness led to the varying extents of particle size reductions observed for DF and DFNa, despite the similar attrition energy used for jet milling (Kubavat et al., 2012; Saleem and Smyth, 2010; Shariare et al., 2011). DFNa is an ionic compound with a higher melting point than DF, which is an organic compound with a lower melting point. Therefore, DFNa requires a higher energy

input to achieve a similar particle size. Comparisons of the PSD results for DFNa and DF should be interpreted with caution, considering that the dispersion media for the laser diffraction were different due to the water solubility of DFNa compared to the pH-dependent solubility of DF. Furthermore, the starting PSD was much smaller for DF compared to DFNa (Figures 5.3 – 5.4, Table 5.2). Additionally, PSD analysis by laser diffraction also has limitations for non-spherical particles. The hollow straws of DF have a high aspect ratio, and the assumptions required by the principle of measurement for this instrument may not be valid.

Regarding the characterization of samples (Table 5.3), the jet-milled DF and DFNa possessed increased SSA compared with DF and DFNa. The abnormally high SSA value of 11.3 ± 0.81 m^2/g for the jet-milled DFNa is clearly an overestimation of SSA since the jet-milled DF with smaller particle size has an SSA of 2.40 ± 0.21 m^2/g. This overestimation of SSA for the jet-milled DFNa is due to the possible formation of a multilayer adsorbate and its condensation on the jet-milled DFNa particles (Bae et al., 2010; Zalepugin et al., 2010). Regarding the true densities, the DF density of 1.48 g/cm^3 corresponded to the literature true density for the denser polymorph of DF (Castellari and Ottani, 1997). The DFNa density of 1.51 g/cm^3 seems to be the first report of the true density for DFNa. Higher true densities were calculated for the jet-milled powders; however, that can be attributed to the low sample mass, the moisture content, and the smaller particle size of the powder. An improved angle of repose, as an indicator for improved flow properties of DFNa following jet milling, can be due to the agglomeration

and the moisture content of the micronized powder. On the other hand, the similar angle of repose for the DF powder following jet milling can be attributed to the small initial size of the DF particles (D_{50} = 6.98 μm) and the presence of agglomerates before jet milling. Following jet milling, HR and CI calculations of flow showed worsening flow for DF; however, they showed improved flow from very poor to fair flow for DFNa.

During jet milling, different percent recoveries in the cyclone, the collection vessel, and the collection bag can be attributed to the smoother, smaller particles of DF compared with DFNa, as the DF particles have a higher degree of adhesion to the surface of the cyclone and cohesion together. Different PSDs for the various segments of the jet mill indicate that particles distribute differently in jet mills as they do in impactors.

There were no detectable transformations of DF and DFNa following jet milling by FT-IR and DSC. Overlapping peaks associated with the FT-IR spectra of DF and jet-milled DF as well as DFNa and jet-milled DFNa signify that following jet milling, the chemical composition of DF and DFNa were not altered. Finally, the similar DSC thermograms for DF, and jet-milled DF, as well as DFNa, and jet-milled DFNa signify that there are no detectable polymorphic changes after the jet milling of DF and DFNa.

As illustrated in Figure 5.7, similar masses of drugs remained in the capsules for DF, and jet-milled DF and DFNa. However, there was a significantly larger mass of jet-milled DFNa deposited in the inhaler base and the mouthpiece compared to DF and jet-milled DF. These differences are not due to the jet-milled DFNa PSD, as its D_{50} value is between the D_{50} for the DF powder and the jet-milled DF powder. Such a deposition

difference may be due to the higher moisture content of DFNa as shown in Table 5.3. Moreover, there were significant differences in the induction port and the pre-separator deposition between the three formulations. Smooth surfaces of the jet-milled DF and DF needles led to increased adhesion to the NGI surfaces and increased cohesion and the agglomeration of particles compared to the rough surface of the jet-milled DFNa (Kubavat et al., 2012). Furthermore, the larger particle size of the DF needles compared with the jet-milled DF and DFNa may be a contributing factor. Such a difference might also be partly due to the drug entrapment in the inhaler base and the mouthpiece for the jet-milled DFNa compared to the jet-milled DF. Furthermore, the jet-milled DFNa fines that reach the NGI stages have the smallest MMAD followed by the jet-milled DF and DF. Particle size reduction through jet milling for DF yielded a formulation with an overall better *in vitro* aerodynamic performance as opposed to the unprocessed DF. However, when comparing the RF% for the three formulations, DF and jet-milled DFNa have a comparable RF%. Even though jet-milled DF does not have the smallest MMAD, it is associated with the largest RF% at 41.7%. The DF hollow needles are remarkable as they are relatively long; however, due to being hollow and being needles have a relatively small MMAD and comparable RF% to the jet-milled powders.

The carrier-free formulation of DF with the 3 mg respirable dose (RF% = 30%) roughly equals to 10% of the 35 mg mass of commercialized DF currently marketed as Zorvolex® (Iroko Pharmaceuticals, LLC, 2013), the estimated theoretical respiratory dose requirements. In 2013, DF was approved for the first time as a capsule containing 18 mg

or 35 mg of DF free acid under the brand name of Zorvolex with a similar pharmacodynamic profile to the higher doses of DF salts. This formulation of DF contains submicron particles of DF free acid to improve dissolution rate, which is dry-milled using the patented SoluMatrix^{TM} technology, developed by iCeutica Pty. Inc. Particle size reduction was achieved using multiple grinding bodies with diameters of 1-15 mm and aggregation was prevented by adding a grinding matrix, which can be separated before further processing, or be formulated into final formulation (Dodd et al., 2014).

As it was discussed in the introduction, one can reduce the aerodynamic diameter by manipulating the dynamic shape factor through needle particle engineering (Ikegami et al., 2003) and decreasing the particle density through the creation of porous particles (Vehring, 2008). The carrier-free, hollow needle formulation of DF, consisting of particles with a high aspect ratio, possesses both the described attributes and was shown to have a good MMAD and a comparable RF% to the jet-milled DF and DFNa. The delivery of the carrier-free formulation to the lung lowers the total dosage requirement and decreases the ADRs associated with the oral delivery of the DF. However, the DF formulation needs to be optimized to minimize the RF% variability and the deposition in the induction port and pre-separator.

5 Conclusion

The DF hollow, crystalline needles were precipitated, characterized, and their *in vitro* aerodynamic performance was compared with the jet-milled DF and DFNa using

NGI. The Jet-milled DF and DFNa with similar PSDs had different deposition patterns in the NGI. However, the DF hollow needles with a large aspect ratio proved to have a comparable RF% to the jet-milled DF and DFNa particles. For a carrier-free, DPI formulation, this formulation can reach deep lungs to act locally, or systemically with reduced ADRs through decreased total dose requirements.

6 Acknowledgements

Authors would like to thank Dr. Kristin Fathe for assistance in editing and reviewing this manuscript.

7 References

Bae, Y.-S., Yazaydın, A.Ö., Snurr, R.Q., 2010. Evaluation of the BET Method for Determining Surface Areas of MOFs and Zeolites that Contain Ultra-Micropores. Langmuir 26, 5475–5483. doi:10.1021/la100449z

Beck, R.C.R., Lionzo, M.I.Z., Costa, T.M.H., Benvenutti, E.V., Ré, M.I., Gallas, M.R., Pohlmann, A.R., Guterres, S.S., 2008. Surface morphology of spray-dried nanoparticle-coated microparticles designed as an oral drug delivery system. Braz. J. Chem. Eng. 25, 389–398. doi:10.1590/S0104-66322008000200016

Boss, A.H., Petrucci, R., Lorber, D., 2012. Coverage of Prandial Insulin Requirements by Means of an Ultra-Rapid-Acting Inhaled Insulin. J. Diabetes Sci. Technol. 6, 773–779. doi:10.1177/193229681200600406

Cabaniss, S.E., McVey, I.F., 1995. Aqueous infrared carboxylate absorbances: aliphatic monocarboxylates. Spectrochim. Acta. A. Mol. Biomol. Spectrosc. 51, 2385–2395. doi:10.1016/0584-8539(95)01479-9

Castellari, C., Ottani, S., 1997. Two Monoclinic Forms of Diclofenac Acid. Acta Crystallogr. Sect. C 53, 794–797. doi:10.1107/S0108270197002126

Center for Drug Evaluation and Research, 2015. Drug Safety and Availability - FDA Drug Safety Communication: FDA strengthens warning that non-aspirin nonsteroidal anti-inflammatory drugs (NSAIDs) can cause heart attacks or strokes [WWW Document]. URL http://www.fda.gov/Drugs/DrugSafety/ucm451800.htm (accessed 8.27.15).

Dodd, A., Meiser, F., Norret, M., Russell, A., Bosch, H.W., 2014. Formulation of diclofenac. US8679544 B2.

Eddleston, M.D., Jones, W., 2010. Formation of Tubular Crystals of Pharmaceutical Compounds. Cryst. Growth Des. 10, 365–370. doi:10.1021/cg900969n

Hickey, A.J., Mansour, H.M., Telko, M.J., Xu, Z., Smyth, H.D.C., Mulder, T., McLean, R., Langridge, J., Papadopoulos, D., 2007. Physical characterization of component particles included in dry powder inhalers. II. Dynamic characteristics. J. Pharm. Sci. 96, 1302–1319. doi:10.1002/jps.20943

Hinds, W.C., 2012. Aerosol Technology : Properties, Behavior, and Measurement of Airborne Particles, 2nd ed. Wiley, Hoboken.

Hira, D., Okuda, T., Kito, D., Ishizeki, K., Okada, T., Okamoto, H., 2010. Inhalation Performance of Physically Mixed Dry Powders Evaluated with a Simple Simulator for Human Inspiratory Flow Patterns. Pharm. Res. 27, 2131–2140. doi:10.1007/s11095-010-0215-6

Ikegami, K., Kawashima, Y., Takeuchi, H., Yamamoto, H., Mimura, K., Mamose, D., Ouchi, K., 2003. A new agglomerated KSR-592 beta-form crystal system for dry powder inhalation formulation to improve inhalation performance in vitro and in vivo. J. Controlled Release 88, 23–33. doi:10.1016/S0168-3659(02)00460-1

Iroko Pharmaceuticals, LLC, 2013. Zorvolex (R) [package insert].

Islam, N., Gladki, E., 2008. Dry powder inhalers (DPIs)—A review of device reliability and innovation. Int. J. Pharm. 360, 1–11. doi:10.1016/j.ijpharm.2008.04.044

Klinge, S.A., Sawyer, G.A., 2013. Effectiveness and Safety of Topical Versus Oral Nonsteroidal Anti-inflammatory Drugs: A Comprehensive Review. Phys. Sportsmed. 41, 64–74. doi:10.3810/psm.2013.05.2016

Kubavat, H.A., Shur, J., Ruecroft, G., Hipkiss, D., Price, R., 2012. Influence of primary crystallisation conditions on the mechanical and interfacial properties of micronised budesonide for dry powder inhalation. Int. J. Pharm. 430, 26–33. doi:10.1016/j.ijpharm.2012.03.020

Labiris, N.R., Dolovich, M.B., 2003. Pulmonary drug delivery. Part I: Physiological factors affecting therapeutic effectiveness of aerosolized medications. Br. J. Clin. Pharmacol. 56, 588–599. doi:10.1046/j.1365-2125.2003.01892.x

Lexi-Comp Inc., 2015. Diclofenac [WWW Document]. URL http://online.lexi.com.ezproxy.lib.utexas.edu/lco/action/doc/retrieve/docid/patch_f/1772963 (accessed 8.26.15).

Llinàs, A., Burley, J.C., Box, K.J., Glen, R.C., Goodman, J.M., 2007. Diclofenac Solubility: Independent Determination of the Intrinsic Solubility of Three Crystal Forms. J. Med. Chem. 50, 979–983. doi:10.1021/jm0612970

Matsui, H., Shimokawa, O., Kaneko, T., Nagano, Y., Rai, K., Hyodo, I., 2011. The pathophysiology of non-steroidal anti-inflammatory drug (NSAID)-induced mucosal injuries in stomach and small intestine. J. Clin. Biochem. Nutr. 48, 107–111. doi:10.3164/jcbn.10-79

Murray, M.D., Brater, D.C., 1993. Renal Toxicity of the Nonsteroidal Anti-Inflammatory Drugs. Annu. Rev. Pharmacol. Toxicol. 33, 435–465. doi:10.1146/annurev.pa.33.040193.002251

Newhouse, M.T., Hirst, P.H., Duddu, S.P., Walter, Y.H., Tarara, T.E., Clark, A.R., Weers, J.G., 2003. Inhalation of a dry powder tobramycin PulmoSphere formulation in healthy volunteers. Chest 124, 360–366. doi:10.1378/chest.124.1.360

Novartis, 2013. Tobi Podhaler (R) [Package insert].

Rodriguez, L.A.G., Jick, H., 1994. Risk of upper gastrointestinal bleeding and perforation associated with individual non-steroidal... Lancet 343, 769.

Saleem, I.Y., Smyth, H.D.C., 2010. Micronization of a Soft Material: Air-Jet and Micro-Ball Milling. AAPS PharmSciTech 11, 1642–1649. doi:10.1208/s12249-010-9542-5

Shariare, M.H., de Matas, M., York, P., 2011. Effect of crystallisation conditions and feedstock morphology on the aerosolization performance of micronised salbutamol sulphate. Int. J. Pharm. 415, 62–72. doi:10.1016/j.ijpharm.2011.05.043

Steckel, H., Bolzen, N., 2004. Alternative sugars as potential carriers for dry powder inhalations. Int. J. Pharm. 270, 297–306. doi:10.1016/j.ijpharm.2003.10.039

Telko, M.J., Hickey, A.J., 2005. Dry Powder Inhaler Formulation. Respir. Care 50, 1209–1227.

Ulrich, J., Schuster, A., Stelzer, T., 2013. Crystalline coats or hollow crystals as tools for product design in pharmaceutical industry. J. Cryst. Growth, The 5th Asia Conference on Crystal Growth and Crystal Technologies 362, 235–237. doi:10.1016/j.jcrysgro.2011.10.060

USP Chapter <1174>, 2014. <1174> Powder flow, in: US Pharmacopeial Convention, Rockville, MD, USA. pp. 1051–54.

USP General Chapter <601>, 2009. Aerosols, Nasal Sprays, Metered Dose Inhalers, and Dry Powder Inhalers, in: US Pharmacopeial Convention, Rockville, MD, USA.

Vehring, R., 2008. Pharmaceutical Particle Engineering via Spray Drying. Pharm. Res. 25, 999–1022. doi:10.1007/s11095-007-9475-1

Wallace, J.L., 2008. Prostaglandins, NSAIDs, and Gastric Mucosal Protection: Why Doesn't the Stomach Digest Itself? Physiol. Rev. 88, 1547–1565. doi:10.1152/physrev.00004.2008

Wilson, R., Welte, T., Polverino, E., Soyza, A.D., Greville, H., O'Donnell, A., Alder, J., Reimnitz, P., Hampel, B., 2013. Ciprofloxacin dry powder for inhalation in non-cystic fibrosis bronchiectasis: a phase II randomised study. Eur. Respir. J. 41, 1107–1115. doi:10.1183/09031936.00071312

Xiao, Y., Liu, Y., Mi, Y., Yuan, D., Zhang, J., Cheng, L., 2005. A Simple Route to Form Straw-like Carbon Microbundles. Chem. Lett. 34, 1422–1423. doi:10.1246/cl.2005.1422

Yazdi, A.K., Smyth, H.D.C., 2015. Effect of Capsule Fill Weight on Device Resistance in Dry Powder Inhalers, in: Respiratory Drug Delivery. CRC Press Boca Raton, pp. 523–528.

Zalepugin, D.Y., Tilkunova, N.A., Fronchek, E.V., Gallyamov, M.O., Chernyshova, I.V., Mishin, V.S., Yashin, Y.S., Grigoryev, T.E., Gamzazade, A.I., Khokhlov, A.R., 2010. Production of new haemostatic materials by deposition of dispersed proteins onto porous matrices using supercritical carbon dioxide. Russ. J. Phys. Chem. B 4, 1047–1050. doi:10.1134/S1990793110070018

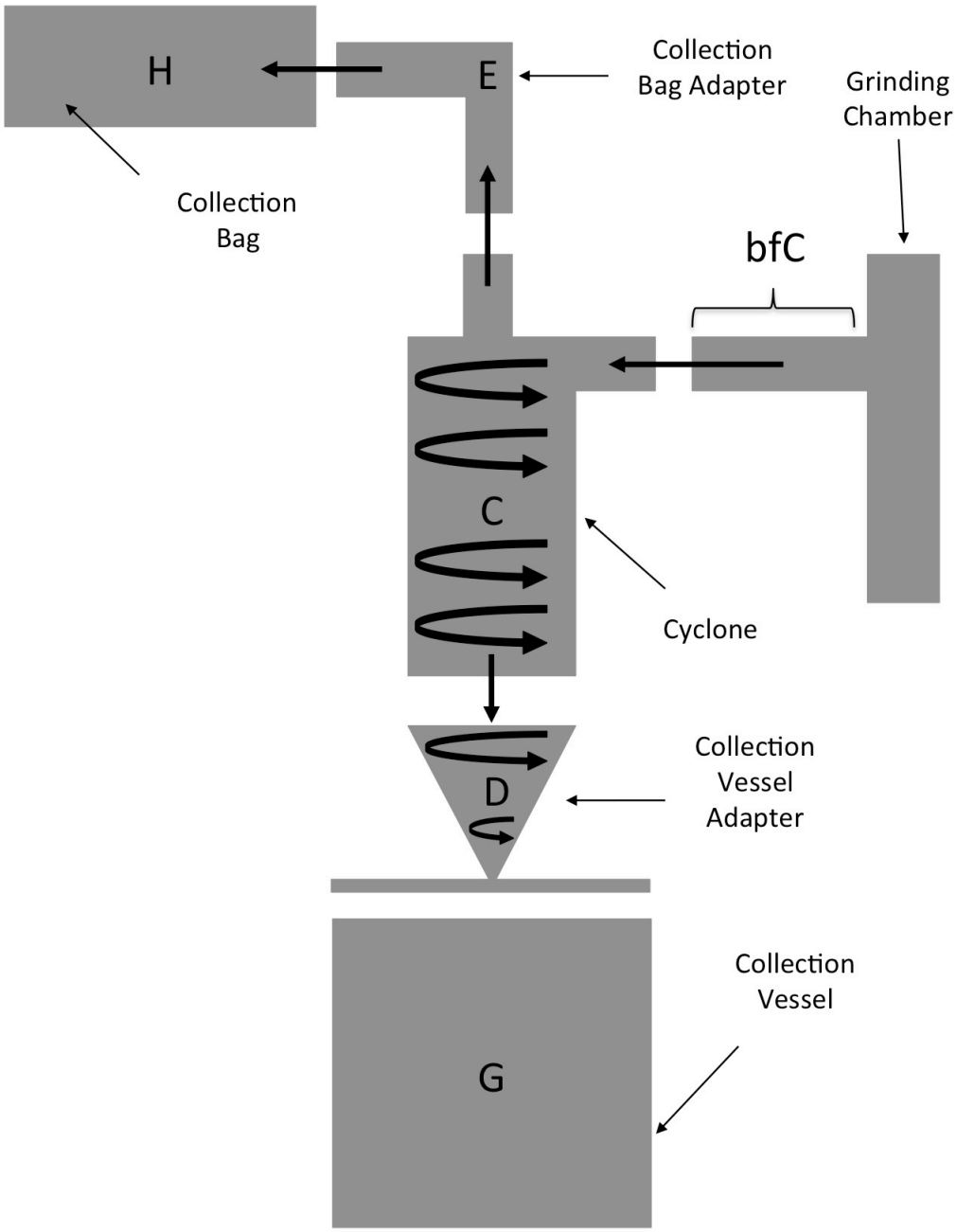

Figure 5.1: Schematic of Aljet mill configuration and setup

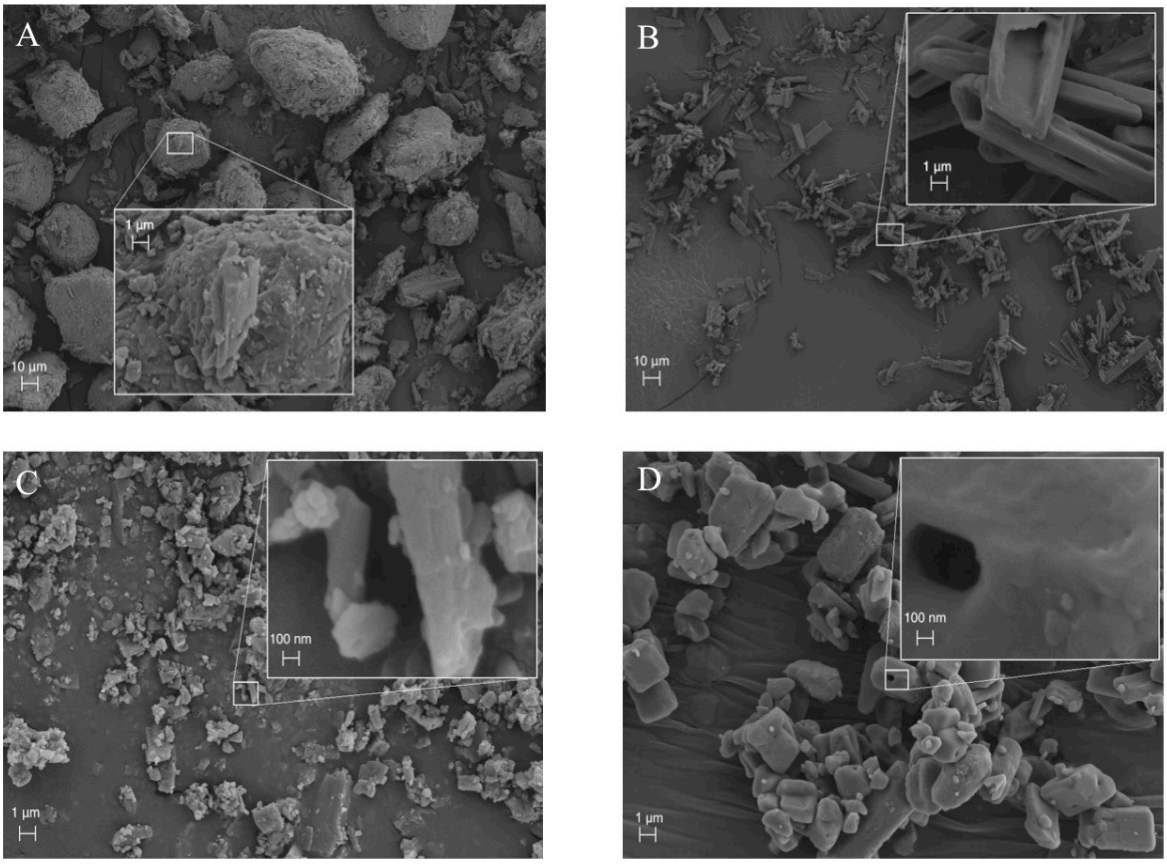

Figure 5.2: A) Unprocessed diclofenac sodium, B) Unprocessed diclofenac, C) Jet milled diclofenac sodium, D) Jet milled diclofenac

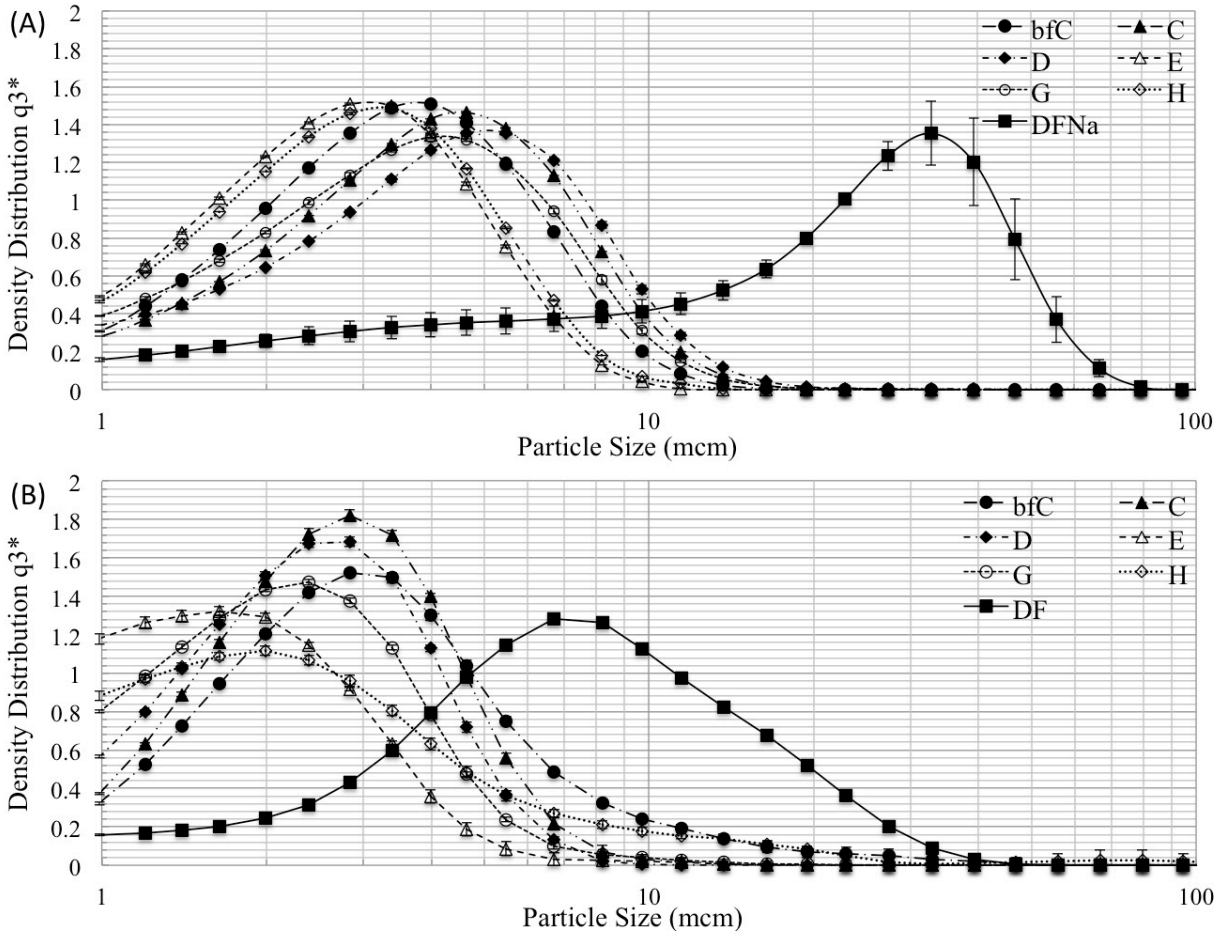

Figure 5.3: Particle size distributions of (A) diclofenac sodium (DFNa) and (B) diclofenac (DF) samples from different sections of Jet mill including: tube after grinding chamber (bfC), cyclone (C), collection vessel adapter (D), collection bag adapter (E), collection vessel (G), and collection bag (H).

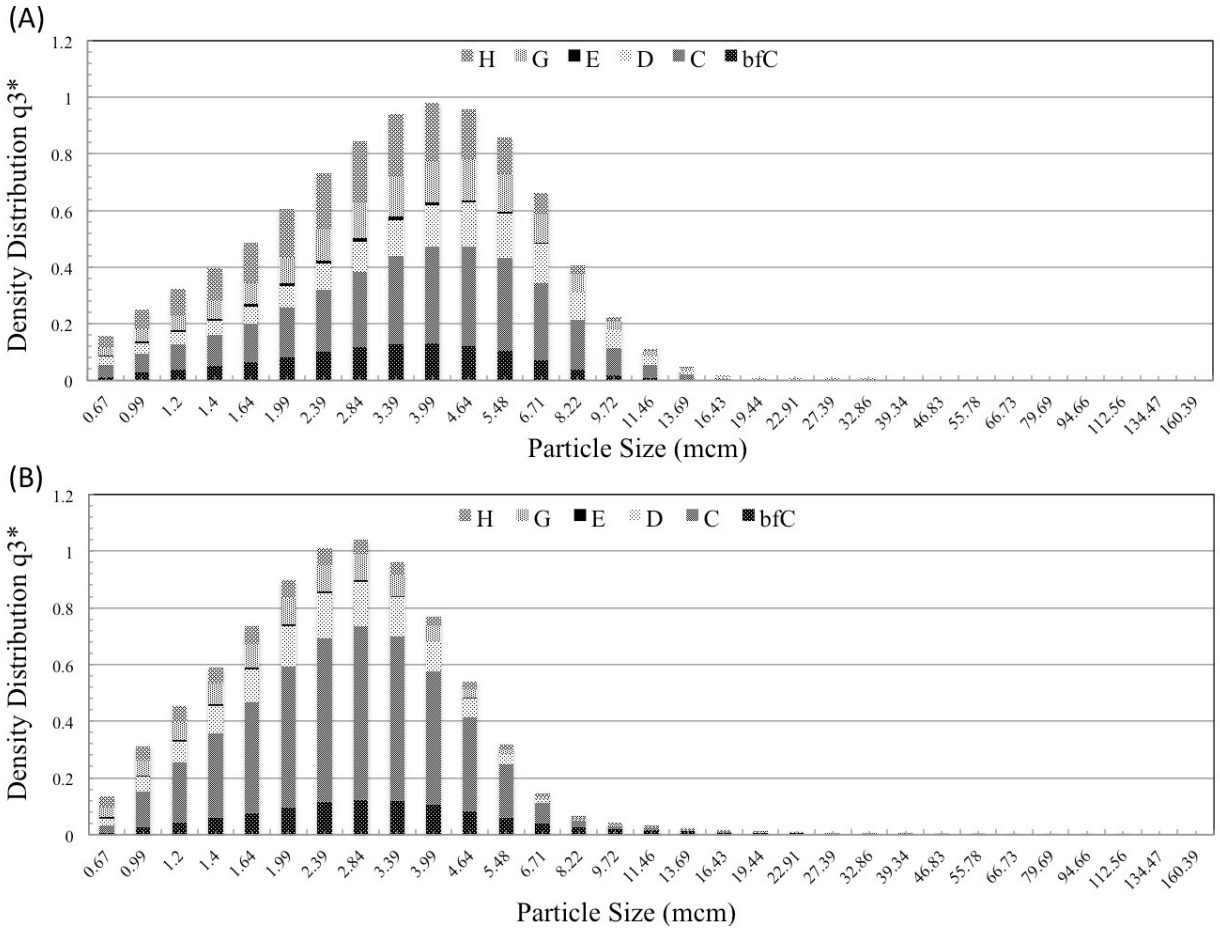

Figure 5.4: Yield normalized cumulative particle size distribution of (A) diclofenac sodium and (B) diclofenac from different sections of Jet mill including: tube after grinding chamber (bfC), cyclone (C), collection vessel adapter (D), collection bag adapter (E), collection vessel (G), and collection bag (H).

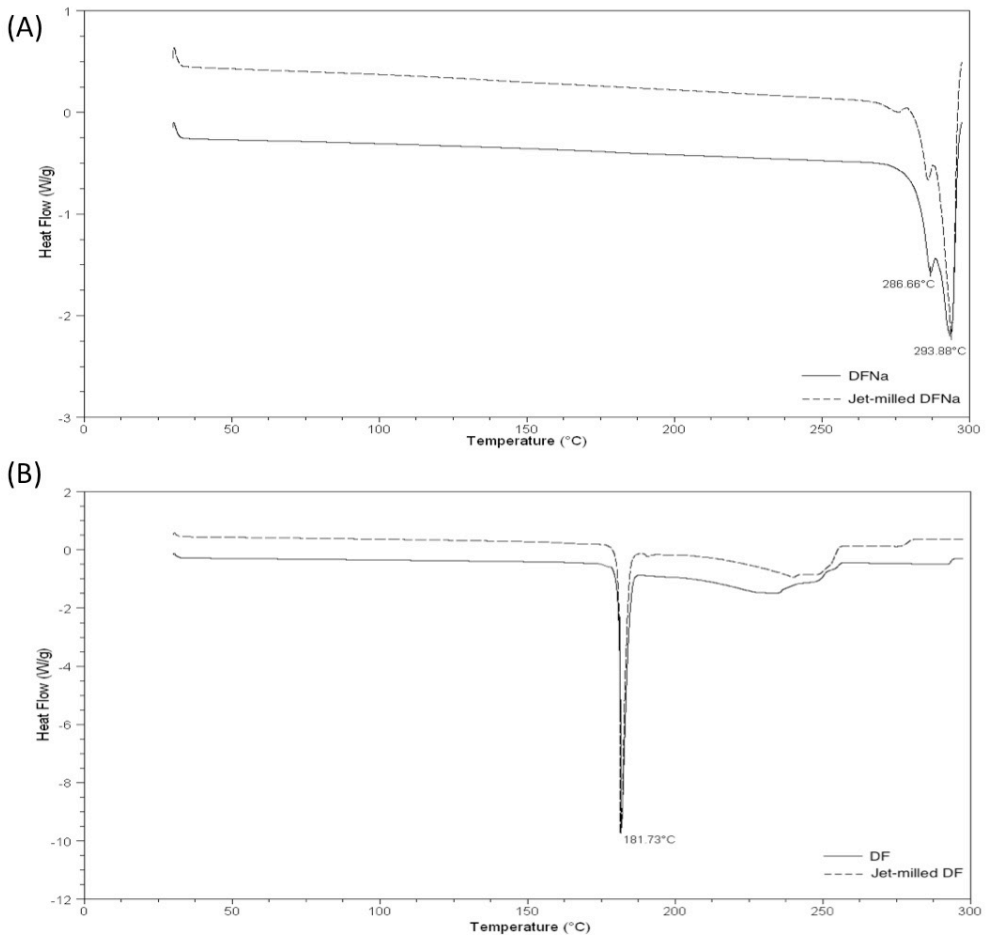

Figure 5.5: DSC thermograms of unprocessed and jet-milled (A) diclofenac sodium (DFNa) and (B) diclofenac (DF)

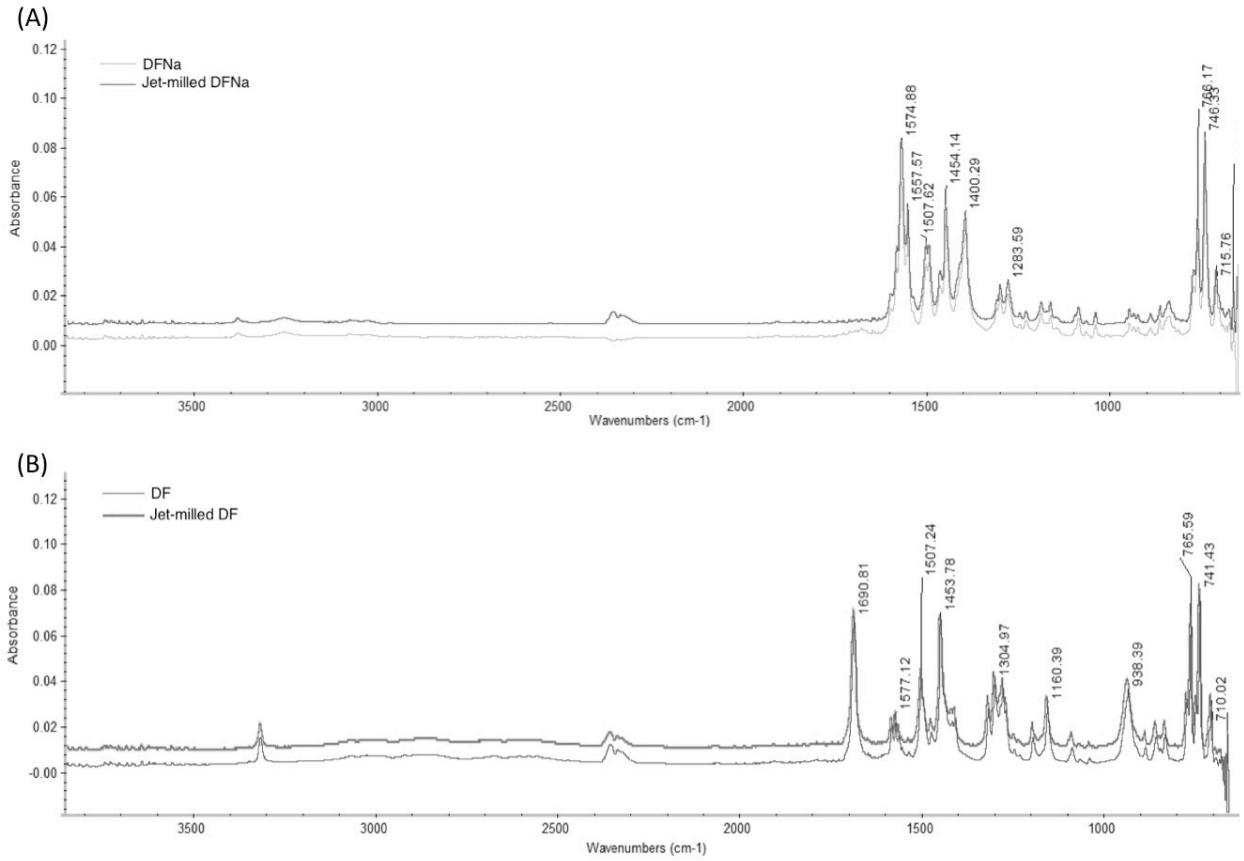

Figure 5.6: FT-IR spectra associated with unprocessed and jet-milled (A) diclofenac sodium (DFNa) and (B) diclofenac (DF)

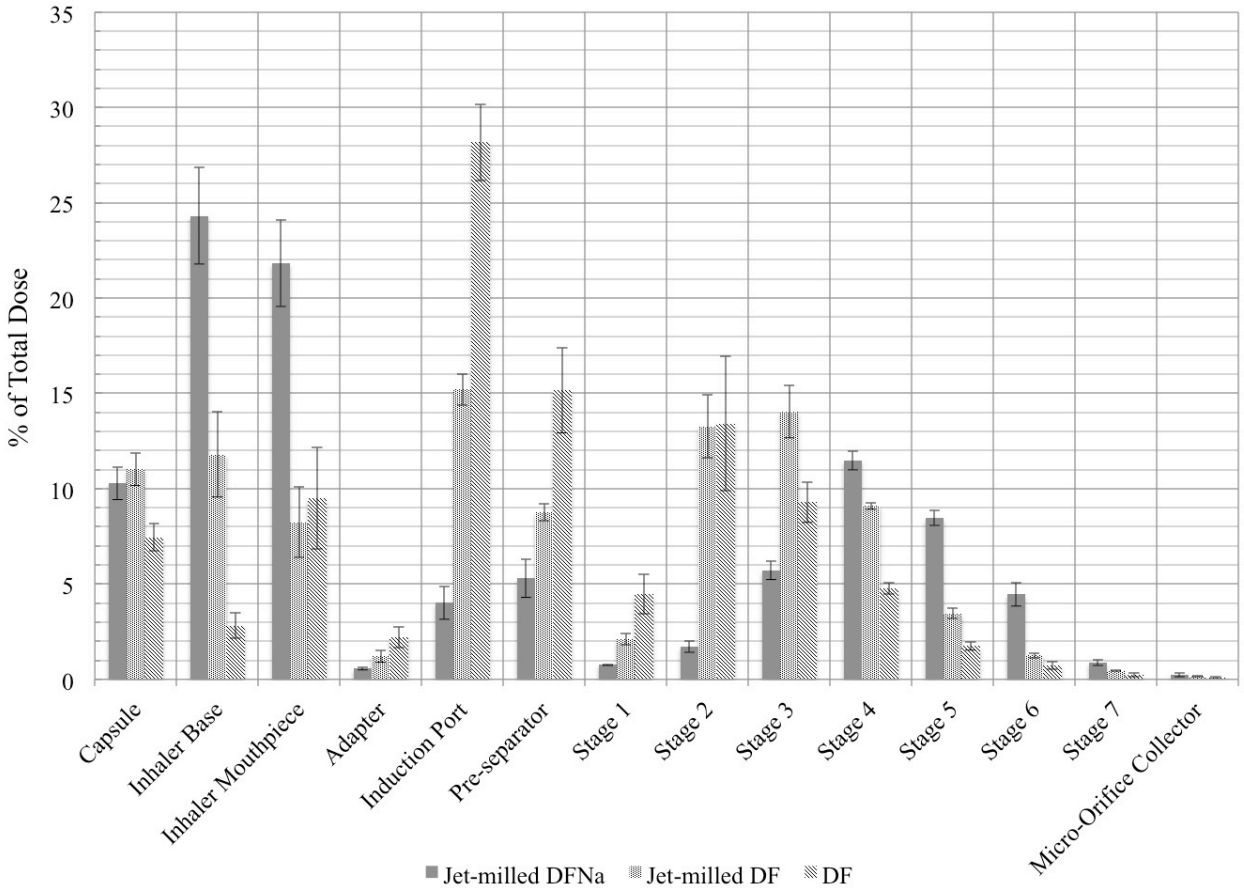

Figure 5.7: In-vitro aerodynamic performance of carrier-free formulations of 10 mg diclofenac (DF), jet-milled DF and jet-milled diclofenac sodium (DFNa) at 4 KPa pressure drop across high-resistance Monodose RS01 (N=3)

Table 5.1: % recovery from different sections of the jet mill including: tube after grinding chamber (bfC), cyclone (C), collection vessel adapter (D), collection bag adapter (E), collection vessel (G), and collection bag (H) for 5 g batches of (A) diclofenac sodium and (B) diclofenac

	bfC	C	D	E	G	H
Diclofenac sodium	8.7	23.9	11.5	0.8	11.1	14.6
Diclofenac	8.0	33.6	9.4	0.4	6.5	5.6

Table 5.2: D_{10}, D_{50}, D_{90}, and span associated with relevant samples of diclofenac sodium (DFNa) vs. diclofenac (DF)

	DFNa vs. DF	**D_{10} (μm)**	**D_{50} (μm)**	**D_{90} (μm)**	**Span**
Normalized cumulative particle size distribution of jet-milled DFNa vs. DF	DFNa	1.29	3.25	6.53	1.61
	DF	1.16	2.36	4.48	1.41
Stock DFNa vs. DF	DFNa	2.02	19.5	42.69	2.08
	DF	2.00	6.98	17.34	2.20
Collection bag from jet-milled DFNa vs. cyclone from jet-milled DF	Jet milled DFNa	1.06	2.72	5.52	1.64
	Jet milled DF	1.31	2.61	4.73	1.31

Table 5.3: Summary table of Powder characterization

Samples	SSA (m^2/g)*	Moisture Content (%)*	ρ (g/cm^3)*	ρ_B (g/cm^3)	ρ_T (g/cm^3)	HR	CI	Angle of Repose (°)*
DF	1.73 ± 0.17	0.78 ± 0.18	1.48 ± 0.01	0.16	0.30	1.88	46.67	34.5 ± 2.3
Jet milled DF	2.40 ± 0.21	0.45 ± 0.10	1.53 ± 0.02	0.12	0.26	2.08	51.85	31.2 ± 1.2
DFNa	1.37 ± 0.20	1.88 ± 0.20	1.51 ± 0.00	0.38	0.69	1.83	45.24	48.7 ± 5.5
Jet milled DFNa	11.3 ± 0.81	2.99 ± 0.10	1.68 ± 0.04	0.17	0.20	1.22	18.18	26.3 ± 1.7

*N=3, Specific Surface Area (SSA), Bulk density (ρ_B), Tapped density (ρ_T), True density (ρ), Compressibility Index (CI) and Hausner Ratio (HR)

Table 5.4: Summary table of parameters for 10 mg diclofenac (DF), jet-milled DF and jet-milled diclofenac sodium (DFNa) carrier-free formulation *in vitro* aerodynamic performance at 4 kPa pressure drop across high-resistance Monodose RS01.

FORMULATION	RF %	ED %	FPF%	FPF5μm%	FPF3μm %	FPF1μm %	MMAD	GSD
Jet-milled DFNa	32.9 ± 1.0	43.6 ± 0.8	75.6 ± 3.3	75.9 ± 3.3	72.0 ± 3.8	34.0 ± 3.0	1.9 ± 0.1	2.0 ± 0.0
Jet-milled DF	41.7 ± 3.5	68.9 ± 2.9	60.4 ± 2.8	60.8 ± 2.8	43.0 ± 1.5	8.6 ± 0.3	3.1 ± 0.1	2.1 ± 0.0
DF	30.3 ± 5.1	80.3 ± 3.5	37.7 ± 5.6	38.4 ± 5.7	22.5 ± 1.9	3.9 ± 0.6	4.2 ± 0.1	2.2 ± 0.1

N=3, respirable fraction percentage (RF%), emitted dose percentage (ED%), particle fraction percentage (FPF%), fine particle fraction (< 5 μm) percentage (FPF5μm %), fine particle fraction (< 3 μm) percentage (FPF3μm %), fine particle fraction (< 1 μm) percentage (FPF1μm %), mass median aerodynamic diameter (MMAD), geometric standard deviation (GSD) for diclofenac (DF), jet-milled DF, and jet-milled diclofenac sodium (DFNa).

REFERENCES

Adams, W.P., Lee, S.L., Plourde, R., Lionberger, R.A., Bertha, C.M., Doub, W.H., Bovet, J.-M., Hickey, A.J., 2012. Effects of device and formulation on in vitro performance of dry powder inhalers. Aaps J. 14, 400–409. doi:10.1208/s12248-012-9352-7

Agent, P., Parrott, H., 2015. Inhaled therapy in cystic fibrosis: agents, devices and regimens. Breathe 11, 111–118. doi:10.1183/20734735.021014

Alhalaweh, A., Velaga, S.P., 2010. Formation of Cocrystals from Stoichiometric Solutions of Incongruently Saturating Systems by Spray Drying. Cryst. Growth Des. 10, 3302–3305. doi:10.1021/cg100451q

Am Ende, D.J., Brenek, S.J., 2004. Strategies to control particle size during crystallization processes. Am Pharm Rev 7, 98–104.

Amidon, G.L., Lennernäs, H., Shah, V.P., Crison, J.R., 1995. A Theoretical Basis for a Biopharmaceutic Drug Classification: The Correlation of in Vitro Drug Product Dissolution and in Vivo Bioavailability. Pharm. Res. 12, 413–420. doi:10.1023/A:1016212804288

Bae, Y.-S., Yazaydın, A.Ö., Snurr, R.Q., 2010. Evaluation of the BET Method for Determining Surface Areas of MOFs and Zeolites that Contain Ultra-Micropores. Langmuir 26, 5475–5483. doi:10.1021/la100449z

BASF Group, n.d. Ibuprofen.

Beck, R.C.R., Lionzo, M.I.Z., Costa, T.M.H., Benvenutti, E.V., Ré, M.I., Gallas, M.R., Pohlmann, A.R., Guterres, S.S., 2008. Surface morphology of spray-dried nanoparticle-coated microparticles designed as an oral drug delivery system. Braz. J. Chem. Eng. 25, 389–398. doi:10.1590/S0104-66322008000200016

Beinborn, N.A., Lirola, H.L., Williams III, R.O., 2012. Effect of process variables on morphology and aerodynamic properties of voriconazole formulations produced by thin film freezing. Int. J. Pharm. 429, 46–57. doi:10.1016/j.ijpharm.2012.03.010

Benson, S.W., Ellis, D.A., 1948. Surface Areas of Proteins. I. Surface Areas and Heats of Absorption1. J. Am. Chem. Soc. 70, 3563–3569.

Bentham, A.C., Kwan, C.C., Boerefijn, R., Ghadiri, M., 2004. Fluidised-bed jet milling of pharmaceutical powders. Powder Technol., Pharmaceutical Particle Formation 141, 233–238. doi:10.1016/j.powtec.2004.01.024

Bhala, N., Emberson, J., Merhi, A., Abramson, S., Arber, N., Baron, J.A., Bombardier, C., Cannon, C., Farkouh, M.E., FitzGerald, G.A., Goss, P., Halls, H., Hawk, E., Hawkey, C., Hennekens, C., Hochberg, M., Holland, L.E., Kearney, P.M., Laine, L., Lanas, A., Lance, P., Laupacis, A., Oates, J., Patrono, C., Schnitzer, T.J., Solomon, S., Tugwell, P., Wilson, K., Wittes, J., Baigent, C., 2013. Vascular and upper gastrointestinal effects of non-steroidal anti-inflammatory drugs: meta-analyses of individual participant data from randomised trials. Lancet Lond. Engl. 382, 769–79. doi:10.1016/S0140-6736(13)60900-9

Boldyrev, V.V., 2004. Mechanochemical modification and synthesis of drugs. J. Mater. Sci. 39, 5117–5120. doi:10.1023/B:JMSC.0000039193.69784.1d

Boss, A.H., Petrucci, R., Lorber, D., 2012. Coverage of Prandial Insulin Requirements by Means of an Ultra-Rapid-Acting Inhaled Insulin. J. Diabetes Sci. Technol. 6, 773–779. doi:10.1177/193229681200600406

Brodka-Pfeiffer, K., Häusler, H., Grass, P., Langguth, P., 2003. Conditioning following powder micronization: influence on particle growth of salbutamol sulfate. Drug Dev. Ind. Pharm. 29, 1077–1084. doi:10.1081/DDC-120025865

Cabaniss, S.E., McVey, I.F., 1995. Aqueous infrared carboxylate absorbances: aliphatic monocarboxylates. Spectrochim. Acta. A. Mol. Biomol. Spectrosc. 51, 2385–2395. doi:10.1016/0584-8539(95)01479-9

Castellari, C., Ottani, S., 1997. Two Monoclinic Forms of Diclofenac Acid. Acta Crystallogr. Sect. C 53, 794–797. doi:10.1107/S0108270197002126

Center for Drug Evaluation and Research, 2015. Drug Safety and Availability - FDA Drug Safety Communication: FDA strengthens warning that non-aspirin nonsteroidal anti-inflammatory drugs (NSAIDs) can cause heart attacks or strokes [WWW Document]. URL http://www.fda.gov/Drugs/DrugSafety/ucm451800.htm (accessed 8.27.15).

Chadwick, K., Davey, R., Cross, W., 2007. How does grinding produce co-crystals? Insights from the case of benzophenone and diphenylamine. CrystEngComm 9, 732–734. doi:10.1039/B709411F

Chen, X., Young, T.J., Sarkari, M., Williams III, R.O., Johnston, K.P., 2002. Preparation of cyclosporine A nanoparticles by evaporative precipitation into aqueous solution. Int. J. Pharm. 242, 3–14. doi:10.1016/S0378-5173(02)00147-3

Clark, A.R., Hsu, C.C., Walsh, A.J., 1998. Preparation of sodium chloride aerosol formulations. US5747002 A.

Clement, S., Purutyan, H., 2002. Narrowing down equipment choices for particle-size reduction. Chem. Eng. Prog. 98, 50–54.

Corrigan, O.I., 1995. Thermal analysis of spray dried products. Thermochim. Acta, Pharmaceuticals and Thermal Analysis 248, 245–258. doi:10.1016/0040-6031(94)01891-J

Dali, M.V., Carstensen, J.T., 1996. Effect of change in shape factor of a single crystal on its dissolution behavior. Pharm. Res. 13, 155–162. doi:10.1023/A:1016010207729

de Boer, A.H., Chan, H.K., Price, R., 2012. A critical view on lactose-based drug formulation and device studies for dry powder inhalation: Which are relevant and what interactions to expect? Adv. Drug Deliv. Rev., Lactose as a carrier for inhalation products 64, 257–274. doi:10.1016/j.addr.2011.04.004

De Yoreo, J.J., Vekilov, P.G., 2003. Principles of crystal nucleation and growth. Rev. Mineral. Geochem. 54, 57–93.

Dellamary, L.A., Tarara, T.E., Smith, D.J., Woelk, C.H., Adractas, A., Costello, M.L., Gill, H., Weers, J.G., 2000. Hollow Porous Particles in Metered Dose Inhalers. Pharm. Res. 17, 168–174. doi:10.1023/A:1007513213292

Descamps, M., Willart, J.F., Dudognon, E., Caron, V., 2007. Transformation of pharmaceutical compounds upon milling and comilling: The role of T-g. J. Pharm. Sci. 96, 1398–1407. doi:10.1002/jps.20939

Dodd, A., Meiser, F., Norret, M., Russell, A., Bosch, H.W., 2014. Formulation of diclofenac. US8679544 B2.

Dokoumetzidis, A., Macheras, P., 2006. A century of dissolution research: From Noyes and Whitney to the Biopharmaceutics Classification System. Int. J. Pharm. 321, 1–11. doi:10.1016/j.ijpharm.2006.07.011

Donovan, M.J., 2015. Influence of carrier particle size and surface roughness on the aerosol performance of DPI formulations (Thesis).

Drying, Y. improvement I., 1872. Improvement in drying and concentrating liquid substances by atomizing. US125406 A.

Dudognon, E., Danède, F., Descamps, M., Correia, N.T., 2008. Evidence for a new crystalline phase of racemic Ibuprofen. Pharm. Res. 25, 2853–2858. doi:10.1007/s11095-008-9655-7

Dudognon, E., Willart, J.F., Caron, V., Capet, F., Larsson, T., Descamps, M., 2006. Formation of budesonide/alpha-lactose glass solutions by ball-milling. Solid State Commun. 138, 68–71. doi:10.1016/j.ssc.2006.02.007

Eddleston, M.D., Jones, W., 2010. Formation of Tubular Crystals of Pharmaceutical Compounds. Cryst. Growth Des. 10, 365–370. doi:10.1021/cg900969n

Engstrom, J.D., Lai, E.S., Ludher, B.S., Chen, B., Milner, T.E., Williams, R.O., Kitto, G.B., Johnston, K.P., 2008. Formation of Stable Submicron Protein Particles by Thin Film Freezing. Pharm. Res. 25, 1334–1346. doi:10.1007/s11095-008-9540-4

Feeley, J.C., York, P., Sumby, B.S., Dicks, H., 1998. Determination of surface properties and flow characteristics of salbutamol sulphate, before and after micronisation. Int. J. Pharm. 172, 89–96. doi:10.1016/S0378-5173(98)00179-3

Fini, A., Fazio, G., Fernandezhervas, M., Holgado, M., Rabasco, A., 1995. Influence of Crystallization Solvent and Dissolution Behavior for a Diclofenac Salt. Int. J. Pharm. 121, 19–26. doi:10.1016/0378-5173(94)00419-6

Fisher, E.S., 2013. Milling of Active Pharmaceutical Ingredients, in: Encyclopedia of Pharmaceutical Technology, Third Edition. Taylor & Francis, pp. 2339–2351.

Friedrich, A.J., 2001. Size reduction overview : Shear, compression, and impact. Powder Bulk Eng. 15, 19–25.

Frijlink, H.W., de Boer, A.H., 2005. Trends in the technology-driven development of new inhalation devices. Drug Discov. Today Technol. 2, 47–57. doi:10.1016/j.ddtec.2005.05.020

Fusaro, F., Mazzotti, M., Muhrer, G., 2004. Gas Antisolvent Recrystallization of Paracetamol from Acetone Using Compressed Carbon Dioxide as Antisolvent. Cryst. Growth Des. 4, 881–889. doi:10.1021/cg034172u

Gabriel, M.C., Mendes, L.B., Carvalho, B.D.M., Pinheiro, L.A., Capocchi, J.D.T., Kubaski, E.T., Cintho, O.M., 2010. High-Energy Mechanical Milling of Ultra-High Molecular Weight Polyethylene (UHMWPE). Mater. Sci. Forum 660-661, 325–328. doi:10.4028/www.scientific.net/MSF.660-661.325

Geller, D.E., Weers, J., Heuerding, S., 2011. Development of an inhaled dry-powder formulation of tobramycin using PulmoSphereTM technology. J. Aerosol Med. Pulm. Drug Deliv. 24, 175–182. doi:10.1089/jamp.2010.0855

Ghadiri, M., Zhang, Z., 2002. Impact attrition of particulate solids. Part 1: A theoretical model of chipping. Chem. Eng. Sci. 57, 3659–3669. doi:10.1016/S0009-2509(02)00240-3

Guinot, S., Leveiller, F., 1999. The use of MTDSC to assess the amorphous phase content of a micronised drug substance. Int. J. Pharm. 192, 63–75. doi:10.1016/S0378-5173(99)00273-2

Hassoun, M., Ho, S., Muddle, J., Buttini, F., Parry, M., Hammond, M., Forbes, B., 2015. Formulating powder-device combinations for salmeterol xinafoate dry powder inhalers. Int. J. Pharm. 490, 360–367. doi:10.1016/j.ijpharm.2015.05.028

Healy, A.M., Amaro, M.I., Paluch, K.J., Tajber, L., 2014. Dry powders for oral inhalation free of lactose carrier particles. Adv. Drug Deliv. Rev. 75, 32–52. doi:10.1016/j.addr.2014.04.005

Hickey, A.J., 2003. Pharmaceutical Inhalation Aerosol Technology, 2nd ed. Informa Healthcare, New York.

Hickey, A.J., Mansour, H.M., Telko, M.J., Xu, Z., Smyth, H.D.C., Mulder, T., McLean, R., Langridge, J., Papadopoulos, D., 2007. Physical characterization of component particles included in dry powder inhalers. II. Dynamic characteristics. J. Pharm. Sci. 96, 1302–1319. doi:10.1002/jps.20943

Hinds, W.C., 2012. Aerosol Technology : Properties, Behavior, and Measurement of Airborne Particles, 2nd ed. Wiley, Hoboken.

Hira, D., Okuda, T., Kito, D., Ishizeki, K., Okada, T., Okamoto, H., 2010. Inhalation Performance of Physically Mixed Dry Powders Evaluated with a Simple Simulator for Human Inspiratory Flow Patterns. Pharm. Res. 27, 2131–2140. doi:10.1007/s11095-010-0215-6

Hu, J., Johnston, K.P., Williams, R.O., 2004a. Stable amorphous danazol nanostructured powders with rapid dissolution rates produced by spray freezing into liquid. Drug Dev. Ind. Pharm. 30, 695–704. doi:10.1081/DDC-120039212

Hu, J., Johnston, K.P., Williams, R.O., 2004b. Rapid dissolving high potency danazol powders produced by spray freezing into liquid process. Int. J. Pharm. 271, 145–154.

Ikegami, K., Kawashima, Y., Takeuchi, H., Yamamoto, H., Mimura, K., Mamose, D., Ouchi, K., 2003. A new agglomerated KSR-592 beta-form crystal system for dry powder inhalation formulation to improve inhalation performance in vitro and in vivo. J. Controlled Release 88, 23–33. doi:10.1016/S0168-3659(02)00460-1

Iroko Pharmaceuticals, LLC, 2013. Zorvolex (R) [package insert].

Islam, N., Gladki, E., 2008. Dry powder inhalers (DPIs)—A review of device reliability and innovation. Int. J. Pharm. 360, 1–11. doi:10.1016/j.ijpharm.2008.04.044

Jansook, P., Kurkov, S.V., Loftsson, T., 2010. Cyclodextrins as solubilizers: Formation of complex aggregates. J. Pharm. Sci. 99, 719–729. doi:10.1002/jps.21861

John S., P., 1996. Mechanisms of macromolecule absorption by the lungs. Adv. Drug Deliv. Rev. 19, 3–36. doi:10.1016/0169-409X(95)00113-L

Joshi, V., Dwivedi, S., Ward, G.H., 2002. Increase in the specific surface area of budesonide during storage postmicronization. Pharm. Res. 19, 7–12. doi:10.1023/A:1013690929173

Katritzky, A.R., Jain, R., Lomaka, A., Petrukhin, R., Maran, U., Karelson, M., 2001. Perspective on the Relationship between Melting Points and Chemical Structure. Cryst. Growth Des. 1, 261–265. doi:10.1021/cg010009s

Kayaert, P., Van den Mooter, G., 2012. Is the amorphous fraction of a dried nanosuspension caused by milling or by drying? A case study with Naproxen and Cinnarizine. Eur. J. Pharm. Biopharm. 81, 650–656. doi:10.1016/j.ejpb.2012.04.020

Kendall, K., 1978. The impossibility of comminuting small particles by compression. Nature 272, 710–711. doi:10.1038/272710a0

Klinge, S.A., Sawyer, G.A., 2013. Effectiveness and Safety of Topical Versus Oral Nonsteroidal Anti-inflammatory Drugs: A Comprehensive Review. Phys. Sportsmed. 41, 64–74. doi:10.3810/psm.2013.05.2016

Konstan, M.W., Byard, P.J., Hoppel, C.L., Davis, P.B., 1995. Effect of high-dose ibuprofen in patients with cystic fibrosis. N. Engl. J. Med. 332, 848–854. doi:10.1056/NEJM199503303321303

Konstan, M.W., VanDevanter, D.R., Rasouliyan, L., Pasta, D.J., Yegin, A., Morgan, W.J., Wagener, J.S., 2010. Trends in the use of routine therapies in cystic fibrosis: 1995–2005. Pediatr. Pulmonol. 45, 1167–1172. doi:10.1002/ppul.21315

Kubavat, H.A., Shur, J., Ruecroft, G., Hipkiss, D., Price, R., 2012. Influence of primary crystallisation conditions on the mechanical and interfacial properties of micronised budesonide for dry powder inhalation. Int. J. Pharm. 430, 26–33. doi:10.1016/j.ijpharm.2012.03.020

Kulshreshtha, A.K., Singh, O.N., Wall, G.M., 2009. Pharmaceutical Suspensions: From Formulation Development to Manufacturing. Springer Science & Business Media.

Labiris, N.R., Dolovich, M.B., 2003. Pulmonary drug delivery. Part I: Physiological factors affecting therapeutic effectiveness of aerosolized medications. Br. J. Clin. Pharmacol. 56, 588–599. doi:10.1046/j.1365-2125.2003.01892.x

Labiris, N.R., Dolovich, M.B., 2003. Pulmonary drug delivery. Part I: Physiological factors affecting therapeutic effectiveness of aerosolized medications. Br. J. Clin. Pharmacol. 56, 588–599. doi:10.1046/j.1365-2125.2003.01892.x

Lands, L.C., Milner, R., Cantin, A.M., Manson, D., Corey, M., 2007. High-dose ibuprofen in cystic fibrosis: Canadian safety and effectiveness trial. J. Pediatr. 151, 249–254. doi:10.1016/j.jpeds.2007.04.009

Larsson, I., Kristensen, H.G., 2000. Comminution of a brittle/ductile material in a Micros Ring Mill. Powder Technol. 107, 175–178. doi:10.1016/S0032-5910(99)00184-9

Lee, S.L., O'Connor, T.F., Yang, X., Cruz, C.N., Chatterjee, S., Madurawe, R.D., Moore, C.M.V., Yu, L.X., Woodcock, J., 2015. Modernizing Pharmaceutical Manufacturing: from Batch to Continuous Production. J. Pharm. Innov. 10, 191–199. doi:10.1007/s12247-015-9215-8

Leuenberger, H., 1982. The compressibility and compactibility of powder systems. Int. J. Pharm. 12, 41–55. doi:10.1016/0378-5173(82)90132-6

Lexi-Comp Inc., 2015. Diclofenac [WWW Document]. URL http://online.lexi.com.ezproxy.lib.utexas.edu/lco/action/doc/retrieve/docid/patch_f/1772963 (accessed 8.26.15).

Lexi-Comp, 2015. Ibuprofen [WWW Document]. URL http://online.lexi.com.ezproxy.lib.utexas.edu/lco/action/doc/retrieve/docid/patch_f/7066#f_dosages (accessed 8.28.15).

Littringer, E.M., Mescher, A., Eckhard, S., Schröttner, H., Langes, C., Fries, M., Griesser, U., Walzel, P., Urbanetz, N.A., 2012. Spray drying of mannitol as a drug carrier—the impact of process parameters on product properties. Dry. Technol. 30, 114–124.

Llinàs, A., Burley, J.C., Box, K.J., Glen, R.C., Goodman, J.M., 2007. Diclofenac Solubility: Independent Determination of the Intrinsic Solubility of Three Crystal Forms. J. Med. Chem. 50, 979–983. doi:10.1021/jm0612970

Lowell, S., Shields, J.E., Thomas, M.A., Thommes, M., 2004. Characterization of Porous Solids and Powders: Surface Area, Pore Size and Density, Particle Technology Series. Springer Netherlands.

Maas, S.G., Schaldach, G., Littringer, E.M., Mescher, A., Griesser, U.J., Braun, D.E., Walzel, P.E., Urbanetz, N.A., 2011. The impact of spray drying outlet temperature on the particle morphology of mannitol. Powder Technol. 213, 27–35. doi:10.1016/j.powtec.2011.06.024

Macfhionnghaile, P., Hu, Y., Gniado, K., Curran, S., Mcardle, P., Erxleben, A., 2014. Effects of Ball-Milling and Cryomilling on Sulfamerazine Polymorphs: A Quantitative Study. J. Pharm. Sci. 103, 1766–1778. doi:10.1002/jps.23978

Mackin, L., Zanon, R., Park, J., Foster, K., Opalenik, H., Demonte, M., 2002. Quantification of low levels (< 10%) of amorphous content in micronised active batches using dynamic vapour sorption and isothermal microcalorimetry. Int. J. Pharm. 231, 227–236.

Magee, G., Vaughan, C., Smith, J., Kraus, D., 2008. Proposing a Design Space – A Case Study Using Design of Experiments and Jet Milling, in: Respiratory Drug Delivery. CRC Press Boca Raton, pp. 259–270.

Marek, S.R., Donovan, M.J., Smyth, H.D.C., 2011. Effects of mild processing pressures on the performance of dry powder inhaler formulations for inhalation therapy (1): Budesonide and lactose. Eur. J. Pharm. Biopharm. 78, 97–106. doi:10.1016/j.ejpb.2010.12.020

Martin, A., Cocero, M.J., 2008. Micronization processes with supercritical fluids: Fundamentals and mechanisms. Adv. Drug Deliv. Rev. 60, 339–350. doi:10.1016/j.addr.2007.06.019

Masuda, H., Ebooks Corporation, 2006. Powder Technology Handbook. CRC Press, Hoboken.

Matsuda, Y., Kawaguchi, S., Kobayashi, H., Nishijo, J., 1984. Physicochemical characterization of spray-dried phenylbutazone polymorphs. J. Pharm. Sci. 73, 173–179. doi:10.1002/jps.2600730209

Matsui, H., Shimokawa, O., Kaneko, T., Nagano, Y., Rai, K., Hyodo, I., 2011. The pathophysiology of non-steroidal anti-inflammatory drug (NSAID)-induced mucosal injuries in stomach and small intestine. J. Clin. Biochem. Nutr. 48, 107–111. doi:10.3164/jcbn.10-79

McConnell, J.F., 1974. 2-(4-Isobutylphenyl) propionic acid. Cryst Struct Commun 3, 73–75.

Merisko-Liversidge, E., Liversidge, G.G., 2011. Nanosizing for oral and parenteral drug delivery: A perspective on formulating poorly-water soluble compounds using wet media milling technology. Adv. Drug Deliv. Rev. 63, 427–440. doi:10.1016/j.addr.2010.12.007

Miller, D.A., Gil, M., 2012. Spray-Drying Technology, in: III, R.O.W., Watts, A.B., Miller, D.A. (Eds.), Formulating Poorly Water Soluble Drugs, AAPS Advances in the Pharmaceutical Sciences Series. Springer New York, pp. 363–442.

Moribe, K., Ueda, K., Limwikrant, W., Higashi, K., Yamamoto, K., 2013. Nano-Sized Crystalline Drug Production by Milling Technology. Curr. Pharm. Des. 19, 6246–6258.

Muhrer, G., Lin, C., Mazzotti, M., 2002. Modeling the gas antisolvent recrystallization process. Ind. Eng. Chem. Res. 41, 3566–3579. doi:10.1021/ie020070+

Muhrer, G., Mazzotti, M., Muller, M., 2003. Gas antisolvent recrystallization of an organic compound. Tailoring product PSD and scaling-up. J. Supercrit. Fluids 27, 195–203. doi:10.1016/S0896-8446(02)00237-1

Mujumdar, A.S., 2006. Handbook of Industrial Drying, Third Edition. CRC Press.

Muller, F., Polke, R., Schadel, G., 1996. Spiral jet mills: Hold up and scale up. Int. J. Miner. Process. 44-5, 315–326. doi:10.1016/0301-7516(95)00042-9

Muller, M., Meier, U., Kessler, A., Mazzotti, M., 2000. Experimental study of the effect of process parameters in the recrystallization of an organic compound using compressed carbon dioxide as antisolvent. Ind. Eng. Chem. Res. 39, 2260–2268. doi:10.1021/ie990828y

Muller, R.H., Becker, R., Kruss, B., Peters, K., 1999. Pharmaceutical nanosuspensions for medicament administration as systems with increased saturation solubility and rate of solution. US5858410 A.

Mullin, J.W., 2001. Crystallization. Butterworth-Heinemann.

Mullins, M.E., Michaels, L.P., Menon, V., Locke, B., Ranade, M.B., 1992. Effect of geometry on particle adhesion. Aerosol Sci. Technol. 17, 105–118.

Mumenthaler, M., Leuenberger, H., 1991. Atmospheric spray-freeze drying: a suitable alternative in freeze-drying technology. Int. J. Pharm. 72, 97–110.

Murray, M.D., Brater, D.C., 1993. Renal Toxicity of the Nonsteroidal Anti-Inflammatory Drugs. Annu. Rev. Pharmacol. Toxicol. 33, 435–465. doi:10.1146/annurev.pa.33.040193.002251

Naik, S., Chaudhuri, B., 2015. Quantifying Dry Milling in Pharmaceutical Processing: A Review on Experimental and Modeling Approaches. J. Pharm. Sci. 104, 2401–2413. doi:10.1002/jps.24512

Nakach, M., Authelin, J.R., Chamayou, A., Dodds, J., 2004. Comparison of various milling technologies for grinding pharmaceutical powders. Int. J. Miner. Process. 74, S173–S181. doi:10.1016/j.minpro.2004.07.039

Nalajala, V.S., Moholkar, V.S., 2011. Investigations in the physical mechanism of sonocrystallization. Ultrason. Sonochem. 18, 345–355. doi:10.1016/j.ultsonch.2010.06.016

Neupert, W., Brugger, R., Euchenhofer, C., Brune, K., Geisslinger, G., 1997. Effects of ibuprofen enantiomers and its coenzyme A thioesters on human prostaglandin endoperoxide synthases. Br. J. Pharmacol. 122, 487–492. doi:10.1038/sj.bjp.0701415

Newell, H.E., Buckton, G., Butler, D.A., Thielmann, F., Williams, D.R., 2001. The Use of Inverse Phase Gas Chromatography to Measure the Surface Energy of

Crystalline, Amorphous, and Recently Milled Lactose. Pharm. Res. 18, 662–666. doi:10.1023/A:1011089511959

Newhouse, M.T., Hirst, P.H., Duddu, S.P., Walter, Y.H., Tarara, T.E., Clark, A.R., Weers, J.G., 2003. Inhalation of a dry powder tobramycin PulmoSphere formulation in healthy volunteers. Chest 124, 360–366. doi:10.1378/chest.124.1.360

Newman, S.P., Chan, H.-K., 2008. In Vitro/In Vivo Comparisons in Pulmonary Drug Delivery. J. Aerosol Med. Pulm. Drug Deliv. 21, 77–84. doi:10.1089/jamp.2007.0643

NIST/SEMATECH e-Handbook of Statistical Methods, n.d.

Nokhodchi, A., Homayouni, A., Araya, R., Kaialy, W., Obeidat, W., Asare-Addo, K., 2015. Crystal engineering of ibuprofen using starch derivatives in crystallization medium to produce promising ibuprofen with improved pharmaceutical performance. RSC Adv. 5, 46119–46131. doi:10.1039/C5RA06183K

Novartis, 2013. Tobi Podhaler (R) [Package insert].

Olsson, B., Bondesson, E., Borgström, L., Edsbäcker, S., Eirefelt, S., Ekelund, K., Gustavsson, L., Hegelund-Myrbäck, T., 2011. Pulmonary drug metabolism, clearance, and absorption, in: Smyth, H.D., Hickey, A.J. (Eds.), Controlled Pulmonary Drug Delivery. Springer, pp. 21–50.

Ostrowska, K., Kropidłowska, M., Katrusiak, A., 2015. High-pressure crystallization and structural transformations in compressed R, S-Ibuprofen. Cryst. Growth Des. 15, 1512–1517. doi:10.1021/cg5018888

Overhoff, K.A., Engstrom, J.D., Chen, B., Scherzer, B.D., Milner, T.E., Johnston, K.P., Williams III, R.O., 2007. Novel ultra-rapid freezing particle engineering process for enhancement of dissolution rates of poorly water-soluble drugs. Eur. J. Pharm. Biopharm. 65, 57–67. doi:10.1016/j.ejpb.2006.07.012

Parrott, E., 1974. Milling of Pharmaceutical Solids. J. Pharm. Sci. 63, 813–829. doi:10.1002/jps.2600630603

Patton, J.S., Fishburn, C.S., Weers, J.G., 2004. The lungs as a portal of entry for systemic drug delivery. Proc. Am. Thorac. Soc. 1, 338–44. doi:10.1513/pats.200409-049TA

Patton, J.S., Platz, R.M., 1992. (D) Routes of delivery: Case studies: (2) Pulmonary delivery of peptides and proteins for systemic action. Adv. Drug Deliv. Rev., Routes of Drug Delivery: Case studies 8, 179–196. doi:10.1016/0169-409X(92)90002-8

Pérez-Maqueda, L.A., Duran, A., Pérez-Rodríguez, J.L., 2005. Preparation of submicron talc particles by sonication. Appl. Clay Sci., EUROCLAY 2003 28, 245–255. doi:10.1016/j.clay.2004.01.012

Planinšek, O., Zadnik, J., Kunaver, M., Srčič, S., Godec, A., 2010. Structural evolution of indomethacin particles upon milling: Time-resolved quantification and

localization of disordered structure studied by IGC and DSC. J. Pharm. Sci. 99, 1968–1981. doi:10.1002/jps.21986

Puri, V., Dantuluri, A.K., Kumar, M., Karar, N., Bansal, A.K., 2010. Wettability and surface chemistry of crystalline and amorphous forms of a poorly water soluble drug. Eur. J. Pharm. Sci. 40, 84–93. doi:10.1016/j.ejps.2010.03.003

Rasenack, N., Müller, B.W., 2004. Micron-Size Drug Particles: Common and Novel Micronization Techniques. Pharm. Dev. Technol. 9, 1–13. doi:10.1081/PDT-120027417

Rasenack, N., Steckel, H., Muller, B.W., 2003. Micronization of anti-inflammatory drugs for pulmonary delivery by a controlled crystallization process. J. Pharm. Sci. 92, 35–44. doi:10.1002/jps.10274

Révész, Á., 2005. Melting behavior and origin of strain in ball-milled nanocrystalline Al powders. J. Mater. Sci. 40, 1643–1646. doi:10.1007/s10853-005-0664-1

Roberts, R.J., Rowe, R.C., 1987. Brittle/ductile behaviour in pharmaceutical materials used in tabletting. Int. J. Pharm. 36, 205–209. doi:10.1016/0378-5173(87)90157-8

Rodriguez, L.A.G., Jick, H., 1994. Risk of upper gastrointestinal bleeding and perforation associated with individual non-steroidal... Lancet 343, 769.

Roos, Y.H., 2002. Importance of glass transition and water activity to spray drying and stability of dairy powders. Le Lait 82, 10. doi:10.1051/lait:2002025

Rowe, J.M., Johnston, K.P., 2012. Precipitation Technologies for Nanoparticle Production, in: III, R.O.W., Watts, A.B., Miller, D.A. (Eds.), Formulating Poorly

Water Soluble Drugs, AAPS Advances in the Pharmaceutical Sciences Series. Springer New York, pp. 501–568.

Saleem, I.Y., Smyth, H.D.C., 2010. Micronization of a Soft Material: Air-Jet and Micro-Ball Milling. AAPS PharmSciTech 11, 1642–1649. doi:10.1208/s12249-010-9542-5

Sander, J.R.G., Zeiger, B.W., Suslick, K.S., 2014. Sonocrystallization and sonofragmentation. Ultrason. Sonochem. 21, 1908–1915. doi:10.1016/j.ultsonch.2014.02.005

Santa-Maria, M., Scher, H., Jeoh, T., 2012. Microencapsulation of bioactives in cross-linked alginate matrices by spray drying. J. Microencapsul. 29, 286–295. doi:10.3109/02652048.2011.651494

Shah, P.N., Marshall-Batty, K.R., Panzer, M.J., Smolen, J.A., Tagaev, J.A., Rodesney, C.A., Le, H.H., Gordon, V.D., Greenberg, D.E., Youngs, W.J., Cannon, C.L., 2015. Antimicrobial and synergistic effects of ibuprofen against resistant cystic fibrosis pathogens. Presented at the 115th General Meeting of American Society of Microbiology.

Shah, R.B., Tawakkul, M.A., Khan, M.A., 2008. Comparative evaluation of flow for pharmaceutical powders and granules. AAPS PharmSciTech 9, 250–258. doi:10.1208/s12249-008-9046-8

Shakhtshneider, T.P., 1997. Phase transformations and stabilization of metastable states of molecular crystals under mechanical activation. Solid State Ion., International

Symposium on the Reactivity of Solids 101–103, Part 2, 851–856. doi:10.1016/S0167-2738(97)00224-5

Shariare, M.H., Blagden, N., de Matas, M., Leusen, F.J.J., York, P., 2012. Influence of solvent on the morphology and subsequent comminution of ibuprofen crystals by air jet milling. J. Pharm. Sci. 101, 1108–1119. doi:10.1002/jps.23003

Shariare, M.H., de Matas, M., York, P., 2011. Effect of crystallisation conditions and feedstock morphology on the aerosolization performance of micronised salbutamol sulphate. Int. J. Pharm. 415, 62–72. doi:10.1016/j.ijpharm.2011.05.043

Sharma, P., Denny, W.A., Garg, S., 2009. Effect of wet milling process on the solid state of indomethacin and simvastatin. Int. J. Pharm. 380, 40–48. doi:10.1016/j.ijpharm.2009.06.029

Shegokar, R., Mueller, R.H., 2010. Nanocrystals: Industrially feasible multifunctional formulation technology for poorly soluble actives. Int. J. Pharm. 399, 129–139. doi:10.1016/j.ijpharm.2010.07.044

Simonell.ap, Mehta, S., Higuchi, W., 1970. Inhibition of Sulfathiazole Crystal Growth by Polyvinylpyrrolidone. J. Pharm. Sci. 59, 633–&. doi:10.1002/jps.2600590512

Smyth, H.D., Saleem, I., Donovan, M., Verschraegen, C.F., 2007. Pulmonary delivery of anti-cancer agents, in: Advanced Drug Formulation Design to Optimize Therapeutic Outcomes. p. 81.

Smyth, H.D.C., 2005. Propellant-driven metered-dose inhalers for pulmonary drug delivery. Expert Opin. Drug Deliv. 2, 53–74. doi:10.1517/17425247.2.1.53

Steckel, H., Bolzen, N., 2004. Alternative sugars as potential carriers for dry powder inhalations. Int. J. Pharm. 270, 297–306. doi:10.1016/j.ijpharm.2003.10.039

Steckel, H., Rasenack, N., Villax, P., Müller, B.W., 2003. In vitro characterization of jet-milled and in-situ-micronized fluticasone-17-propionate. Int. J. Pharm. 258, 65–75. doi:10.1016/S0378-5173(03)00153-4

Strydom, S.J., Rose, W.E., Otto, D.P., Liebenberg, W., de Villiers, M.M., 2013. Poly(amidoamine) dendrimer-mediated synthesis and stabilization of silver sulfonamide nanoparticles with increased antibacterial activity. Nanomedicine Nanotechnol. Biol. Med. 9, 85–93. doi:10.1016/j.nano.2012.03.006

Suslick, K., 1989. The Chemical Effects of Ultrasound. Sci. Am. 260, 80–86.

Suslick, K.S., 1990. Sonochemistry. Science 247, 1439–1445. doi:10.1126/science.247.4949.1439

Takagi, T., Ramachandran, C., Bermejo, M., Yamashita, S., Yu, L.X., Amidon, G.L., 2006. A Provisional Biopharmaceutical Classification of the Top 200 Oral Drug Products in the United States, Great Britain, Spain, and Japan. Mol. Pharm. 3, 631–643. doi:10.1021/mp0600182

Telko, M., Hickey, A., 2007. Critical assessment of inverse gas chromatography as means of assessing surface free energy and acid-base interaction of pharmaceutical powders. J. Pharm. Sci. 96, 2647–2654. doi:10.1002/jps.20897

Telko, M.J., Hickey, A.J., 2005. Dry Powder Inhaler Formulation. Respir. Care 50, 1209–1227.

Teng, S., Wang, P., Zhu, L., Young, M.-W., Gogos, C.G., 2009. Experimental and numerical analysis of a lab-scale fluid energy mill. Powder Technol. 195, 31–39. doi:10.1016/j.powtec.2009.05.013

Ticehurst, M.D., Basford, P.A., Dallman, C.I., Lukas, T.M., Marshall, P.V., Nichols, G., Smith, D., 2000. Characterisation of the influence of micronisation on the crystallinity and physical stability of revatropate hydrobromide. Int. J. Pharm. 193, 247–259.

Ticehurst, M.D., Rowe, R.C., York, P., 1994. Determination of the surface properties of two batches of salbutamol sulphate by inverse gas chromatography. Int. J. Pharm. 111, 241–249. doi:10.1016/0378-5173(94)90347-6

Troy, D.B., 2005. Remington: The science and practice of pharmacy. Lippincott, Williams & Wilkins, Philadelphia, PA.

Ulrich, J., Schuster, A., Stelzer, T., 2013. Crystalline coats or hollow crystals as tools for product design in pharmaceutical industry. J. Cryst. Growth, The 5th Asia Conference on Crystal Growth and Crystal Technologies 362, 235–237. doi:10.1016/j.jcrysgro.2011.10.060

USP General Chapter, 2015a. <1174> Powder flow, in: US Pharmacopeial Convention, Rockville, MD, USA. pp. 1326–30.

USP General Chapter, 2015b. <616> Bulk density and tapped density of powders, in: US Pharmacopeial Convention, Rockville, MD, USA. pp. 7059–63.

USP General Chapter, 2015c. <601> Inhalation and nasal drug products: aerosols, sprays, and powders - performance quality tests, in: US Pharmacopeial Convention, Rockville, MD, USA. pp. 388–414.

Van Oort, M.M., Sacchetti, M., 2007. Spray-drying and supercritical fluid particle generation techniques. LUNG Biol. Health Dis. 221, 307.

Vatsaraj, N.B., Gao, D., Kowalski, D.L., 2003. Optimization of the operating conditions of a lab scale Aljet mill using lactose and sucrose: A technical note. AAPS PharmSciTech 4, 141–146. doi:10.1208/pt040227

Vehring, R., 2008. Pharmaceutical Particle Engineering via Spray Drying. Pharm. Res. 25, 999–1022. doi:10.1007/s11095-007-9475-1

Viçosa, A., Letourneau, J.-J., Espitalier, F., Inês Ré, M., 2012. An innovative antisolvent precipitation process as a promising technique to prepare ultrafine rifampicin particles. J. Cryst. Growth, 6th National Congress on Industrial Crystallization (CRISTAL-6) 342, 80–87. doi:10.1016/j.jcrysgro.2011.09.012

Wallace, J.L., 2008. Prostaglandins, NSAIDs, and Gastric Mucosal Protection: Why Doesn't the Stomach Digest Itself? Physiol. Rev. 88, 1547–1565. doi:10.1152/physrev.00004.2008

Ward, G.H., Schultz, R.K., 1995. Process-induced crystallinity changes in albuterol sulfate and Its effect on powder physical stability. Pharm. Res. 12, 773–779. doi:10.1023/A:1016232230638

Weiler, C., Egen, M., Trunk, M., Langguth, P., 2010. Force control and powder dispersibility of spray dried particles for inhalation. J. Pharm. Sci. 99, 303–316. doi:10.1002/jps.21849

Wildfong, P.L.D., Hancock, B.C., Moore, M.D., Morris, K.R., 2006. Towards an understanding of the structurally based potential for mechanically activated disordering of small molecule organic crystals. J. Pharm. Sci. 95, 2645–2656. doi:10.1002/jps.20672

Williams, R.O., Johnston, K.P., Young, T.J., Rogers, T.L., Barron, M.K., Yu, Z., Hu, J., 2005. Process for production of nanoparticles and microparticles by spray freezing into liquid. US6862890 B2.

Wilson, R., Welte, T., Polverino, E., Soyza, A.D., Greville, H., O'Donnell, A., Alder, J., Reimnitz, P., Hampel, B., 2013. Ciprofloxacin dry powder for inhalation in non-cystic fibrosis bronchiectasis: a phase II randomised study. Eur. Respir. J. 41, 1107–1115. doi:10.1183/09031936.00071312

Witkin, D.B., Lavernia, E.J., 2006. Synthesis and mechanical behavior of nanostructured materials via cryomilling. Prog. Mater. Sci. 51, 1–60. doi:10.1016/j.pmatsci.2005.04.004

Xiao, Y., Liu, Y., Mi, Y., Yuan, D., Zhang, J., Cheng, L., 2005. A Simple Route to Form Straw-like Carbon Microbundles. Chem. Lett. 34, 1422–1423. doi:10.1246/cl.2005.1422

Xu, Z., Hickey, A.J., 2011. The physics of aerosol droplet and particle generation from inhalers, in: Smyth, H.D., Hickey, A.J. (Eds.), Controlled Pulmonary Drug Delivery. Springer, pp. 75–100.

Xu, Z., Mansour, H.M., Mulder, T., McLean, R., Langridge, J., Hickey, A.J., 2010. Dry powder aerosols generated by standardized entrainment tubes from drug blends with lactose monohydrate: 2. Ipratropium bromide monohydrate and fluticasone propionate. J. Pharm. Sci. 99, 3415–3429. doi:10.1002/jps.22100

Yang, W., Iii, D.E.O., Iii, R.O.W., 2012. Pharmaceutical Cryogenic Technologies, in: III, R.O.W., Watts, A.B., Miller, D.A. (Eds.), Formulating Poorly Water Soluble Drugs, AAPS Advances in the Pharmaceutical Sciences Series. Springer New York, pp. 443–500.

Yazdi, A.K., Smyth, H.D.C., 2015. Effect of capsule fill weight on device resistance in dry powder inhalers, in: Respiratory Drug Delivery. CRC Press Boca Raton, pp. 523–528.

Yazdi, A.K., Smyth, H.D.C., 2015. Effect of Capsule Fill Weight on Device Resistance in Dry Powder Inhalers, in: Respiratory Drug Delivery. CRC Press Boca Raton, pp. 523–528.

Yu, L., 2001. Amorphous pharmaceutical solids: preparation, characterization and stabilization. Adv. DRUG Deliv. Rev. 48, 27–42.

Yu, Z., Johnston, K.P., Williams III, R.O., 2006. Spray freezing into liquid versus spray-freeze drying: Influence of atomization on protein aggregation and biological activity. Eur. J. Pharm. Sci. 27, 9–18. doi:10.1016/j.ejps.2005.08.010

Zalepugin, D.Y., Tilkunova, N.A., Fronchek, E.V., Gallyamov, M.O., Chernyshova, I.V., Mishin, V.S., Yashin, Y.S., Grigoryev, T.E., Gamzazade, A.I., Khokhlov, A.R., 2010. Production of new haemostatic materials by deposition of dispersed proteins onto porous matrices using supercritical carbon dioxide. Russ. J. Phys. Chem. B 4, 1047–1050. doi:10.1134/S1990793110070018

Zeiger, B.W., Suslick, K.S., 2011. Sonofragmentation of Molecular Crystals. J. Am. Chem. Soc. 133, 14530–14533. doi:10.1021/ja205867f

Zhang, Z., Ghadiri, M., 2002. Impact attrition of particulate solids. Part 2: Experimental work. Chem. Eng. Sci. 57, 3671–3686. doi:10.1016/S0009-2509(02)00241-5

Zheng, J., 2009. Formulation and Analytical Development for Low-Dose Oral Drug Products. John Wiley & Sons.

Zijlstra, G.S., Rijkeboer, M., Van Drooge, D.J., Sutter, M., Jiskoot, W., Van De Weert, M., Hinrichs, W.L., Frijlink, H.W., 2007. Characterization of a cyclosporine solid dispersion for inhalation. AAPS J. 9, E190–E199.

VITA

Ashkan Khakparvar Yazdi was born in Ahwaz, Iran. He was raised in Tehran, Iran and moved with his parents and brother to Austin, TX in 2003. In 2005, he graduated from L.C. Anderson H.S. in Austin, TX. He transferred to The University of Texas at Austin from Austin Community College in Spring 2006. He completed his Doctor of Pharmacy (Pharm.D.) degree in the College of Pharmacy at The University of Texas at Austin from Fall 2007 until May 2011. He pursued the Pharm.D./Ph.D. program following his first year in the College of Pharmacy. He conducted research rotations in the labs of Dr. Sean M. Kerwin, Dr. Jason T. McConville, and Dr. Christine L. Duvauchelle prior to formally starting the Ph.D. in the division of Pharmaceutics under supervision of Dr. McConville. In 2012, he joined Dr. Hugh D.C. Smyth lab following the relocation of Dr. McConville. During his Ph.D. studies, he served as the vice-president and the president of Pharmacy Graduate Students Association and the master of ceremony for the new graduate student orientation from 2012-13. Furthermore, he is an author to multiple manuscripts as well as abstracts and posters presented in the ExcipientFest Americas, the American Association of Pharmaceutical Scientists (AAPS), and the Respiratory Drug Delivery (RDD). He is currently residing in Austin, TX.

Email Address: ashkan.k.yazdi@utexas.edu

This dissertation was typed by Ashkan K. Yazdi.